



**UNIVERSITÁ DEGLI STUDI DI NAPOLI  
FEDERICO II**

**Dipartimento di Ingegneria dei Materiali e della Produzione**

**Insight of thermo-mechanical and fire  
properties of an aerospace epoxy matrix  
loaded with micro and nano fillers.**

**CRISTINA FORMICOLA**

**Ph.D. Dissertation**

**TUTOR**

**Dr. Michele Giordano**

**Dr. Mauro Zarrelli**

**COORDINATOR**

**Ch.mo Domenico Acierno**

**December 2008**



# UNIVERSITÀ DEGLI STUDI DI NAPOLI FEDERICO II

Dipartimento di Ingegneria dei Materiali e della Produzione

## Insight of thermo-mechanical and fire properties of an aerospace epoxy matrix loaded with micro and nano fillers.

**CRISTINA FORMICOLA**

Ph.D. Dissertation

**TUTOR**

**Dr. Michele Giordano  
Dr. Mauro Zarrelli**

**COORDINATOR**

**Ch.mo Domenico Acierno**

**December 2008**

**In collaboration with:**



**Technological District in Polymer  
and Composite Engineering**



# ***Table of Contents***

## ***Chapter 1***

### ***Introduction***

- 1.1 Combustion mechanism
  - 1.2 Fire test for composites materials
- References

## ***Chapter 2***

### ***Materials***

- 2.1 Thermosetting resin: RTM6
    - 2.1.1 Characterization of RTM6
  - 2.2 Micro materials: Introduction on flame retardant
    - 2.2.1 Zinc Borate
    - 2.2.2 Aluminium Trihydrate
    - 2.2.3 Zinc Hydroxystannate
    - 2.2.4 Zinc Stannate
  - 2.3 Nano materials: Introduction on carbon nanotubes
    - 2.3.1 Multi walled carbon nanotubes
- References

## ***Chapter 3***

### ***Experimental techniques***

- 3.1 Methods
  - 3.1.1 Micro particles: Mechanical stirring
  - 3.1.2 Nano particles: Sonication
  - 3.1.3 Vacuum infusion process
- 3.2 Characterization
  - 3.2.1 Cone calorimeter
  - 3.2.2 Scanning Electron Microscope
  - 3.2.3 Thermal mechanical analysis

### 3.2.4 Thermal gravimetric analysis

References

## **Chapter 4**

### ***Flame retardant of epoxy resin with inorganic compounds***

**4.1** The state of the art on flame retardant of inorganic compounds

**4.2** Cone calorimeter test

4.2.1 Flame retardant of RTM6 and inorganic compounds

4.2.2 Synergistic effect of zinc borate

4.2.3 Scanning electron micrograph of residue

4.2.4 Flame retardant of panels of RTM6 and inorganic compounds

**4.3** Thermal mechanical analysis of RTM6 and inorganic compounds

References

## **Chapter 5**

### ***Flame retardant of epoxy resin with carbon nanotubes***

**5.1** The state of the art on flame retardant of carbon nanotubes

**5.2** Cone calorimeter test

5.2.1 Flame retardant of RTM6 and multi walled carbon nanotubes

5.2.2 Flame retardant of panels of RTM6 and carbon nanotubes

**5.3** Thermal mechanical analysis of RTM6 and carbon nanotubes

References

## **Chapter 6**

### ***Kinetic degradations: Kissinger and Ozawa methods***

**6.1** The state of the art on Kissinger and Ozawa methods for epoxy resin

**6.2** Kinetic degradations of RTM6 and inorganic compounds

**6.3** Kinetic degradations of RTM6 and carbon nanotubes

## **6.4** Analysis of residue

References

## ***Chapter 7***

### ***Conclusions and future perspectives***

**7.1** Conclusions

**7.2** Future Perspectives

# *ACKNOWLEDGMENTS*

I want to thank Dr. Engineer Giordano for this opportunity and to Dr. Engineer Zarrelli for having believed in my possibilities and for allowing me to fulfill them.

To Professor Camino and Dr. Engineer Frache of Turin Polytechnic for having welcomed me in their structure with professionalism and kindness.

To my family for their (also monetary) support.

To my friends/colleagues for their help and for putting up with me and my temper and

Especially "Thank you" to my beloved *Ciro*, who has always been by my side despite everything.

To *Daniele* who supported me and was tortured by me.

To *Anna*, who has been a moral and professional support and for not having sent me to hell yet.

# CHAPTER 1

## INTRODUCTION

### 1.1 Combustion mechanisms

The use of polymer composites has grown at a phenomenal rate since the 1960s, and these materials now have an impressive and diverse range of applications in aircraft, spacecraft, boats, ships, automobiles, civil infrastructure, sporting goods and consumer products. The growth in the use of composite materials by various industry sectors in the United States since 1960 is reported in figure 1.1. Growth in the use of composites has reached a level where they are now challenging the use of traditional materials - most notably steels and aluminium alloys - in many markets; particularly the aircraft, boat-building and chemical processing industries.

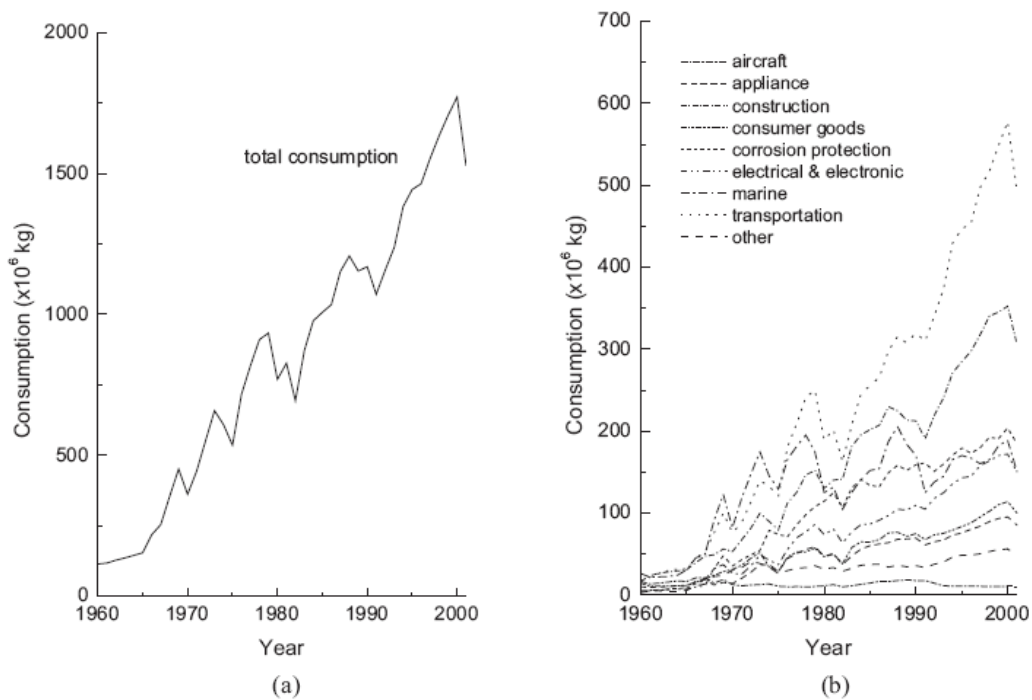


**Figure 1.1.** Growth in the (a) total use and (b) use by individual market sectors in the United States. (Source: Composite Fabrication Association).

The use of composites in a wide variety of applications is due to their many outstanding physical, thermal, chemical and mechanical properties. Key advantages of composites over many metal alloys include low density, high specific stiffness and specific strength, good fatigue endurance, excellent corrosion resistance, outstanding thermal insulation and low thermal expansion. However, there are several disadvantages with composites that have impacted on their growth in some markets. Composites are plagued by problems such as low through-thickness mechanical properties, poor impact damage tolerance, and anisotropic properties. A major disadvantage of many composite materials is poor performance in fire. When composites are exposed to high temperatures (typically above 300-400°C) the organic matrix decomposes with the release of heat, smoke, soot and toxic volatiles. Composites also soften, creep and distort when heated to moderate temperature (>100-200°C), that can result in buckling and failure of load-bearing composite structures. The heat, smoke and gases released by a burning composite and the degradation in structural integrity can make fire-fighting extremely hazardous and increase the likelihood of serious injury and death. The susceptibility of composites to fire has been the key issue in curtailing their use in many infrastructure and public transportation applications.

Although many polymer composites are flammable, their resistance to pyrolysis can be improved. Furthermore, these materials possess some potentially useful properties in fire that are not inherent with metals. Composites have excellent thermal insulation properties and slow burn-through. The rate of heat conduction through composites is much slower than metals, and this is a significant benefit in slowing the spread of fire from room-to-room. Composites can provide an effective protective barrier against flame, heat, smoke and toxic fumes.

Fire is a complicated phenomenon that can develop in stages of increasing temperature and size before decaying. The fire event becomes

more complex when a polymer composite material is involved because it can control the temperature, size and spread of the flame. A turbulent flame consists of three zones, and from the base to top can be divided into the solid flame region, intermittent flame region and thermal plume (Fig. 1.2). The solid flame region near the plume base is where the majority of the flammable vapours undergo exothermic chain-branching reactions that generate most of the heat.

The temperature within this zone is reasonably constant at about 830-900°C for most types of solid fuels [1], although the maximum temperature in hydrocarbon pool fires and natural gas flames can reach 1150-1250°C [2]. Above the solid flame is the intermittent flame region, and the temperature drops continuously the higher up this zone. The average temperature at the visible tips of a flame is about 400°C [3], although it can vary over a wide range from 300 to 600°C [1]. The boundary between the solid flame and intermittent regions is not well defined in a turbulent flame, and some overlap or changes in the boundary location do occur. Above the flame tips is the thermal plume region, where no flames are visible and the temperature drops with height. The thermal plume consists of hot gases, vapours and soot particles that can be carried upwards by convective heat.

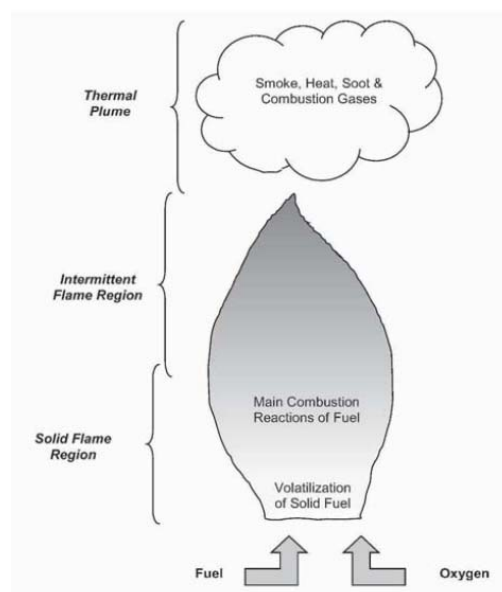


**Figure 1.2.** Schematic showing the different zones within a turbulent plume.

The initiation and growth of fire is determined by a multitude of factors including the type (caloric value) of fuel, fuel load, fuel size (area), oxygen content in the flame, wind speed, and whether the fire is within an open or enclosed space. In the case of polymer composites exposed to fire, the material itself can be a rich source of fuel that causes the temperature to rise and the flame to spread.

A serious concern with using composites in enclosed spaces, such as an aircraft cabin, ship compartment or rail carriage, is that the heat, smoke and toxic gases are trapped which seriously increases the fire hazard. It is therefore useful to examine the development of fire within a closed compartment. Figure 1.3 shows how the temperature can vary with time for a closed compartment fire.

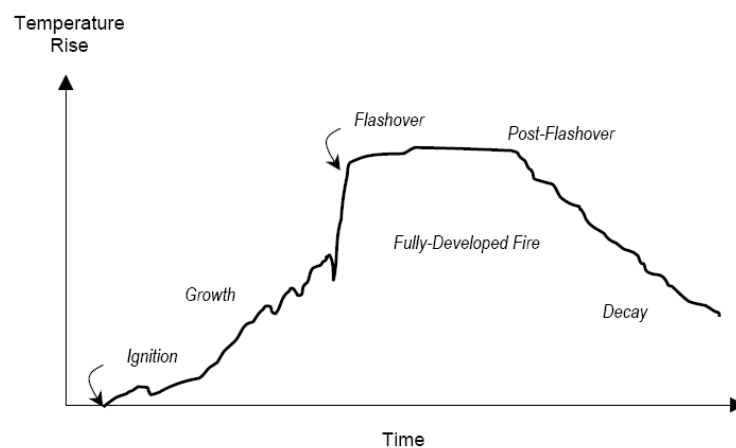


**Figure 1.3.** Growth stages of a compartment fire.

A fire can undergo several stages of growth, and in order these are:

1. **Ignition.** This is the point when the fuel source ignites and undergoes sustained flaming combustion.
2. **Growth.** The initial growth of a fire is dependent mainly on the fuel itself, with little or no influence from the combustible materials within the compartment. The fire will grow and the compartment temperature will continue to rise if sufficient fuel and oxygen are available. It is often in this stage that composite

materials exposed to the flame will ignite when the temperature exceeds 350-500°C.

3. **Flashover**. This occurs when the fire is fully developed and all combustible items in the compartment (including any composite materials) are involved in the fire. Flashover usually occurs when the average upper gas temperature in the room exceeds about 600°C.
4. **Fully developed fire**. This stage occurs when the heat release rate and temperature of a fire are at their greatest. The peak temperature of a typical post-flashover room fire is 900-1000°C, although it can reach as high as 1200°C.
5. **Decay**. The final decay stage occurs as the fuel and combustible materials become consumed, causing the compartment temperature to fall. Obviously, decay can also be caused by active fire suppression systems, such as sprinklers.

When a composite is heated to a sufficiently high temperature the polymer matrix and (if present) organic fibres will thermally decompose. Most polymer matrixes and organic fibres decompose over the temperature range of about 350 to 600°C with the production of flammable gases. Decomposition occurs by a series of reactions that breaks down the polymer chains into low molecular weight volatiles that diffuse into the flame. Depending on the chemical composition and molecular structure of the polymer, the thermal degradation reactions may proceed by various paths. The majority of organic resins and fibres used in composites degrade thermally by a random chain scission process. This basically involves the break-down of the long organic chains at the lowest-energy bond sites into small fragments. Polymers can also decompose by other processes, including de-polymerisation (that involves the breakdown of the chain into monomers) and chain-end initiated scission (that involves the process starting from the chain ends and propagating along the chain length until it is completely degraded).

The combustion cycle of organic polymers is illustrated in fig. 1.4 and the cycle stops only when the fuel source has been exhausted, which is usually when the organic components in a composite have been completely degraded.

It is common practice by fire scientists to quantify the intensity of a fire by the radiant heat flux rather than flame temperature.

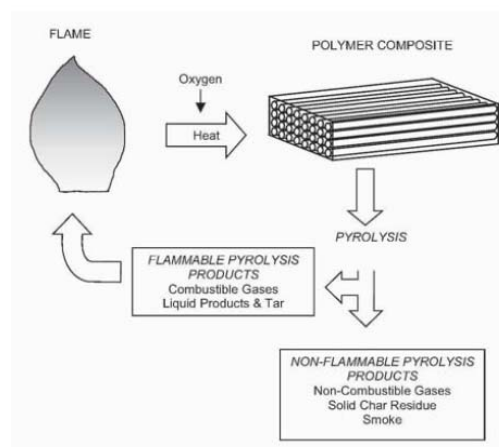


**Figure 1.4.** The combustion cycle of organic polymers.

The diverse range of uses for composite materials means they can be exposed to a variety of fire threats, and their increasing use in high fire risk applications raises the likelihood of severe fire incidents. Several case studies of fires in aircraft and ships are given to demonstrate the importance of understanding the fire behaviour of composites, and the need for more flame resistant polymeric materials.

The fire behaviour of composites materials is distinct by two important properties: ***Fire reaction and Fire resistant.***

***Fire reaction*** describes the flammability and combustion properties of a material from ignition to flashover and also explains the smoke toxicity of a combustible material. The fire reaction properties that influence fire growth are the heat release rate, time to ignition, flame spread rate and oxygen index.

**The heat release rate (HRR)** is a quantitative measure of the amount of thermal energy released by a material per unit area when exposed to a fire radiating a constant heat flux (or temperature) and its unit is kW/m<sup>2</sup>. The heat release rate value of a composite material is determined by the thermal energy liberated in several thermo-chemical decomposition processes, with the most important being exothermic combustion at the composite/flame boundary of flammable gas products released by the decomposing polymer matrix and (if present) organic fibres. Two parameters describe the heat release rate: **average HRR and peak HRR**. The average heat release rate is the averaged value over a certain period of time (usually three or five minutes). The peak heat release rate is the maximum amount of heat liberated by a material during the combustion process, and it often occurs over a very short period of time (less than a few seconds). The peak heat release rate is considered a critical property controlling the maximum temperature and flame spread rate.

**Time to ignition (TTI)** is the period that a combustible material can withstand exposure to a constant radiant heat flux before igniting and undergoing sustained flaming combustion.

**Flame spread rate** describes the speed at which the flame front will travel over the surface of a combustible material. The flame spread rate is an experimentally measured value, and various experimental techniques with important differences in test configuration are used. Some tests are used to measure the rate of flame spread in a downward direction while other techniques measure it in a vertical or inclined direction. Consequently, the value for flame spread rate is test-dependent. **Oxygen index** is defined as the minimum oxygen content in the fire environment required to sustain flaming combustion of a material. Materials with high oxygen index values should be used in high fire risk applications, particularly for internal structures and components, because they offer the potential to self-extinguish when the fire becomes deprived of oxygen.

Two other important fire reaction properties are **smoke density** and **gas toxicity** because they have a major impact on the ability of humans to survive a fire. Smoke density is defined and measured in several ways, but basically it is the concentration of smoke particles (e.g. soot, water vapour) within the plume of a fire. Gas toxicity is a generic term that describes the concentration and lethality of gas products within the smoke plume.

While many fire reaction properties are important in the development of fire up to the point of flashover, the fire resistant properties are critical when the fire has fully developed.

**Fire resistance** defines the ability of a material or structure to impede the spread of fire and retain mechanical integrity. In other words, fire resistance describes the ability of a construction to prevent a fire from spreading from one room to neighbouring rooms. Fire resistance also describes the ability of a construction to retain structural integrity (ie. shape, load-bearing properties) in a fire. The main fire resistant properties are heat insulation, burn-through resistance, and structural integrity. **Heat insulation** is simply the resistive property that describes the rate of heat conduction through a material when exposed to fire. Obviously, materials that are good heat insulators are best suited for slowing the spread of fire from room-to-room, and this is one of the attributes of composites compared to metals. **Burn-through resistance** is the time taken for a flame to penetrate a material and emerge from the opposing side. Composites generally have better burn-through resistance than metals that melt at temperatures below the flame temperature, such as aluminium alloys. **Mechanical integrity** is another important fire resistant property, and this defines the ability of a material or structure to retain mechanical properties such as stiffness, creep resistance and strength when exposed to fire and after the fire has been extinguished. The behaviour of composites materials in fire is based by chemical and thermal decomposition of the matrix used. In figure 1.5 is showed the decomposition process of polymer

composites exposed to a heat flux radiated from a fire. When the material is exposed to a fire, the matrix decomposes to volatile gases, solid carbonaceous char and smoke. The volatiles consist of a variety of vapours and gases, both flammable as carbon monoxide, methane, low molecular organics and non flammable as carbon dioxide and water. The flammable volatiles extend from composites material into the flame zone where they react with oxygen and lead to the formation of the final combustion products accompanied by the liberation of heat.

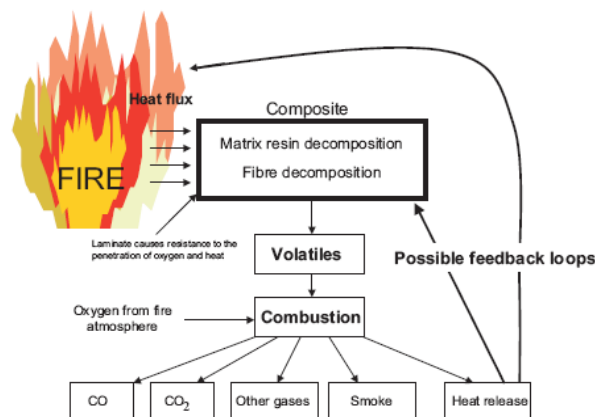


**Figure 1.5.** The decomposition mechanisms of composites materials.

Several analytical technique can be used to characterise the decomposition reactions and the chemical nature of the reaction volatiles of polymers. The three important technique are TGA, in which the weight loss is measured with increasing temperature or time; differential scanning calorimetry (DSC), in which heat absorption or evolution due to chemical changes of the polymer are measured; and gas chromatography/mass spectrometry (GC/MS), in which the chemical composition of the volatile gases are determined. Other methods may also be used, including thermal volatilisation analysis (TVA) and differential thermal analysis (DTA). It is often necessary to use a combination of methods to obtain a complete understanding of the decomposition reaction rate, reaction mechanisms, volatile gases and char yield.

## **1.2 Fire test for composites materials**

A large quantity of information is available on the fire reaction properties of polymer composites, and the level of fire hazard associated with their use is known for a large number of materials. We also have a good understanding of the chemical, thermal and physical mechanisms that control reaction properties such as time-to-ignition, heat release rate, flame spread rate, smoke production and toxicity.

In short, we have quite a good quantitative understanding of the fire reaction behavior of composites. Unfortunately, less is known about the fire resisting properties, such as burn-through resistance, dimensional stability and structural integrity, especially when the structure is under load. Moreover it is not usually possible to estimate the fire resistive behavior based solely on the known fire reaction properties. A composite that has good fire reaction properties, such as low heat release rate and smoke yield, may not necessarily have good fire resistive properties. Composites with a polymer matrix having high thermal stability, decomposition temperature and char yield may not necessarily have better fire resistive properties than more flammable materials.

The first fire test was developed in the early twentieth century, and over the last one hundred years a large number of tests have been used to characterise the fire properties of combustible materials. The number of tests available to characterise fire reaction is now immense. For example, the American Society for Testing and Materials (ASTM) have over 80 fire test standards in the 1999 edition of their handbooks on testing standards. The standards are applicable to a wide range of materials, including building products, woods, plastics and other combustible materials. None of the ASTM fire standards are specific to polymer composites, but are instead generic to a wide range of materials. The ASTM is one of many international standardisation organisations that publish fire test methods. Not all of the tests, of

course, are relevant for testing composites; many tests are only suitable for evaluating building materials, woods or some other type of combustible material. Only a relatively small number of tests are suitable for determining the fire properties of composite materials or structures.

Experimental techniques used to measure the fire properties of composites range in size from bench-top apparatus for testing small specimens weighing only a few grams up to full-scale tests for large structures.

Regardless of scale, it is important that fire reaction tests are performed in conditions that closely replicate the type of fire to which the composite will be exposed. These fires range in heat flux from low intensity fires where the radiant heat flux is under  $20 \text{ kW/m}^2$  to intense fires where the heat flux can exceed  $150 \text{ kW/m}^2$ .

The range of test methods for determining the fire reaction and fire resistive properties of composites is clearly very diverse, although some attempts are now being made to rationalize this situation. The tests vary in scale and complexity, and considerable care must be exercised when selecting the most appropriate procedure. Most fire reaction testing is performed using bench-scale apparatus because of the lower cost and greater simplicity. Test methods such as the cone calorimeter, OSU calorimeter and radiant flame spread technique have an excellent track record and are widely used for determining the fire behaviour of composites. However, the problem of scaling-up from small-scale test results to fire performance of large structures in real fires is a major difficulty.

Problems common to bench-scale tests are that the ignition, heating and atmospheric (oxygen content) conditions are not representative of an actual fire. The growth and spread of fire cannot be accurately replicated using these tests, and it is usually not possible to achieve flashover. Further, the specimens are rarely tested in the end-use condition.

Large-scale fire tests, such as the room calorimeter, avoid many of the problems associated with small size, and allow the composite article to be tested in the end-use condition. However, large fire tests are generally slow and expensive to perform and may only produce data relevant to one particular situation [4].

It is also important to recognise that no single test method is adequate to evaluate all the fire properties of a composite. Table 1.1 lists the properties that can be determined using the test methods. Of these, it is those methods capable of determining the heat release rate that are most important when characterising the fire reaction of composites. While a few methods have the capability to determine the heat release rate together with several other properties, it is necessary to use two or more methods to obtain a complete understanding of the fire behaviour of a composite material.

Test Method	Heat Release Rate	Ignition Time	Flame -Out Time	Heat of Combustion	Mass Loss Rate	Flame Spread	Smoke Density	Soot Yield	Gas Emissions
Cone calorimeter	✓	✓	✓	✓	✓		✓	✓	✓
OSU calorimeter	✓						✓		
Bomb calorimeter				✓					
LOI test		✓	✓						
Radiant panel flame spread		✓	✓			✓	✓		
NBS smoke chamber							✓		✓
NFPA 269 toxicity test									✓
Room calorimeter	✓	✓	✓			✓	✓		✓

**Table 1.1.** The decomposition Fire reaction properties measured using test methods

**References**

- [1] H.Ingason, Two dimensional rack storage fires, Proceedings of the Fourth International Symposium on Fire Safety Science, 1994,1209-1220.
- [2] K.S. Mudan and P.A. Croce, Fire hazard calculations for large open hydrocarbon fires, in SFPE Handbook of Fire Protection Engineering, ed. P.J. DiNenno et al., 1995, 2-13.
- [3] H. Inganson and J. de Ris, Flame heat transfer in storage geometries, Journal of Fire Safety, 1997.
- [4] Mouritz AP., Gibson AG. Fire Properties of Polymer Composite Materials. Springer

# **CHAPTER 2**

## **MATERIALS**

### **2.1 Thermosetting resin: RTM6**

Epoxy resins are used worldwide on a large scale for adhesive, lamination, coating, casting applications and contain a very large number of chemical types. All such resins rely on the reactivity of the three member epoxy group at both ends of the molecule. Other more complex types of epoxy resins are employed when a higher level of functionality is needed, ie. when a greater number of cross-linking points per epoxy group (fig.2.1) is required, as for instance in some of the higher performance resins used in aerospace. Traditionally, epoxy resins are cured by reacting them with amines or anhydrides; these materials being known as “hardeners”. There are also catalysts that will polymerise the resin via the end groups and hydroxyls without the need for a hardener.

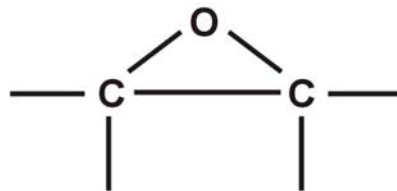


**Figure 2.1.** Epoxy group

Many epoxy resins and hardeners are viscous or even solid at room temperature and may require preheating or dilution to lower their viscosity prior to processing into composites. Further heating, sometimes to temperatures up to 150-180°C, is often needed to promote resin gelation and curing. Nevertheless, epoxies are used in all the traditional composite processes, including wet laminating, resin transfer moulding and filament winding. Decomposition of most epoxies occurs via random chain scission reactions over the temperature range of about 380 to 450°C.

HexFlow® RTM6, provided by Hexcel, is a premixed, monocomponent epoxy resin system, specially developed to fulfil the requirements of the aerospace and space industry in advanced resin transfer moulding processes (RTM). The expected service temperatures of final products range from -60°C to 180°C. At room temperature, RTM6 is a translucent paste and its viscosity drops very quickly upon heating. The uncured resin has a density of 1.117 g/cm<sup>3</sup> and the fully cured resin 1.141 g/cm<sup>3</sup>. When fully cured, it exhibits high glass transition temperatures, excellent hot/ wet properties and low moisture absorption. According to the manufacturer, the shelf life of this resin at 23°C is at least 15 days, whereas at -18°C it is approximately 9 months [1].

The main advantage of this epoxy resin called RTM6 is that it is a monocomponent system and is already degassed and its properties are reported in table 2.1.

<b>Epoxy resin RTM6</b>	
T <sub>g0</sub>	-11°C
T <sub>g∞</sub>	190°C
Density uncured resin (g/cm <sup>3</sup> )	1.11 at 25°C
Density cured resin (g/cm <sup>3</sup> )	1.14 at 25°C

**Table 2.1:** Properties of monocomponent epoxy resin

In figures 2.2 and 2.3 are reported the molecule from which RTM6 derives: carbon glycidyl diamino-diphenyl-methane (TGDMM) and the molecule-diamino-diphenyl sulfone (DDS), as agent crosslinker.

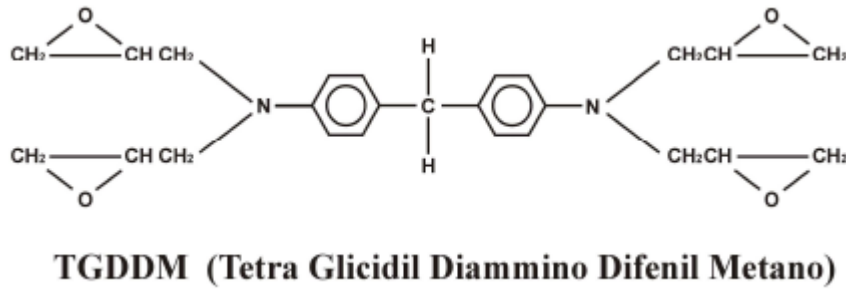


**Figure 2.2.** Formula of structure of TGDDM

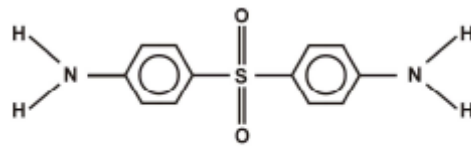


**Figure 2.3.** Formula of structure of DDS

### 2.1.1 Characterization of RTM6

To define the parameters of resin process a preliminary screening by a kinetic analysis by differential scanning calorimeter (DSC) is necessary to understand the mechanisms with which the molecules inside the composites are organized depending on the temperature variations. In figure 2.4 and 2.5 the kinetic analysis, dynamical and isothermal, of epoxy resin RTM6 neat are reported.

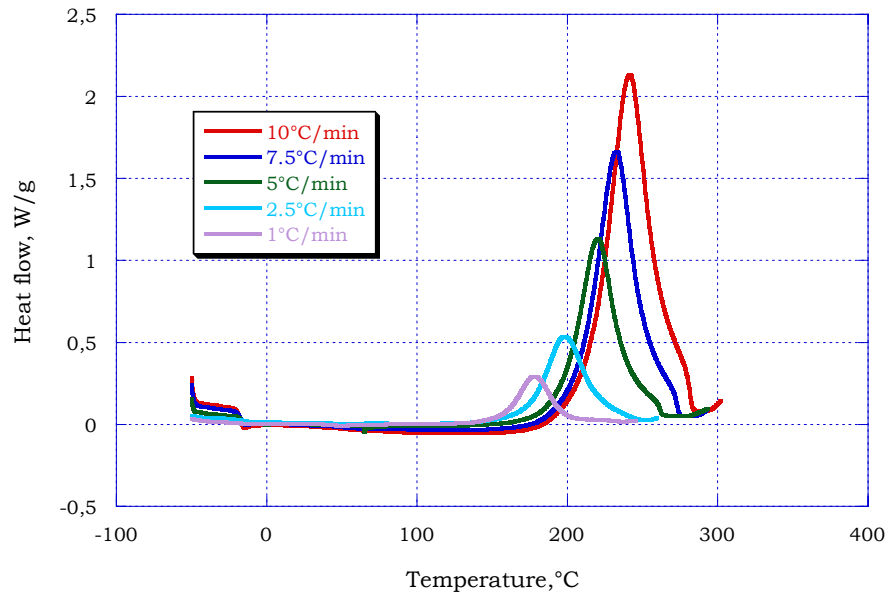


**Figure 2.4.** Dynamic analysis of RTM6 neat

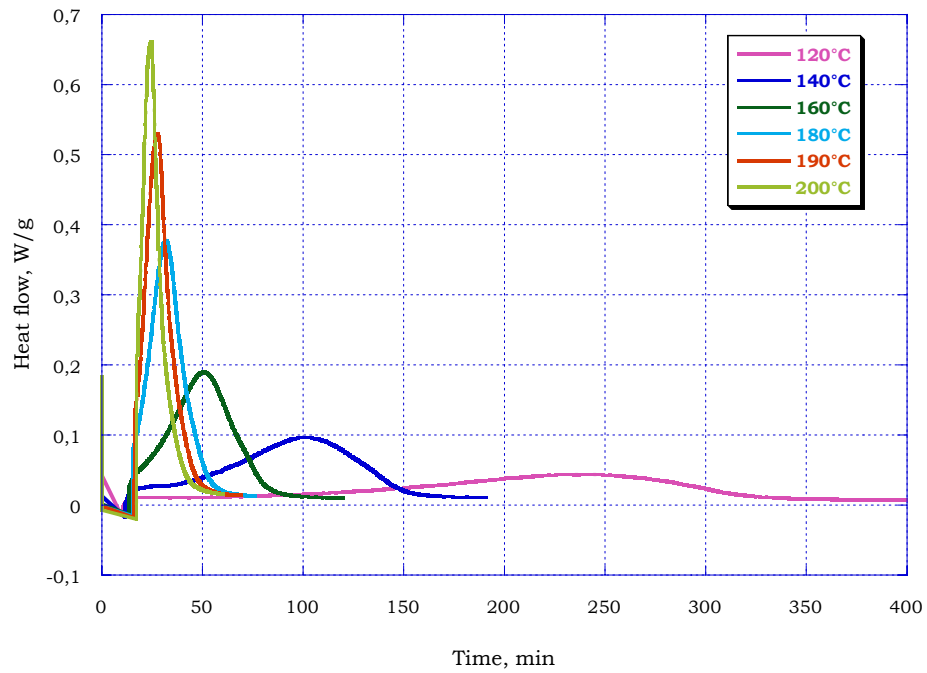


**Figure 2.5.** Dynamic analysis of RTM6 neat

The dynamical analysis (fig.2.4) show that the reticulation peak has a maximum at the temperature 241°C and a energy amounted to 470J/g. From the data of the isotherm analysis (fig.2.5) it is clear that curing for 90 minutes at 160°C results in a cross-linking of molecules equal to

83%. In addition, to obtain a complete cross-linking, there should be a next step of treatment at a temperature greater than 160°C, but that does not exceed the value of glass transition temperature of 196°C.

The choice of temperature for the second step of treatment was 180°C because the isothermal measure carried out this value of temperature is slow enough to allow the molecules to rearrange within the matrix partially cured before completing the reaction.

## **2.2 Micro materials: Introduction on flame retardants**

Flame retardation is a process by which the normal degradation or combustion of polymers is altered by addition of certain chemicals. Some plastics are inherently fire retardant or smoke retardant and their fire performance is acceptable for certain applications. However, [2] for many plastic materials, it is necessary to improve their fire performance by incorporating flame retardants.

Flame retardants are chemical agents which are added to combustible materials to make them more resistant to ignition and they are intended to minimise the risk of a fire starting in case the contact with a small heat source. Hence the term “flame retardants” describe a function and not a chemical class and their aim is to break the cycle of self-combustion of polymeric materials reducing the speed of chemical and physical process that develop. Often they are applied in combinations and this variety of products is necessary because the materials are very different in nature and composition.

Flame retardants interfere with combustion processes during a particular stage of this process, during heating, decomposition, ignition or flame spread and the amount of flame retardant one has to add to achieve the desired level of fire safety can range from less than one percent for highly effective flame retardants up to more than 50 percent for inorganic fillers, but typical ranges are 5 to 20 percent by weight.

Flame retardants acting by chemical and physical actions which are divided into:

- **Chemical action**

1. Reaction in the gas phase: The radical gas phase combustion process is interrupted by flame retardant, resulting in cooling of the system, reducing and eventually suppressing the supply of flammable gases.
2. Reaction in the solid phase (fig.2.6): The flame retardant builds up a char layer and shields the materials against oxygen and provides a barrier against the heat source (flame).

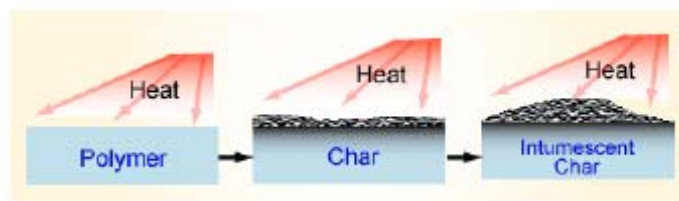


**Figure 2.6.** Reaction in the solid phase

- **Physical action** (fig.2.7)

1. Cooling: Energy absorbing (endothermic) processes triggered by additives and the chemical release of water cool the substrate of material to a temperature below that required for sustaining the combustion process.
2. Formation of a protective layer (coating): The material is protected with a solid or gaseous protective layer and protected from heat and oxygen necessary for the combustion process.
3. Dilution: Inert substances and additives evolving non-combustible gases dilute the fuel in the solid and gaseous phases.

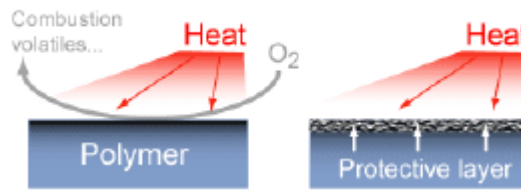


**Figure 2.7.** Physical action of flame retardant

Flame retardants can be placed into the polymer material or by reacting chemically with the polymer (reactive mode) or by mixing (additive mode) or in both modes. The choice of a flame retardant must be based on the knowledge its toxicity, action and its impact on environment. The main categories of flame retardants are based on compounds containing (fig 2.8):

1. Halogens (Bromine and Chlorine).
2. Phosphorus.
3. Nitrogen.
4. Inorganic compounds: Minerals (based on aluminium and magnesium).
5. Borates and Stannates.
6. Intumescent systems.

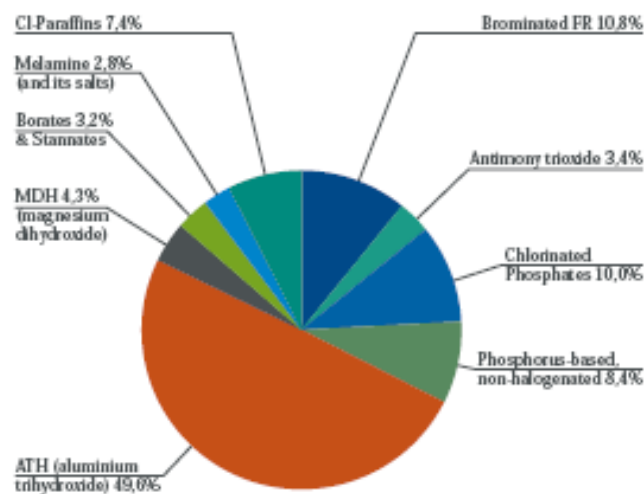


**Figure 2.8.** Classes of flame retardant

Flame retardants work in a number of different ways, in fact some flame retardant are effective on their own but other are used mainly as “synergists” acting to increase the effect of other types of flame retardants. Almost all flame retardants generate a stable carbonaceous barrier called “char” which protects and at the same time cools the surface of the material.

**Halogenated flame retardants**, when exposed to high temperatures release bromine (Br) or chlorine (Cl) as free radicals ( $\text{Br}^\cdot$  or  $\text{Cl}^\cdot$ ) which react with hydrocarbon molecules (flammable gases) to give HBr or HCl. These then react with the high-energy  $\text{H}^\cdot$  and  $\text{OH}^\cdot$  radicals to give water and the much lower energy  $\text{Br}^\cdot$  or  $\text{Cl}^\cdot$  radicals, which are then available to begin a new cycle of  $\text{H}^\cdot$  and  $\text{OH}^\cdot$  radical removal. They act by effectively removing the  $\text{H}^\cdot$  and  $\text{OH}^\cdot$  radicals in the gas flame phase thus reducing heat generation and so the production of further gaseous flammable materials.

**Phosphorus-containing flame retardants**, when heated, reacts to give a polymeric form of phosphoric acid. This acid crates a glass layer (char) on the surface of the material and inhibits the pyrolysis process which is necessary to feed flames. Char plays an important role in fact it acts as a two-way barrier that both prevents the passage of the combustible gases and shields the polymer from the heat of the flame.

A wide range of different phosphorus based flame retardants is available, including elemental red phosphorus, which is oxidised to phosphoric acid with heat, ammonium polyphosphate, melamine polyphosphate, phosphonates, phosphinates and phosphate esters.

**Nitrogen-containing flame retardant** (pure melamine and derivates) are believed to act by several mechanisms. In fact, in the condensed phase, melamine is transformed into cross-linked structures which promotes char formation releasing ammonia. In conjunction with phosphorus, the nitrogen appears to enhance the attachment of the phosphorus to the polymer. A mechanism in the gas phase may be the

release of molecular nitrogen which dilutes the volatile polymer decomposition products.

**Antimony trioxide** does not have flame retarding properties of its own, but is an effective synergist for halogenated flame retardants. It acts as a catalyst, facilitating the breakdown of halogenated flame retardants into active molecules. It also reacts with the halogens to produce volatile antimony halogen compounds, which are themselves directly effective in removing the high energy H<sup>+</sup> and OH<sup>-</sup> radicals which feed the flame phase of the fire, thus reinforcing the flame suppressing effect of the halogenated flame retardants. When added to PVC, antimony trioxide acts to suppress flames by activating the chlorine present in the plastic itself.

**Inorganic compounds** are used as flame retardants interfering through various physical processes with the burning process: release of water or non-flammable gases which dilute the gases feeding flames, absorption of heat energy thus cooling the fire, production of a non-flammable and resistant layer on the surface of material (char). These mechanisms of inorganic compounds are however of a relatively low efficiency and the products have to often be used in large concentrations, or more usually, in combination with other types of flame retardants.

**Boron containing compounds** act through the stepwise release of water and the formation of a glassy coating protecting the surface. Zinc borate, in halogen-free systems, is normally used in conjunction with aluminium trihydrate, magnesium hydroxide or red phosphorus. Zinc stannate and zinc hydroxystannate are used to reduce smoke emission from PVC, to promote charring or as synergists to increase the effectiveness of halogenated or nitrogen flame retardants.

Finally **intumescent coatings** are fire protection systems which are used to protect materials such as wood or plastic from fire but also to protect steel and other materials from the high temperatures of fire. The coatings are made of a combination of products, applied to the surface

like a paint, which are designed to expand to form an insulating and fire-resistant covering when subject to heat.

### 2.2.1 Zinc Borate

Zinc borate ZB ( $2\text{ZnO} \cdot 3\text{B}_2\text{O}_3 \cdot 3.5\text{H}_2\text{O}$ ) is a multifunctional flame retardant which can function as a flame retardant in synergy with halogen, smoke suppressant because promote char formation and afterglow suppressant. It is a synergist of chlorine and bromine-containing flame retardants or polymers. Its efficacy depends on the type of halogen source (aliphatic versus aromatic) and the base polymer used. The zinc borate can generally display synergistic effects with antimony oxide in fire retardancy. This synergy [3] can be more remarkable when used in conjunction with aluminium trihydrate (ATH) or magnesium hydroxide (MDH).

Zinc borate decomposition has been studied by thermogravimetric analyses TGA reported in figure 2.9 and its decomposition temperature is about  $436^\circ\text{C}$ .

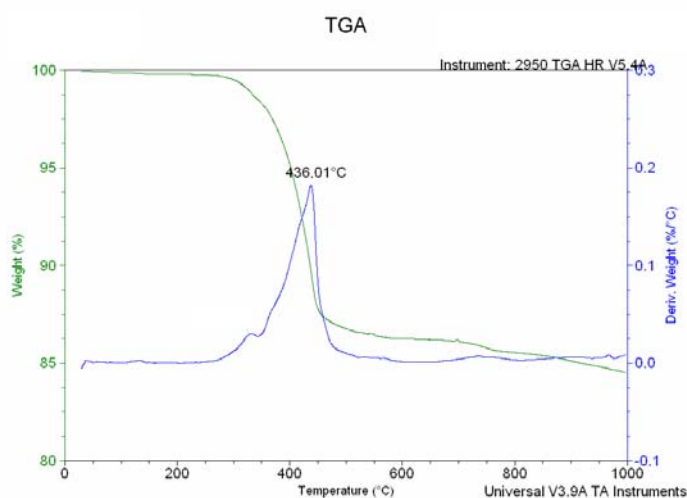


**Figure 2.9.** TGA and DTG in nitrogen of zinc borate

Zinc borate works as an antitracking agent in both halogen-containing and halogen-free polymers in different ways.

In halogen-containing polymers:

- Zinc borate possesses a synergistic effect with halogen sources.
- Zinc borate display synergistic effects with antimony oxide in fire retardancy. In the presence of ATH or MDH, this synergy can be augmented significantly.
- In some polymer systems, zinc borate can completely replace antimony oxide.
- In contrast to antimony oxide, zinc borate is predominant in the condensed phase and can work as a smoke suppressant.
- Zinc borate promotes char formation and prevents burning drips. The zinc oxide moiety can promote char formation with halogen sources and  $B_2O_3$  moiety can stabilize the char.
- Zinc borate can improve the thermal stability of polyamides containing halogen/antimony trioxide and improve the aged elongation property of polyolefin.
- Improves corrosion resistance.

In halogen-free polymers:

- Zinc borate are multifunctional fire retardants in halogen-free polymers.
- When used in combination with metal hydroxides, zinc borate can work as a sintering aid to promote the formation of a strong char/ceramic residue that can act as an insulator for underlying polymer.
- Zinc borate can reduce the heat release rate, smoke evolution, carbon monoxide generation, and afterglow combustion.
- The use of a co-additive such as the silicone/silica, melamine polyphosphate, talc, or red phosphorous can increase the fire test performance of zinc borate/metal hydroxide combination.
- Zinc borate alone can work as a flame retardant in certain halogen-free systems.

Zinc borate used is produced by Joseph Storey & Company LTD and its name is Storflam ZB 2335 and its physical and chemical properties are reported in table 2.2 [4].

<b>Zinc Borate ZB</b>	
Appearance	Power dust
Colour	White
Molecular weight	434.64
Bulk density (Kg/m <sup>3</sup> )	400-700
Soluble in	Acids and Bases
Solubility value (g/100g H <sub>2</sub> O/20°C)	<1%
pH	7-8 (aqueous filtrate of 20% suspension)

**Table 2.2:**Physical and chemical properties of zinc borate

### 2.2.2 Aluminium trihydrate

Aluminium trihydrate ATH ( $2\text{Al}(\text{OH})_3$ ) is the most widely used flame retardant. It is an inert mineral filler, a non-toxic, white, crystalline powder and is included in the inorganic flame retardants. It acts with all three of mechanisms indicated in the figure 2.10. At around 300°C (fig.2.11), it is decomposed to aluminium oxide which forms a protective, non-flammable layer on the material surface and water.

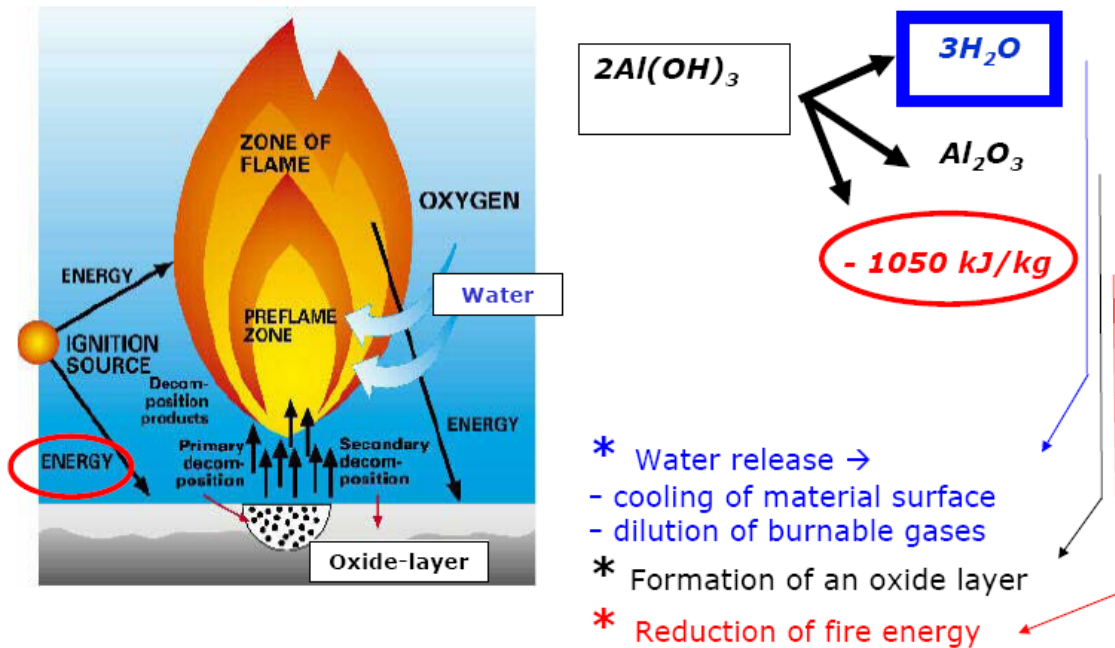


**Figure 2.10.** Mechanism of Aluminium trihydrate ATH

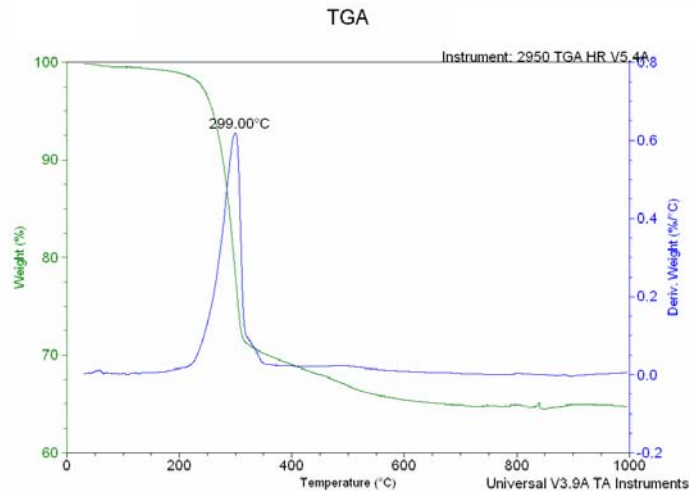


**Figure 2.11.** TGA and DTG in nitrogen of aluminium trihydrate

Water forms a layer of non-flammable gas near the material's surface, inhibiting flames. The reaction is endothermic, it absorbs heat, thus cooling the material and slowing burning. The water vapour produced during ATH decomposition dilutes both the combustible gases and oxygen in the vicinity of the flame, making combustion more difficult. For smoke suppression the heat dissipation by the ATH is thought to

aid in forming char rather than forming smoke by favouring crosslinking reactions over soot formation. The char provides a fuel-oxygen barrier on the surface of the burning polymer.

Aluminium trihydrate used in this work is produced by Dadco and provided by Joseph Storey & Company LTD [4] and its physical and chemical properties are reported in table 2.3.

<b>Aluminium trihydrate ATH</b>	
L.O.I. (110°C-1.100°C) (%)	34.6
Specific gravity (g/cm <sup>3</sup> )	2.4
Whiteness (%)	> 91
Bulk density (Kg/m <sup>3</sup> )	500-700
Medium grain size diameter (µm)	4.0-7.5
Boiling point (°C)	2700 (Al <sub>2</sub> O <sub>3</sub> decomposition product)
Density at 20°C (g/ml)	2.42

**Table 2.3:** Physical and chemical properties of aluminium trihydrate

### 2.2.3 Zinc Hydroxystannate

Zinc hydroxystannate ZHS (ZnSn(OH)<sub>6</sub>) is a fire retardant and a smoke suppressant additive for polymeric materials [5]. It was developed as a smoke suppressant for PVC but later it was found that it also acts as a flame retardant in certain plastics mainly by promoting char formation and can usually partly substitute antimony trioxide. Recent studies to develop flame retardants formation have used inorganic tin compounds such as zinc hydroxystannate because it is less toxic [2]. The physical and chemical properties of ZHS are reported in table 2.4 and it is provided by Joseph Storey & Company LTD [4] and its decomposition temperature (225°C) is reported in figure 2.12

<b>Zinc Hydroxystannate</b>	
Physical state	Power
Colour	White
Bulk density (Kg/m <sup>3</sup> )	400-500
Soluble in	Strong Acids and Bases
Solubility in water (% in weight)	0.003%
pH	7

**Table 2.4:**Physical and chemical properties of zinc hydroxystannate

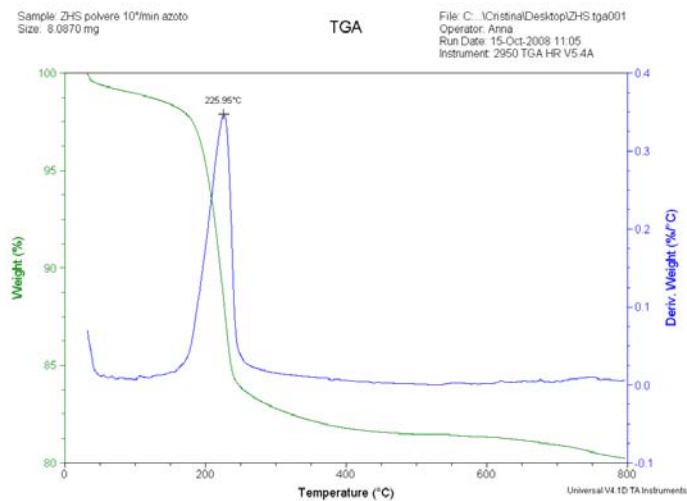


**Figure 2.12.** TGA and DTG in nitrogen of zinc hydroxystannate

#### 2.2.4 Zinc Stannate

Zinc stannate ZS ( $\text{ZnSnO}_3$ ) has excellent flame retardant and smoke suppressant properties and its advantage, as zinc hydroxystannate, is that it is less toxic than antimony compounds. In fact ZS and ZHS are used instead of antimony trioxide because they are less toxic [6]. Zinc stannate, as zinc hydroxystannate, is provided by Joseph Storey & Company LTD [4] and its properties are listed in table 2.5 and in figure 2.13.

<b>Zinc Stannate</b>	
Appearance	Power dust
Colour	White
Bulk density (Kg/m <sup>3</sup> )	400-500
Soluble in	Strong Acids and Bases
Solubility value (g/100g H <sub>2</sub> O/20°C)	0.003%
pH	7
Molecular weight	232.07

**Table 2.5:**Physical and chemical properties of zinc stannate

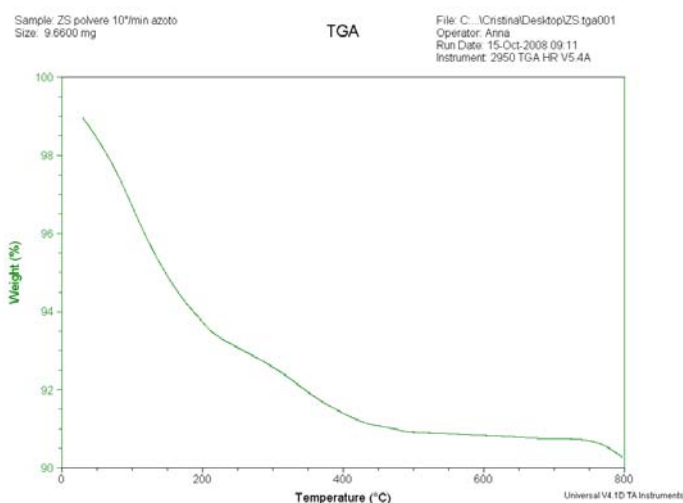


**Figure 2.13.** TGA in nitrogen of zinc hydroxystannate

Zinc hydroxystannate shows several degradation steps and different decomposition temperatures hence its DTG is not reported.

### 2.3 Nano materials: Introduction on carbon nanotubes

The discovery of carbon nanotubes can be traced back to the origin of fullerene chemistry (buckyball, C<sub>60</sub>) in 1985 [7]. Fullerenes have provided an exciting new insight into carbon nanostructures built from sp<sup>2</sup> carbon units based on geometric architectures. In 1991, Iijima [8]

discovered carbon nanotubes (CNTs) that are elongated fullerenes where the walls of the tubes are hexagonal carbon and often capped at each end. The nanotube is typically closed at each end by hemispherical caps that are constituted by at least 12 pentagons. According to the Euler theorem [9], which relates the number of vertices, edges and faces, a convex structure can be created by introducing a positive curvature and, therefore, pentagons to close up the hexagonal lattice of the tube (fig.2.14).

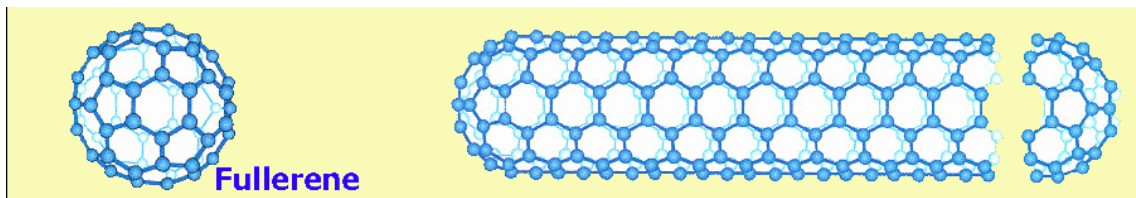


**Figure 2.14.** Schematic of the nanotube formation

Due to the hexagonal symmetry of the carbon atoms in the graphitic sheet, different structural isomers are possible depending on how the planar graphite sheet is folded. The rolling up can be accomplished in several different ways requiring only the matching of the dangling bonds at each end. However, the nanotubes can present a different helicity degree with respect to the tube axis. Figure 2.15 shows the three different possible nanotubes: armchair, zig zag and chiral.

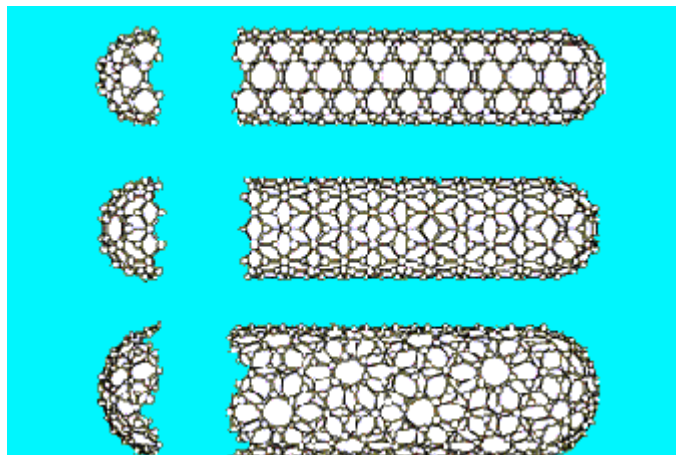


**Figure 2.15.** Schematic of the three different nanotubes structure

The characteristic of helicity in nanotubes has a great relevance affecting the physical properties that depend also on the tube diameter [10]. For example, it has been shown that all the armchair tubes are metallic whereas the zig zag and chiral tubes are either metallic or semiconducting.

The nanotubes can exist in two forms: multi-walled and single-layer (fig.2.16). The multi-wall carbon nanotubes were the first to be discovered. They consist of concentric cylinders placed around a common central hollow area with a constant separation between the layers close to the graphite interlayer spacing (0.34 nm). Each individual cylinder can be characterized by a different helicity and has diameter ranging from 2 to 25 nm and length of several microns.

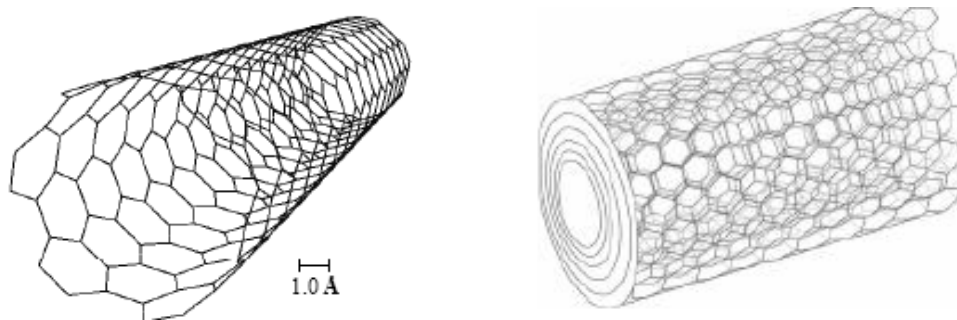


**Figure 2.16.** Single walled and multi walled carbon nanotubes

The single walled nanotubes were synthesized in 1993 when it was found that the addition of metals such as cobalt to the graphite electrodes in the arc evaporation method resulted in tubes with single layer walls [11]. A single walled nanotube is close to an ideal fullerene fiber and consists of a single layer cylinder extending from end to end with a narrow distribution in diameter range (1-2 nm). When produced in vapour phase, the single wall nanotube can self-assemble into larger bundles, called ropes consisting of several tens of nanotubes arranged in a one-dimensional triangular lattice. It is important to observe that the discovery of single wall tubes has been very significant allowing

researchers to verify and test some of the theoretical predictions about the nanotube properties.

Due to the combination of size, structure and topology, the nanotubes display remarkable features. In particular, the graphitic nature of the nanotube lattice contributes to provide high conductivity, high strength and stiffness, chemical specificity and inertness, while the lattice helicity and elasticity provide optimal electronic properties. Further, the nanoscale size and the high aspect ratio are advantageous for many applications that require large surface area to volume ratio. However, due to their very small size and often presence of defects, mechanical property characterization is a challenge. Nevertheless, it is possible to imagine that their stiffness and strength are very high if one uses graphite as reference. The in-plane elastic modulus of graphite is estimated to be 1.06 TPa ( $1.06 \times 10^{12}$  Pa) and the tensile stiffness as 0.8 TPa, due to the very strong covalent C-C bonds in the plane [10].

The elastic properties evaluation of carbon nanotube has been performed by:

- measuring their thermal vibration amplitudes;
- atomic force microscopy measurement during bending.

The first technique provided the Young's modulus equal to 1.8 TPa, while a modulus close to 1 TPa has been determined by the second method. Further, the maximum tensile strength has been determined close to 30 GPa ( $30 \times 10^9$  Pa) [8]. Many other observations have shown that carbon nanotubes have other intriguing properties such as:

- high flexibility, related to the ability of the carbon atoms to rehybridize with the degree of rehybridization depending on the strain;
- high capability to sustain strain in tension (40%) without brittleness, plastic deformation or bond rupture.

These features make the carbon nanotubes ideal candidates for reinforcing fibers in polymer-based composites. In particular, due to

their ability to sustain high deformations, they have a significant advantage over carbon fibers in composites for structural and strength applications. However, the effective reinforcement action due to the nanotubes hinges on the success of the preparation techniques and stable dispersion of the nanotubes in the polymer matrix. In most cases, since the nanotubes have many entanglements, it is a challenge and an unresolved issue to disperse them effectively with polymer systems to make strong and stiff components.

Carbon nanotubes have extraordinary properties that have attracted the attention of several researchers from diverse fields. Substantial effort has been devoted to the experimental evaluation and theoretical calculation of their physical, electronic, magnetic, electrical and mechanical properties.

Because of their promising physical and mechanical properties, the most common commercial application of carbon nanotubes is based on their use as filler elements for metals, ceramic or polymers matrix. In particular, carbon nanotubes may exhibit characteristics that can be beneficial. For example, they can be used as

- reinforcement of polymer based composite materials which improve structural properties;
- polymer modifiers for high temperature uses;
- conductive filler in insulating polymer matrices to provide electrostatic discharge and electromagnetic-radio frequency interference protection;
- doping of conjugated luminescent polymers to produce active materials for electronic applications.

The use of carbon nanotubes as reinforcing systems of polymer matrix would offer several advantages over the conventional reinforcements including continuous and short fibers (glass, carbon). In the case of continuous fibers reinforcements, the advanced composite material has much higher mechanical properties in the direction parallel to the fibers

or in the plane of the lamina than in the transverse direction. Furthermore, since the conventional polymer processing equipment cannot process the long continuous fibers, their use is limited to simple shapes and limited production. On the other hand, it's established that the fiber aspect ratio represents the critical factor affecting the resulting structural properties of short fiber composites. As the aspect ratio increases, the composite stiffness and strength increase. However, the packing of short fibers in a polymer matrix is a percolation phenomenon, so the maximum packing decreases with increasing aspect ratio (see figure 16) and may not be sufficient to manufacture a very strong material [12].

Dispersion process of carbon nanotubes represents a very complex phenomenon due to their natural tendency to bundle together due to van der Waals interactions. A non uniform dispersion can lead to many defect sites and reach resin area limiting not only the efficiency of CNTs as reinforcement filler for the polymer composite matrix [13-18]. A good dispersion and possibly, the alignment of CNTs within a matrix is still a challenge and it could play the main factor driving the diffusion of CNT or MWCNT as nano-reinforcement on industrial scale [17,18] in fact are used several dispersion technique to separate the agglomerates into individual nanotubes.

Carbon nanotubes are another candidate as a FR additive because of their highly elongated shape (high aspect ratio). The in situ formation of a continuous, network structured protective layer from the tubes is critical for significant reduction in heat release rate, because the layer thus acts as a thermal shield from energy feedback from the flame [19].

### **2.3.1 Multi walled carbon nanotubes: Nanocyl 7000**

The multi walled carbon nanotubes used in this work are provided by Nanocyl S.A. (Belgium) and are denominated Nanocyl 7000. This multi walled carbon nanotubes are produced via the catalytic carbon vapour deposition (ccvd) process. Nanotubes exit the reactor with a purity of

90% carbon to produce the 7000 grade [20]. Its properties are reported in table 2.6.

<b>Multi-walled carbon nanotubes (MWNTs)</b>	
Average diameter	10 nm
Length	0.1-10 $\mu\text{m}$
Carbon Purity	90%

**Table 2.6:** Properties of MWNT

## References

- [1] [www.hexcel.com/...../HexFlowRTM6.pdf](http://www.hexcel.com/...../HexFlowRTM6.pdf).
- [2] Petsom A., Roengsumran S., Ariyaphattanakul A., Sangvanich P. *Polym. Degrad. Stab.* 2003,(80):17-22.
- [3] Shen KK., Kochesfahani S., Jouffret F. *Polym.Adv.Technol.* 2008, (19):469-474.
- [4] Data sheet provided by Joseph Storey & Company LTD.
- [5] Hornsby PR., Cusack PA., Cross M., Toth A., Zelei B., Marosi G. *Journal of materials science* 2003, (38):2893-2899.
- [6] Cusack PA., Heer MS., Monk AW. *Polymer Degradation and Stability* 1997, (58):229-237.
- [7] Kroto HW., Heath JR., O'Brien SC., Curl RF., Smalley RE. *Nature* 1985, 318: 162.
- [8] Iijima S. *Nature* 1991, 354: 56.
- [9] Ebbesen WT. *Physics Today* 1996, 26-32.
- [10] Ajayan PM. *Chem. Rev.* 1999, (99):1787-1799
- [11] Ebbesen WT. *CRC* 1997.
- [12] Calvert P. *Nature* 1999, (399):210-211.
- [13] Qian D., Dickey EC., Andrews R., Rantell T. *Appl. Phys. Lett.* 2000; 76 (20):2868-2870.
- [14] Park C. et al. *Chemical Physical Letters* 2002, (364):303-308.
- [15] Ham HT., Choi YS., Chung JI. *Journal of Col. and Inter. Science* 2005, 286 (1):216-223.
- [16] Salvétat JP., Briggs AD., Bonard JM., Bacsá RR., Kulik AJ., Stockli T., Burnham NA., Forró L. *Phys. Rev. Lett.* 1999, 82 (5):944-947.
- [17] Jin L., Bower C., Zhou O. *Appl. Phys. Lett.* 1998, 73 (9):1197-1199.
- [18] Choi ES., Brooks JS., Eaton DL., Al-Haik MS., Hussaini MY., Garmestani H., Li D., Dahmen KJ. *Appl. Phys.* 2003, (94):5451-5473.
- [19] Kashiwagi T., Du F., Winey KI., Groth KM., Shields JR., Bellayer SP., Kim H., Douglas JF. *Polymer* 2005, (46):471-481.
- [20] Data sheet provided by Nanocyl S.A.

# **CHAPTER 3**

## **EXPERIMENTAL TECHNIQUES**

### **3.1 Methods**

#### **3.1.1 Micro particles: Mechanical stirring**

The flame retardant composites were prepared by mixing the epoxy resin RTM6 with zinc borate, aluminium trihydrate, zinc stannate and zinc hydroxystannate at different percentage (5 wt%, 10 wt%, 20 wt%, 30 wt%, 40 wt%). The mixing was made by using a Heidolph RZR mechanical stirring equipment (fig. 3.1). The additives were included into the matrix at 400 rpm to avoid disperse the additive on the walls of beaker [1].

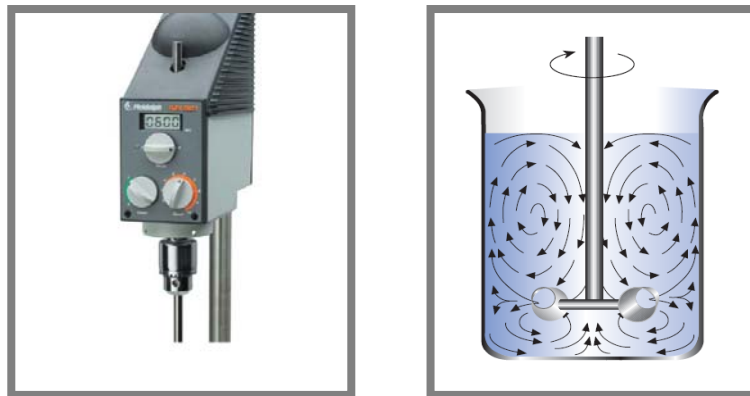


**Figure 3.1.** Heidolph RZR mechanical stirring

Afterwards the mixing was continued for 10 minutes at 1050 rpm and 10 minutes at 2000 rpm and then the mixture were degassed for 30 minutes at 90°C in a vacuum oven to eliminate entrapped air and humidity. Finally the liquid system was poured in mould and cured at 160°C and 180°C respectively for 90 mins and 120 mins, according to the curing schedule sheet of the neat epoxy resin.

The quality of dispersion of all additives into the epoxy resin after the mixing process was observed by Scanning Electron Microscope (1450VP LEO).

For example the SEM micrograph of zinc borate 20 wt% is reported where the dust of zinc borate (fig. 3.2) is well dispersed into the epoxy matrix and it maintains its original grain size. Analogous behaviour is noticed for the aluminium trihydrate, zinc stannate and zinc hydroxystannate (fig. 3.3)

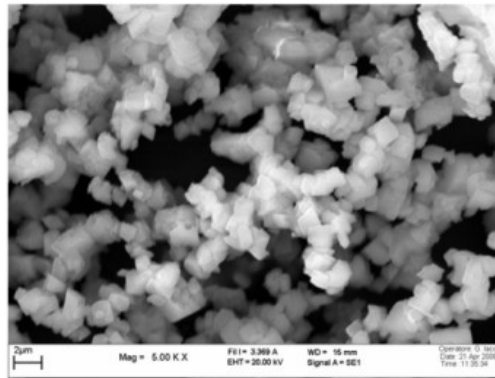


**Figure 3.2.** Scanning electron micrograph of zinc borate dust

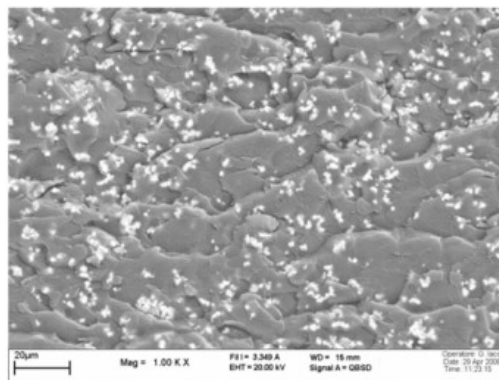


**Figure 3.3.** Scanning electron micrograph of the composite of RTM6 and ZB 20wt%

### 3.1.2 Nano particles: Sonication

The nanocomposites were prepared by using sonication process (fig. 3.4) for a constant time (1 hour) at temperature of 120°C with the

MWNTs content of 0.1 % fraction by weight. We selected this process and this percentage of carbon nanotubes by previous studies and experimental analysis that we conducted [2]. All the obtained samples were then degassed in vacuum oven at 90°C for 30 min, and then cured considering an identical temperature cycle (1 h at 160°C followed by 2 h at 180°C) according to the specified curing schedule.



**Figure 3.4.** Misonix Sonicator S3000

The SEM micrograph of fracture surface of multi walled carbon nanotubes into the epoxy resin was obtained by fragile failure of nitrogen cooled samples and this surface is reported in figure 3.5 at different level of magnitude.

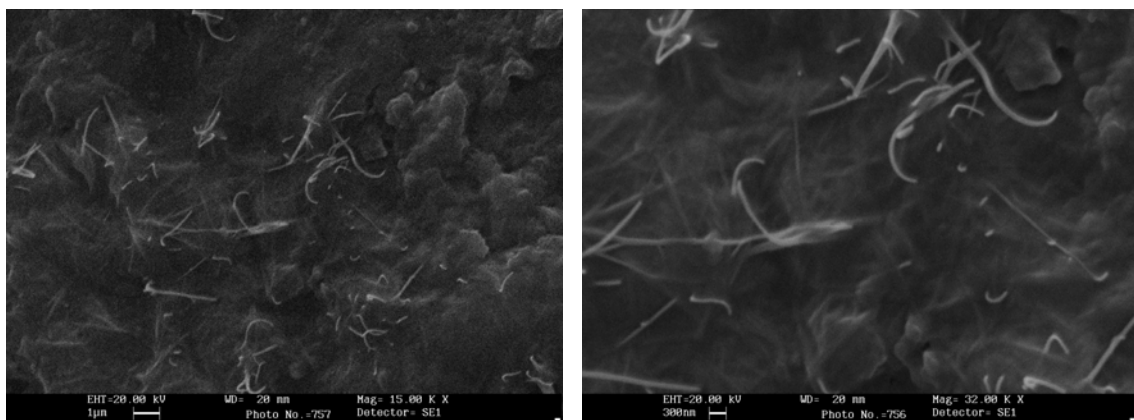


**Figure 3.5.** SEM images of fracture surface of specimen taken at different magnitudes (1 µm-300 nm)

The nanotubes, reported in figure 3.5, are present and well separated each other, showing a good level of adhesion with the matrix, in fact it appears a satisfactory uniformity of single or agglomerated of nanotube.

### **3.1.3 Vacuum infusion process**

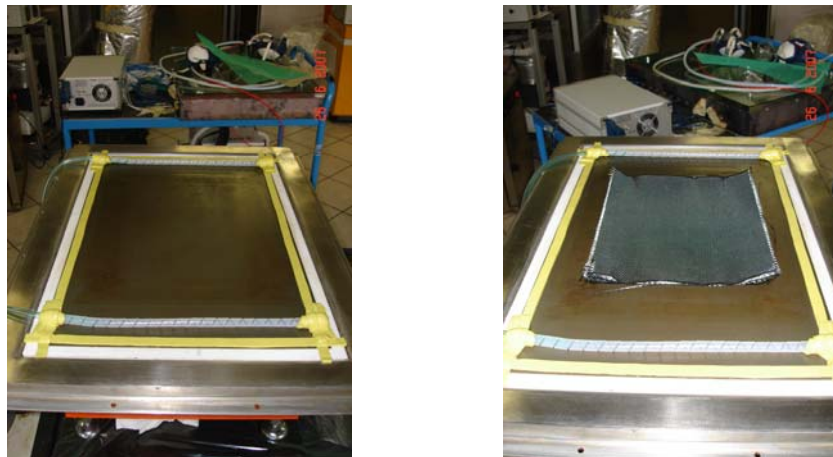
The vacuum infusion process (VIP) is a technique that uses vacuum pressure to drive resin into a laminate. Materials are laid dry into the mould and the vacuum is applied before resin is introduced. Once a complete vacuum is achieved, resin is literally sucked into the laminate via carefully placed tubing. This process is aided by an assortment of supplies and materials. Vacuum infusion provides a number of improvements over traditionally vacuum bagged parts. These benefits include:

- Better fiber-to-resin ratio
- Less wasted resin
- Very consistent resin usage
- Unlimited set-up time
- Cleaner

The samples were obtained by a preform of 8 plies of overlaid unidirectional carbon fibres at zero degrees. We chose 20x20cm samples.

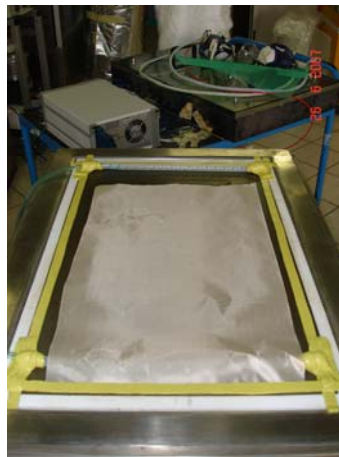
Operations to prepare the samples are:

1. Cleaning mould with acetone;
2. Application of realising agent to make the mould hydrophobic. The realising agent used in this work is LOCTITE® FREWAX FREKOTE® and adheres to the surface of the mould, creating a barrier between materials and mould;
3. Application of sealing tape GS AT200Y. This tape is softened by temperature so to enable the perfect adherence of the bag to the plate while maintaining the vacuum (figs. 3.6a)-b))



**Figures 3.6.** Application of sealing tape a) and position of carbon plies b)

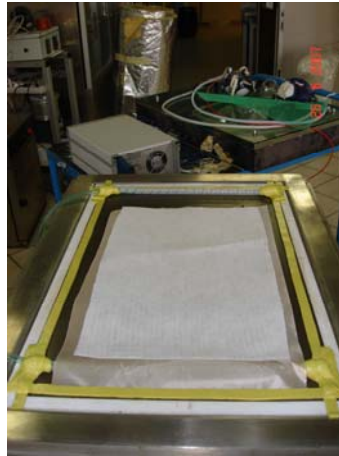
4. Application of “peel ply” under and over the carbon fibres plies to avoid damage to the composite surface in the successive phases (fig. 3.7). The peel ply used in this work is RELEASE EASE 234TFP and it is provided by Airtech. It is also placed on the aspiration pipe because it allows to keep the vacuum.



**Figures 3.7.** Application of “peel ply”

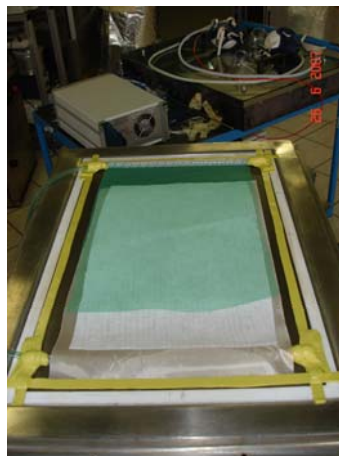
5. Application of “breather and bleeder” provided by Airtech. It is the AIRWEAVE® Super and it is useful to ensure the vacuum distribution. When the panels of epoxy resin are micro and nano additived, the breather/bleeder is placed only beside the carbon

fibres plies because it doesn't absorb the additives but it guarantees the vacuum distribution (fig. 3.8).



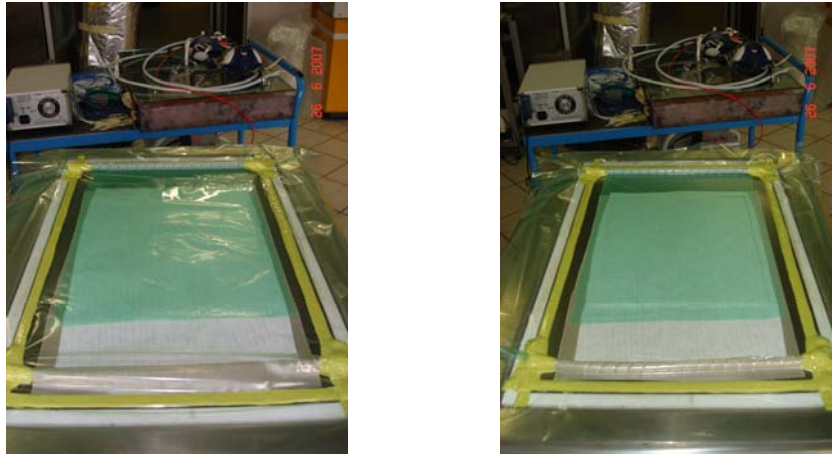
**Figures 3.8.** Application of “breather/bleeder”

6. Application of “network” (fig 3.9) to facilitate the advancement of the resin flow in the mould.



**Figures 3.9.** Application of “network”

7. Application of a vacuum bag (figs. 3.10a)-b)) that is sealed by sealing tape.



**Figures 3.10.** Application of vacuum bag a) and creation of vacuum b)

At the end, the vacuum is applied and a compaction of the different layers is obtained (fig. 3.10b)) and the breather allows the vacuum to spread throughout the mould.

## **3.2 Characterization**

### **3.2.1 Cone Calorimeter**

The cone calorimeter has become one of the most important and widely used instruments for the research and development of fire retarded polymeric materials. The cone calorimeter is a performance-based bench scale fire testing apparatus [3-7].

The cone calorimeter provides comprehensive insight into not only fire risks such as heat release rate, total heat release, and time to ignition, but also fire hazards such as smoke release and CO production. Cone calorimeter investigations can be used as a universal approach to ranking and comparing the fire behaviour of materials.

However, each experimental setup defines a specific fire scenario. As is typical for all fire tests, samples' performance in the cone calorimeter depends on the specific characteristics of the test, including ignition source, ventilation, irradiance (external heat flux), temperature, and the geometry of the specimen.

The cone calorimeter test characterizes the performance resulting from an interaction of material properties, specimen, and the defined fire scenario.

Lower external heat fluxes such as below  $20 \text{ kW/m}^2$  target ignition and flammability, whereas higher external heat flux such as  $50 \text{ kW/m}^2$  target flame spread and combustion properties. The relevant and active mechanisms can change significantly. Hence, the external heat flux influences the conclusions implied by the cone calorimeter studies. The frequently used irradiances of  $35 \text{ kW/m}^2$  or even  $50 \text{ kW/m}^2$  deliver reproducible results for forced flaming conditions with respect to flame spread and combustion properties (fig. 3.11).

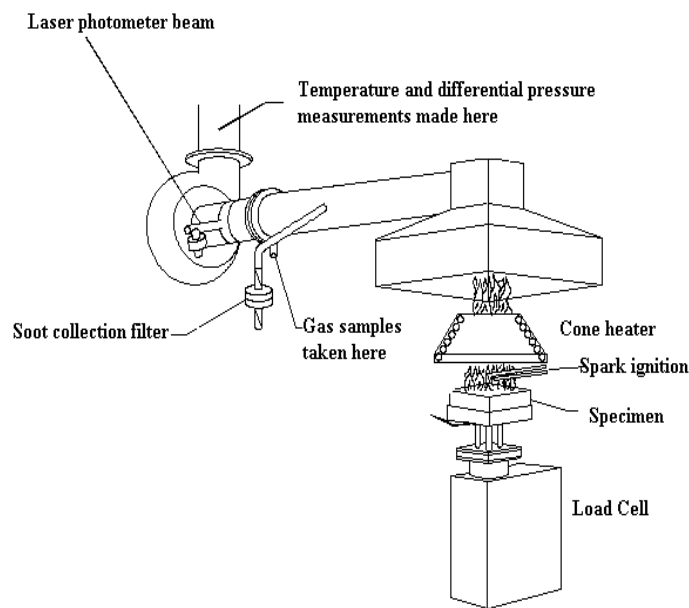


**Figure 3.11.** Schematic diagram of the cone calorimeter

The main capability of the instrument is that the heat release response of a burning material can be measured continuously to a high degree of accuracy and values for peak and average heat release rate can be determined. The technique can also be used to measure time to ignition, time of sustained flaming, effective heat of combustion, smoke density, soot yield, mass loss rate, and yield of  $\text{CO}$ ,  $\text{CO}_2$  and other combustion

gases. The only fire reaction property that cannot be directly determined is the flame spread rate.

Specimens tested within the cone calorimeter are flat plates that are 100mm long, 100mm wide and up to 50mm thick. The specimen is placed inside a sample holder lined with a low-density refractory material to minimise heat losses from the unexposed face. It is also necessary to insulate the specimen sides to minimise edge burning, which can give an artificially high heat release rate. The sides of composite specimens should also be sealed and insulated to avoid the escape of volatile gases from the edges, which can also affect the fire reaction properties. During fire testing the mass loss of the specimen is recorded continuously using a load cell located beneath the sample holder.

The top surface of the specimen is positioned 25mm from the cone heater (fig.3.12).



**Figure 3.12.** Positioning of the sample

A spark igniter may be placed mid-way between the sample and heater, and is used to ignite combustible gases released from the thermally decomposing material when the concentration reaches the critical level needed to sustain flaming. Most fire tests on composites are performed

using the igniters, although it is possible not to use the igniters to study the effect of auto-ignition on the reaction properties.

During fire testing (fig.3.13) a constant flow rate of air at 24 litres per second is maintained in the heating chamber.

This air flow rate is needed to force all the gaseous combustion products released by the burning specimen up through the orifice of the cone heater and into the gas exhaust system above the heating chamber. As the entrained air and combustion products enter the exhaust system they are thoroughly mixed to avoid stratification of the gases that can cause inaccurate heat release, smoke or toxic gas measurements.



**Figure 3.13.** Burning of sample

In this work the combustion tests [8], according to ASTM E 1354-04, are carried out with irradiance of  $50 \text{ kW/m}^2$  for samples of a thickness between 6-8mm and size  $100 \times 100 \text{ mm}$  using the cone calorimeter produced by Fire Testing Technology Ltd (fig. 3.14).



**Figure 3.14.** Cone calorimeter provided by Fire Testing Technology Ltd.

The information provided by cone calorimeter are:

- Time to ignition (TTI): which corresponds to the period that a combustible material can withstand when exposed to a constant radiant heat flux before igniting and undergoing sustained flaming combustion.
- Mass lost: different between the initial and final mass of the sample.
- Heat Release Rate peak (pHRR), average (HRR average) and Time To Peak (TTP): are a quantitative measure of the amount of thermal energy released by a material per unit area when exposed to a fire radiating at constant heat flux (or temperature).
- Mean CO/CO<sub>2</sub> Yield: the average return of CO and CO<sub>2</sub> related to the mass of the sample.
- Total Heat Evolved (THR).
- Total Smoke Released (TSR).

### 3.2.2 Scanning Electron Microscope

The Scanning Electron Microscope (SEM) is a microscope that uses electrons rather than light to form an image (fig. 3.15). The SEM has a large depth of field, which allows a large amount of the sample to be in focus at one time. The SEM also produces images of high resolution,

which means that closely spaced features can be examined at a high magnification. The combination of higher magnification, larger depth of focus, greater resolution, and ease of sample observation makes the SEM one of the most heavily used instruments in research areas today. The SEM is designed for direct studying of the surfaces of solid objects. By scanning with an electron beam that has been generated and focused by the operation of the microscope, an image is formed in much the same way as a TV. The SEM allows a greater depth of focus than the optical microscope. For this reason the SEM can produce an image that is a good representation of the three-dimensional sample.

The SEM uses electrons instead of light to form an image. A beam of electrons is produced at the top of the microscope by heating of a metallic filament. The electron beam follows a vertical path through the column of the microscope. It makes its way through electromagnetic lenses which focus and direct the beam down towards the sample. Once it hits the sample, other electrons (backscattered or secondary) are ejected from the sample. Detectors collect the secondary or backscattered electrons, and convert them to a signal that is sent to a viewing screen similar to the one in an ordinary television, producing an image.

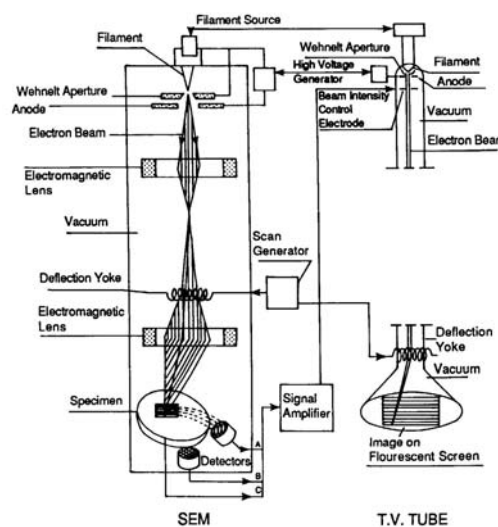


**Figure 3.15.** Scanning Electron Microscope

When a SEM is used, the column and sample must always be at vacuum. A vacuum environment means that most of the air molecules have been removed from the inside of the microscope.

Since the SEM uses electrons to produce an image, most conventional SEM's require that the samples be electrically conductive. The sputter coater uses argon gas and a small electric field. The sample is placed in a small chamber which is at vacuum. Argon gas is then introduced and an electric field is used to cause an electron to be removed from the argon atoms to make the atoms ions with a positive charge. The Ar ions are then attracted to a negatively charged piece of gold foil. The Ar ions act like sand in a sandblaster, knocking gold atoms from the surface of the foil. These gold atoms now settle onto the surface of the sample, producing a gold coating.

### 3.2.3 Thermo mechanical analysis

Thermo mechanical analysis (TMA) is a well-known technique [9] that measures linear or volumetric changes as a function of time, temperature and force. TMA is the measurement of materials behaviour, expansion and /or contraction, as a function of an applied load or temperature. A scan of dimensional changes related to time or load provides invaluable information about the samples mechanical properties. Most analyses are presented in the form of the coefficient of thermal expansion:

$$dL/(dT \cdot L_0) = \text{CTE (coefficient of thermal expansion)}$$

where  $dL$  is the change in length ( $\mu\text{m}$ ),  $dT$  is the change in temperature ( $^{\circ}\text{C}$ ), and  $L_0$  is the initial length (m). Thermo mechanical analysis were conducted using a TMA-60WS (fig.3.16) provided by SHIMADZU.

We measured the CTE of epoxy resin with additives and panels obtained by using VIP, with a force of 0.03N from 25 $^{\circ}\text{C}$  to 250 $^{\circ}\text{C}$  at 3 $^{\circ}\text{C}/\text{min}$  in

double scan and expansion mode. The sample measure 3x3x15mm in accordance to ASTM E831-06.



**Figure 3.16.** TMA-60WS

### 3.2.4 Thermal gravimetric analysis

Thermogravimetric analysis (TGA) (fig.3.17) is an analytical technique used to determine the thermal stability of a material and its fraction of volatile components by monitoring the weight change that occurs when a specimen is heated. The measurement is normally carried out in air or in an inert atmosphere and the weight loss is recorded as a function of increasing temperature.

Analysis of the TGA curves and DTG signals reports two temperature:

- The onset temperature ( $T_{\text{onset}}$ ) calculated from the TGA curves by extrapolating from the curve at the peak of degradation back to the initial weight of the polymer.
- The temperature maximum ( $T_{\text{max}}$ ) calculated from the DTG curves by extrapolating from the curve at the peak of degradation forward to the final weight of the polymer.



**Figure 3.17.** TGA 2920 TA Instruments

Differential thermal analysis was carried out using a TGA 2950 by TA Instruments [10]. All measurements were conducted under air or inert atmosphere, with a sample weight of about 7-8mg; for each test the heating rate was 5, 7.5, 10 and 20°C/min, and the test temperature ranged from 30°C to 800°C.

## References

- [1] [www.heidolph.it](http://www.heidolph.it)
- [2] Formicola C., Martone A., Zarrelli M., Giordano M. Dispersion of carbon nanotubes in a monocomponent epoxy system. 2008 proceeding of AIDC workshop.
- [3] Schartel B., Bartholmai M., Knoll. Some comments on the use of cone calorimeter data. *Polym. Degrad. Stab.* 2005, (88):540–547.
- [4] Schartel B., Hull T.R. Development of fire-retarded materials- Interpretation of cone calorimeter data. *Fire and materials* 2007, (31):327–354.
- [5] Fire Testing Technology. User's Guide for the Cone Calorimeter, February 2000.
- [6] Grant G.B. Quick operation procedure for the cone calorimeter. Unit of fire safety engineering, Edinburgh University, 2nd edition, January 1993.
- [7] Babrauskas V. and Grayson S.J. *Heat Release in Fires*. Elsevier Applied Science, 1992.
- [8] Committee E05.21 on Smoke Combustion Products. ASTM 1354-03 Standard test methods for heat and visible smoke release for materials and products using an oxygen consumption calorimeter. ASTM, 10 February 2003.
- [9] [www.shimadzu.it](http://www.shimadzu.it)
- [10] [www.tainstruments.com](http://www.tainstruments.com)

# **CHAPTER 4**

## **FLAME RETARDANT OF EPOXY RESIN WITH INORGANIC COMPOUNDS**

### **4.1 The state of the art on flame retardant of inorganic compounds**

Flame retardants are chemical agents which are added to combustible materials to make them more resistant to ignition and they are intended to minimise the risk of a fire starting in case of contact with a small heat source.

Inorganic flame retardant as zinc borate, aluminium trihydrate, zinc stannate and zinc hydroxystannate are used in this study because they have shown very low toxicity, they are compatible with a variety of flame retardants while acting as smoke suppressants for various polymer systems. Synergistic effects are envisaged when these smoke suppressants are combined with conventional flame retardants and/or nanoclays. Recent studies to develop flame retardants formation have used inorganic compounds because they have less toxicity. Bourbigot et al. [1] demonstrated that zinc borates are useful synergistic agents in Ethylene vinyl acetate EVA and aluminium trihydrate ATH and magnesium hydroxide  $Mg(OH)_2$  formulations and that they act as smoke suppressant. Moreover they demonstrated that zinc borate develops a vitreous protective residual layer which reduces the combustion rate.

Carpentier et al. [2] studied the synergistic effect of zinc borate on EVA8 filled with magnesium hydroxide (MH), by LOI, cone calorimeter, and TGA. Solid-state NMR was employed to study the carbon in the residues collected after thermal treatment. It is suggested that zinc borate slows the degradation of the polymer and creates a vitreous protective

residual layer, which could act as a physical barrier and a glassy cage for polyethylene chains.

Wu et al [3] studied the synergistic flame retarding effect of ultrafine zinc borate on LDPE/IFR based on LOI, UL94 test and cone calorimeter and established that the flame retardancy is improved when incorporating zinc borate to LDPE/IFR system in fact HRR, THR and mass loss is reduced significantly.

Petsom et al. [4] described a study on zinc hydroxystannate and zinc stannate in combination with 1,2 bis-tribromophenoxy ethane (BTBPE) to increase flame retardancy and reduce smoke emission in an acrylonitrile-butadiene-styrene (ABS) copolymer. They concluded that the combination of tin compounds and BTBPE was found more effective as flame retardant than the individual components when used alone.

Cusak et al. [5] found that zinc hydroxystannate is a good synergist alternative to antimony trioxide, particularly with regard to reducing heat release rates and smoke generation. They demonstrated that ZHS is the best alternative synergist to  $Sb_2O_3$  in halogen-containing polyester resins.

Ning et al. [6] studied the effects of zinc borate, aluminium trihydrate and their mixture on the flame retardant and smoke suppressant properties of polyvinyl chloride PVC as well as their mechanism for flame retardancy and smoke suppression. They concluded that ZB and ZB-ATH reduced the activation energy of PVC and their mixture had a good synergistic effect on the flame retardance and smoke suppression of PVC.

It's clear that different authors [1-11] analyzed the fire and smoke behaviour of zinc borate, zinc stannate, aluminium trihydrate, zinc hydroxystannate and their synergist effect in thermoplastic matrix or in thermosetting bi-component matrix.

## 4.2 Cone calorimeter test

Cone calorimeter represents a small-scale testing configuration which provides important correlating parameters with real fire scenario; data obtained from cone calorimeter can provide plentiful information on fire scenario material behaviour [12].

The values provided by cone calorimeter are mainly: Time To Ignition (TTI), which corresponds to the period that a combustible material can withstand when exposure to a constant radiant heat flux before igniting and undergoing sustained flaming combustion; Heat Release Rate peak (pHRR), average (HRRaverage) and Time To Peak (TTP) are a quantitative measure of the amount of thermal energy released by a material per unit area when exposed to a fire radiating at constant heat flux (or temperature); Total Heat Evolved (THR), Total Smoke Released (TSR).

Cone calorimeter tests were performed using a Fire Testing Technology Ltd. cone calorimeter according to the ASTM E1354-04 procedure. Samples, with nominal dimensions of 100x100x7 mm, were tested horizontally under an incident flux of 50 kW/m<sup>2</sup>. This level was chosen as it corresponds to the evolved heat during a fire.

### 4.2.1 Flame retardant of epoxy resin with inorganic compounds

The composite flame retardant were prepared by mixing the epoxy resin RTM6 with zinc borate, aluminium trihydrate, zinc stannate and zinc hydroxystannate at different percentage (5 wt%, 10 wt%, 20 wt%, 30 wt%, 40 wt%) using a Heidolph RZR mechanical stirring equipment (Chap. 3).

Cone calorimeter data, reported in tables 4.1 and 4.2, show that the presence of zinc borate at 5 and 10 wt % does not change substantially the flame behaviour of the matrix as drawn by analysing the time to ignition and heat release rate peak values. Instead, the presence of zinc borate at 20, 30, 40 wt % induces the flame retardant effect as

supported by the recorded values of pHRR and HRR average. The cone calorimeter data reported in table 4.1 are averaged over two replicate experiments.

Samples	TTI (s)	pHRR (kW/m <sup>2</sup> )	HRR average (kW/m <sup>2</sup> )	TTP (s)	THR (MJ/m <sup>2</sup> )	TSR (m <sup>2</sup> /m <sup>2</sup> )
RTM6 neat	43	702	382	290	189	9260
RTM6+ZB 5wt%	48	523	265	297	176	8282
RTM6+ZB 10wt%	44	682	354	325	184.2	8442
RTM6+ZB 20wt%	49	428	251	455	188	9275
RTM6+ZB 30wt%	47	396	193	65	186	10296
RTM6+ZB 40wt%	63	315	148	82	161	7474

**Table 4.1.** Main cone calorimeter parameters evaluated for RTM6 epoxy with ZB at different percentage

Samples	$\Delta$ TTI (s)	$\Delta$ pHRR (kW/m <sup>2</sup> )	FIP (kW/m <sup>2</sup> *s)	FIGRA (kW/m <sup>2</sup> *s)
RTM6 neat	–	–	16.32	2.42
RTM6+ZB 5wt%	5	179	10.79	1.75
RTM6+ZB 10wt%	1	20	15.5	2.09
RTM6+ZB 20wt%	6	274	8.61	0.94
RTM6+ZB 30wt%	4	306	8.42	6.09
RTM6+ZB 40wt%	20	387	5	3.84

**Table 4.2.** Parameters calculated by cone calorimeter data for RTM6 epoxy with ZB at different percentage

Where FPI and FIGRA are respectively  $pHRR/TTI$  ( $kW/m^2*s$ ) and  $pHRR/TTP$  ( $kW/m^2*s$ ).

Decreasing values for the  $pHRR$  and  $HRR$  average may be correlated with the formation of a char layer over the surface of tested sample, during the combustion process.

A visual inspection of the final residual sample reports the presence of the char layer (fig. 4.1).

In figure 4.1 the  $HRR$  peak of RTM6/ZB 10 wt % system is higher than corresponding peak for the ZB 5 wt % system; this curve's behaviour could be attributed to a local instability of the heat flux during the test which lead to a wider cracked area and therefore, a localised combustion growth.

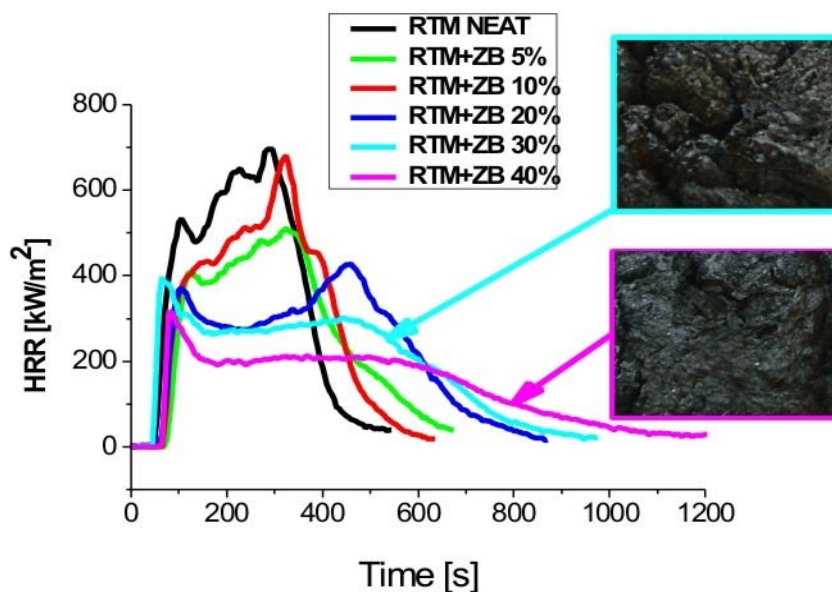


**Figure 4.1.** HRR curves of RTM6/ZB at different percentage

Whereas the aluminium trihydrate shows a negative effect, as showed by preliminary thermo-gravimetric analysis, probably due an acceleration of decomposition of the epoxy resin the presence of ATH from 20 to 40 wt % reduced the  $HRR$  peak and the  $HRR$  average (fig. 4.2).

In figure 4.2 the images of the residues of 30 and 40 wt % RTM6-ATH system with the whitish surface characteristic of the aluminium trihydrate are reported.

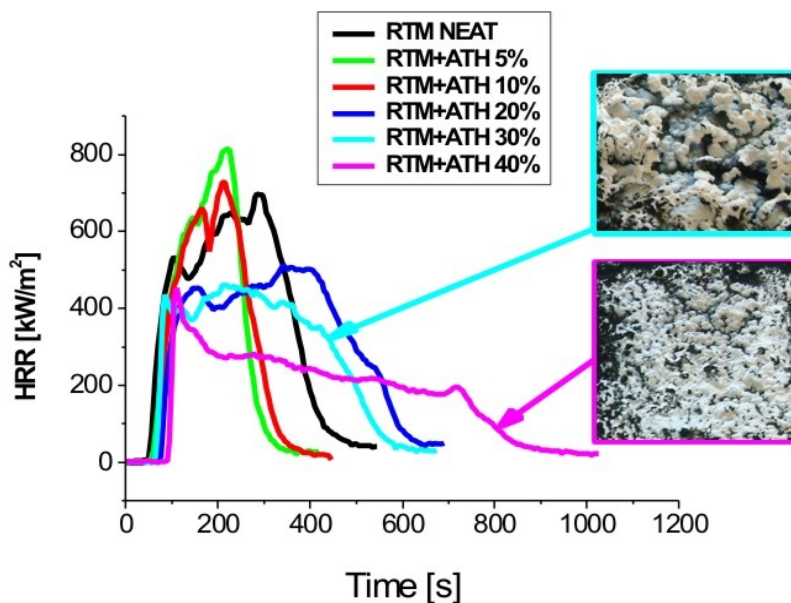


**Figure 4.2.** HRR curves of RTM6/ATH at different percentage

The cone calorimeter data for ATH are reported in table 4.3 and FPI and FIGRA in table 4.4 and are averaged over two replicate experiments.

Samples	TTI (s)	pHRR (kW/m <sup>2</sup> )	HRR average (kW/m <sup>2</sup> )	TTP (s)	THR (MJ/m <sup>2</sup> )	TSR (m <sup>2</sup> /m <sup>2</sup> )
RTM6 neat	43	702	382	290	189	9260
RTM6+ATH 5%	33	815	413	220	126	5099
RTM6+ATH 10%	51	728	383	210	126	5246
RTM6+ATH 20%	52	510	368	340	199	9109
RTM6+ATH 30%	64	468	324	232	174	7648
RTM6+ATH 40%	93	453	193	110	172	8238

**Table 4.3.** Main cone calorimeter parameters evaluated for RTM6 epoxy with ATH at different percentage

Samples	$\Delta$ TTI (s)	$\Delta$ pHRR (kW/m <sup>2</sup> )	FIP (kW/m <sup>2</sup> *s)	FIGRA (kW/m <sup>2</sup> *s)
RTM6 neat	-	-	16.32	2.42
RTM6+ATH 5%	-10	-113	24.7	3.70
RTM6+ATH 10%	8	-26	14.27	3.46
RTM6+ATH 20%	9	192	9.8	1.5
RTM6+ATH 30%	21	234	7.31	2.01
RTM6+ATH 40%	50	249	4.87	4.11

**Table 4.4.** Parameters calculated by cone calorimeter data for RTM6 epoxy with ZB at different percentage

Where FPI and FIGRA are respectively pHRR/TTI (kW/m<sup>2</sup>\*s) and pHRR/TTP (kW/m<sup>2</sup>\*s).

Zinc hydroxystannate and zinc stannate, such as zinc borate and aluminium trihydrate, reduced HRR peak and HRR average with the presence of ZS and ZHS of 30 and 40 wt%. ZS and ZHS weren't prepared at 5 wt% percentage because previously test on zinc borate and aluminium trihydrate have failed the cone calorimeter tests.

Cone calorimeter data are reported in table 4.5 for ZHS and in table 4.7 for ZS.

In figure 4.3 HRR curves of ZHS at different percentage are reported and the residual image shows a densified structure (char) that forms a barrier to inhibit combustible gases.

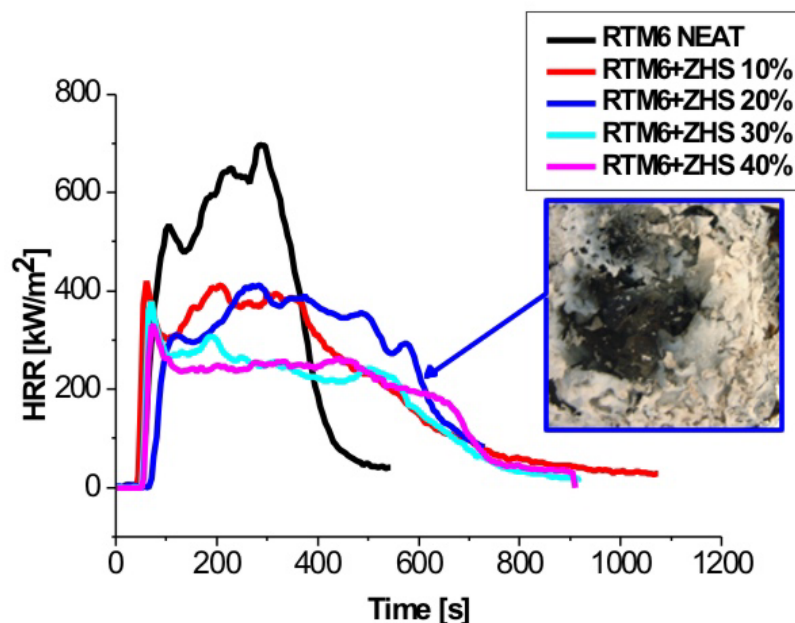


**Figure 4.3.** HRR curves of RTM6/ZHS at different percentage

Samples	TTI (s)	pHRR (kW/m <sup>2</sup> )	HRR average (kW/m <sup>2</sup> )	TTP (s)	THR (MJ/m <sup>2</sup> )	TSR (m <sup>2</sup> /m <sup>2</sup> )
RTM6 neat	43	702	382	290	189	9260
RTM6+ZHS 10%	44	469	203	255	202	9070
RTM6+ZHS 20%	43	465	286	417	194	7092
RTM6+ZHS 30%	52	379	192	70	153	6726
RTM6+ZHS 40%	51	329	214	75	153	72

**Table 4.5.** Main cone calorimeter parameters evaluated for RTM6 epoxy with ZHS at different percentage

Samples	$\Delta$ TTI (s)	$\Delta$ pHRR (kW/m <sup>2</sup> )	FIP (kW/m <sup>2</sup> *s)	FIGRA (kW/m <sup>2</sup> *s)
RTM6 neat	–	–	16.32	2.42
RTM6+ZHS 10%	1	233	10.65	1.84
RTM6+ZHS 20%	0	237	10.82	1.11
RTM6+ZHS 30%	9	323	7.28	5.41
RTM6+ZHS 40%	8	373	6.45	4.38

**Table 4.6.** Parameters calculated by cone calorimeter data for RTM6 epoxy with ZHS at different percentage

Instead in the residual image of ZS (fig. 4.4) a crack on the surface is observed probably due to a local instability of the heat flux during the test which lead to a wider cracked area and therefore, a localised combustion growth such as zinc borate.

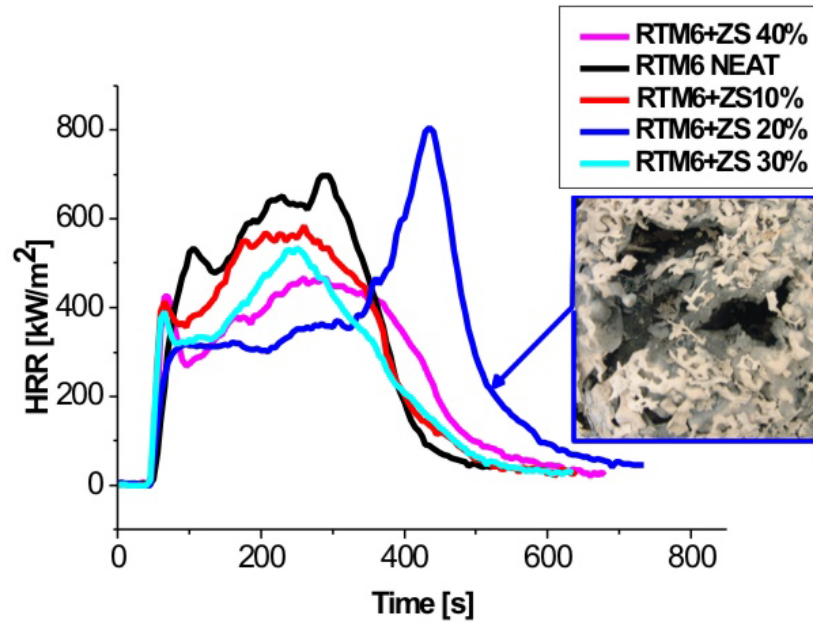


**Figure 4.4.** HRR curves of RTM6/ZS at different percentage

Samples	TTI (s)	pHRR (kW/m <sup>2</sup> )	HRR average (kW/m <sup>2</sup> )	TTP (s)	THR (MJ/m <sup>2</sup> )	TSR (m <sup>2</sup> /m <sup>2</sup> )
RTM6 neat	43	702	382	290	189	9260
RTM6+ZS 10%	45	583	313	260	176	7505
RTM6+ZS 20%	46	803	336	475	200	6747
RTM6+ZS 30%	43	551	274	262	152	6509
RTM6+ZS 40%	45	470	293	282	163	7096

**Table 4.7.** Main cone calorimeter parameters evaluated for RTM6 epoxy with ZS at different percentage

Samples	$\Delta TTI$ (s)	$\Delta p HRR$ (kW/m <sup>2</sup> )	FIP (kW/m <sup>2</sup> *s)	FIGRA (kW/m <sup>2</sup> *s)
RTM6 neat	–	–	16.32	2.42
RTM6+ZS 10%	2	119	12.95	2.24
RTM6+ZS 20%	3	-101	17.45	1.69
RTM6+ZS 30%	0	151	12.81	2.10
RTM6+ZS 40%	2	232	10.44	1.66

**Table 4.8.** Parameters calculated by cone calorimeter data for RTM6 epoxy with ZS at different percentage

In conclusion, the effect of all additives on the HRR peak value of epoxy resin RTM6 is considerable for percentages of 30 and 40 wt%. In particular the best result has been achieved with zinc borate 40 wt% and the heat release rate peak enhancement was 55%.

#### 4.2.2 Synergistic effect of zinc borate with aluminium trihydrate

The synergy between the zinc borate and aluminium trihydrate was investigated on four different percentages (10, 20, 30 and 40 wt %) of additives into neat system, considering the total amount split between zinc borate and aluminium trihydrate according to the ratio 1:1.

In order to study the synergistic effects of zinc borate with aluminium trihydrate, samples of composite of RTM6 and ZB/ATH, dispersed at total percentage of 20 wt%, were mapped by SEM. The presence of ZB and ATH within the same area of the sample lead to the reasonable conclusion that an interaction between the two additives is taking place (fig. 4.5).

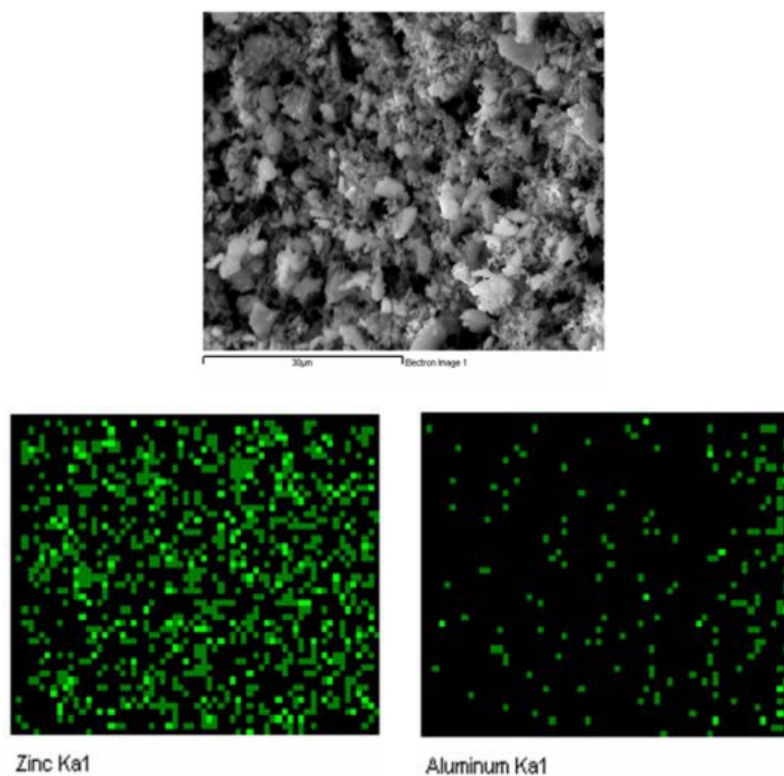


**Figure 4.5.** Mapping of ZB/ATH sample dispersed into the epoxy resin

Preliminary thermogravimetric analysis shows that the synergic effect due to the presence of both, ZB and ATH, is highlighted by the value of onset temperature which decreases to about 355°C for the higher concentrations. Theoretical (calculation) and experimental TG-DTG curves have been superimposed in figures 4.6 and 4.7 for the 30 wt%; similar results were also obtained for the 40 wt% mixture. It results that the addition of ZB and ATH synergistically drives the degradation behaviour of neat matrix system as showed by the remarkable shifting of the experimental curve toward higher onset temperature compared with the calculated one.

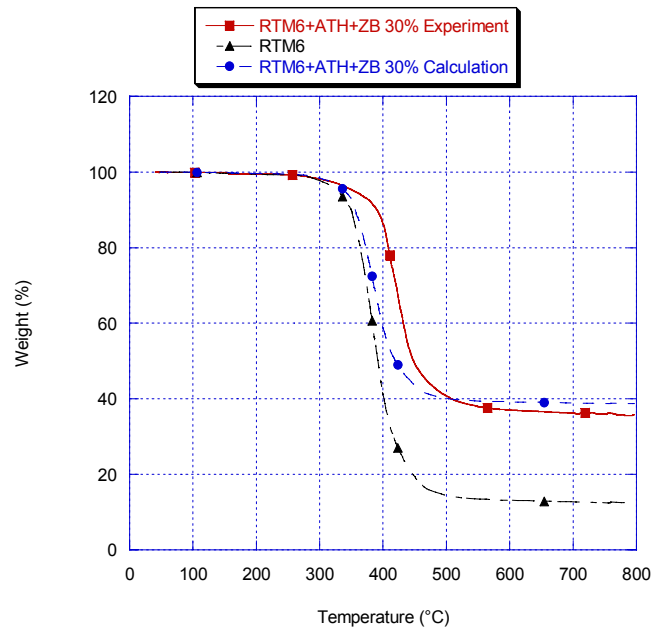


**Figure 4.6.** Experimental and calculated TGA curves for RTM6/ATH/ZB 30 wt% system

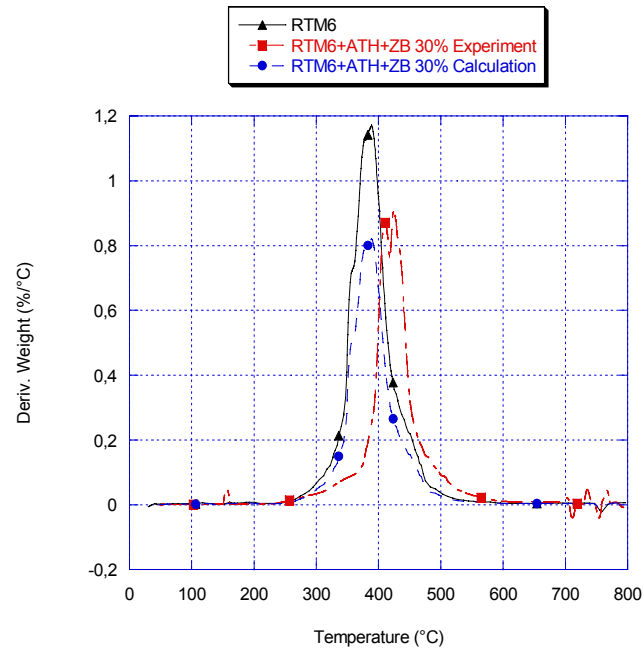


**Figure 4.7.** Experimental and calculated DTG curves for RTM6/ATH/ZB 30 wt% system

Cone calorimeter data of synergic effect of zinc borate is reported in tables 4.9 and 4.10.

Samples	TTI (s)	pHRR (kW/m <sup>2</sup> )	HRR average (kW/m <sup>2</sup> )	TTP (s)	THR (MJ/m <sup>2</sup> )	TSR (m <sup>2</sup> /m <sup>2</sup> )
RTM6 neat	43	702	382	290	189	9260
RTM6+ZB+ATH 10%	52	679	285	200	122	5702
RTM6+ZB+ATH 20%	52	468	337	140	195	10086
RTM6+ZB+ATH 30%	55	431	249	95	174	8966
RTM6+ZB+ATH 40%	87	437	74	100	173	7184

**Table 4.9.** Main cone calorimeter parameters evaluated for RTM6/ZB/ATH system at different percentage

Samples	$\Delta$ TTI (s)	$\Delta$ pHRR (kW/m <sup>2</sup> )	FIP (kW/m <sup>2</sup> *s)	FIGRA (kW/m <sup>2</sup> *s)
RTM6 neat	–	–	16.32	2.42
RTM6+ZB+ATH 10%	9	23	13.05	3.4
RTM6+ZB+ATH 20%	9	234	9.17	3.34
RTM6+ZB+ATH 30%	12	271	7.83	4.53
RTM6+ZB+ATH 40%	44	265	5.02	4.37

**Table 4.10.** Parameters calculated by cone calorimeter data for RTM6/ZB/ATH system at different percentage

The synergy of zinc borate is effective above content of 20 wt %, in fact the heat release rate average undergoes a significant decrease by 382 kW/m<sup>2</sup> for epoxy resin to 249 kW/m<sup>2</sup> for system ZB/ATH 30 wt % and 74 kW/m<sup>2</sup> for ZB/ATH 40 wt % (fig. 4.8). Comparing the  $\Delta$ TTI and the

HRR average values for RTM6/ZB 20 wt %, RTM6/ATH 20 wt % and RTM6/ZB/ATH system at 40 wt %, the effect synergic of zinc borate and aluminium trihydrate improves significantly the flame retardancy, respectively from 6 to 44 sec for TTI; and from 251 kW/m<sup>2</sup> to 74 kW/m<sup>2</sup> for HRR compared.

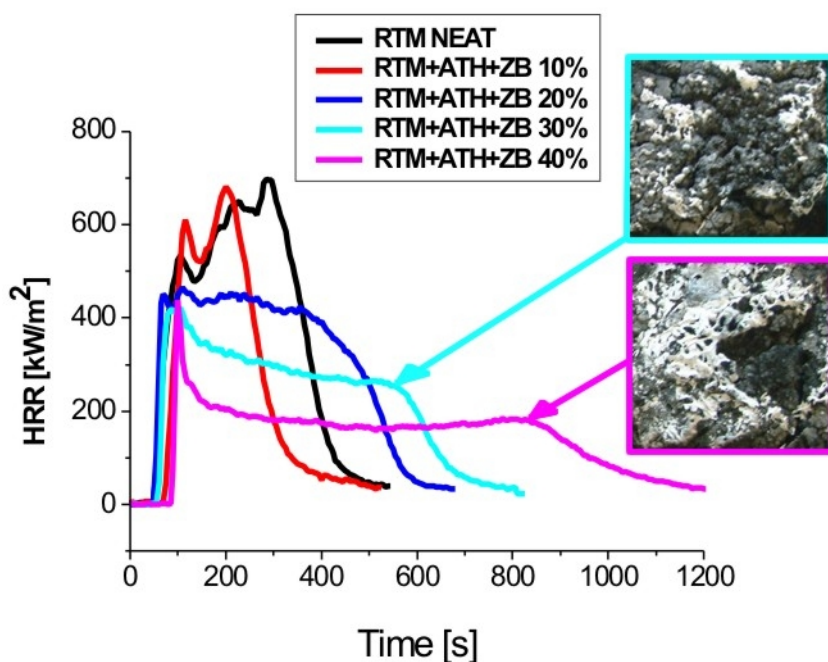


**Figure 4.8.** HRR curves of RTM6/ZB/ATH system at different percentage

#### 4.2.3 Scanning electron micrograph of residual

The scanning electron micrographs of dust, cryogenically fractured composite samples and their residuals were taken by a 1450VP LEO.

The analyses made with the electronic scanning microscope were made to observe the morphology of the material both before and after the combustion process occurred in the cone calorimeter.

We used two different methodologies, one for observing the morphology of the material (ion secondary SE1) and the other for the phase difference (ions scatter QBSD) and the EDS analysis was also carried out to view the compounds contained in the sample examined.

Analysis of SEM micrographs on residual of system of epoxy resin, zinc borate and aluminium trihydrate indicates that char topography varies from a compact like-amalgam structure for the RTM6+ZB (fig.4.9-4.11) to a granular porous-like structure characterized by very small particles of degraded resin and additive, for the ATH mixture (fig.4.12-4.14). Reported SEM image are taken for the 20 wt % content system as this percentage represents the first useful composition to observe a delayed effect of flame retardancy.

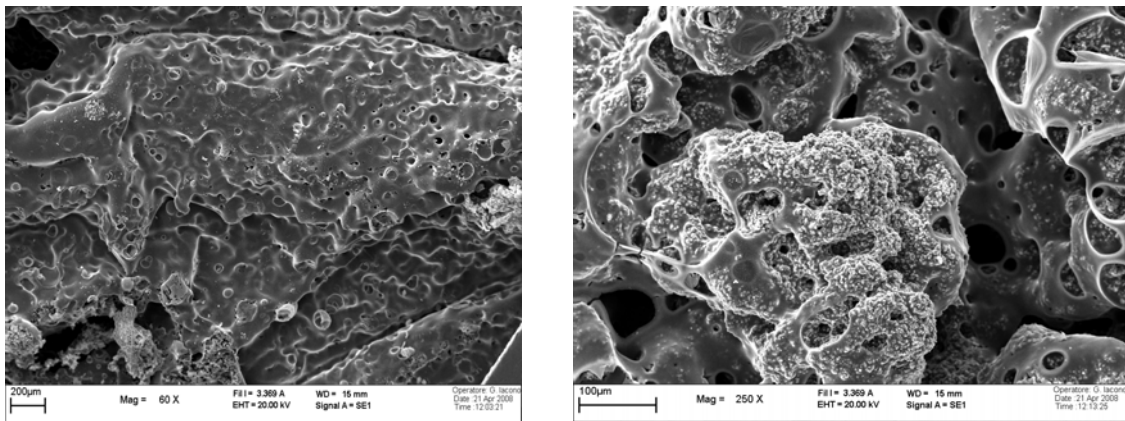


**Figure 4.9 and 4.10.** Scanning electron micrograph of residual of RTM6/ZB system

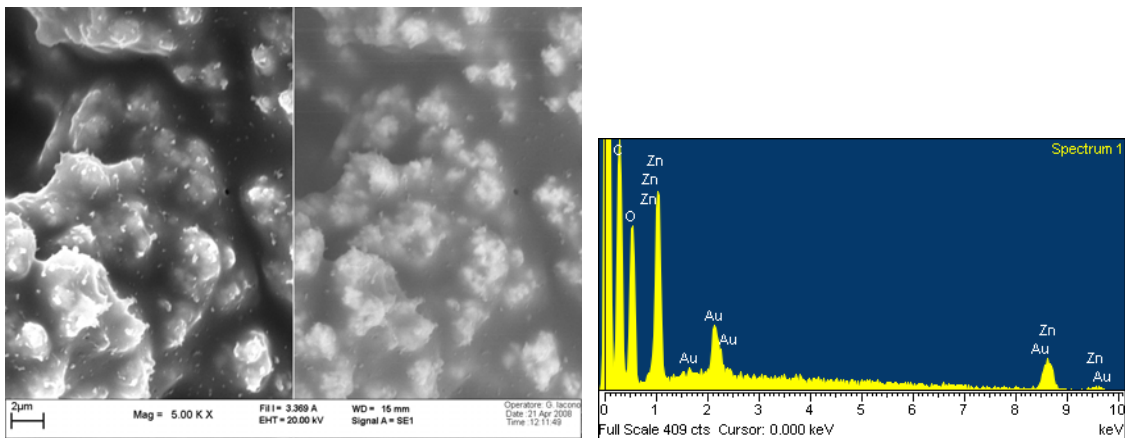


**Figure 4.11.** Scanning electron micrograph (SE1 and QBSD) and EDS of residual of RTM6/ZB system

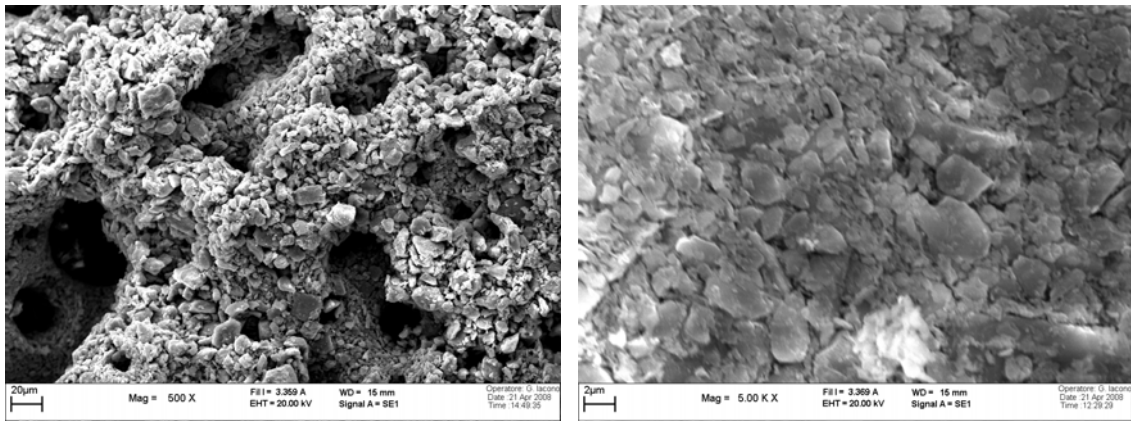


**Figure 4.12 and 4.13.** Scanning electron micrograph of residual of RTM6/ZB system

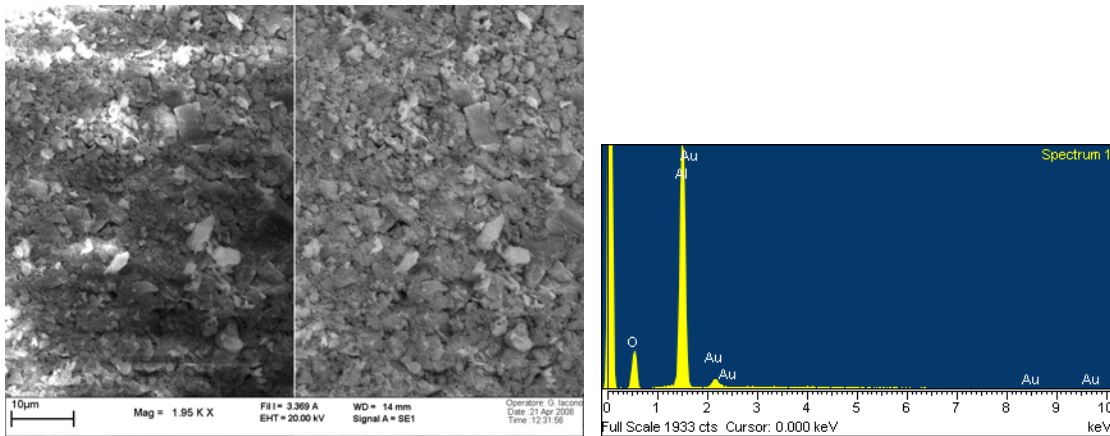


**Figure 4.14.** Scanning electron micrograph (SE1 and QBSD) and EDS of residual of RTM6/ZB system

In figure 4.15 the scanning electron micrograph of residual samples of RTM6/ZB/ATH system is reported and the formation of char layer on the surface due to zinc borate that reduces the HRR peak and average of the burning surface is observe.

Scanning electron micrographs indicate that the synergistic flame retardant effects of these additives result from the excellent quality of char that can better endure the oxidation of high temperatures slowing, at same time, the degradation of epoxy resin.

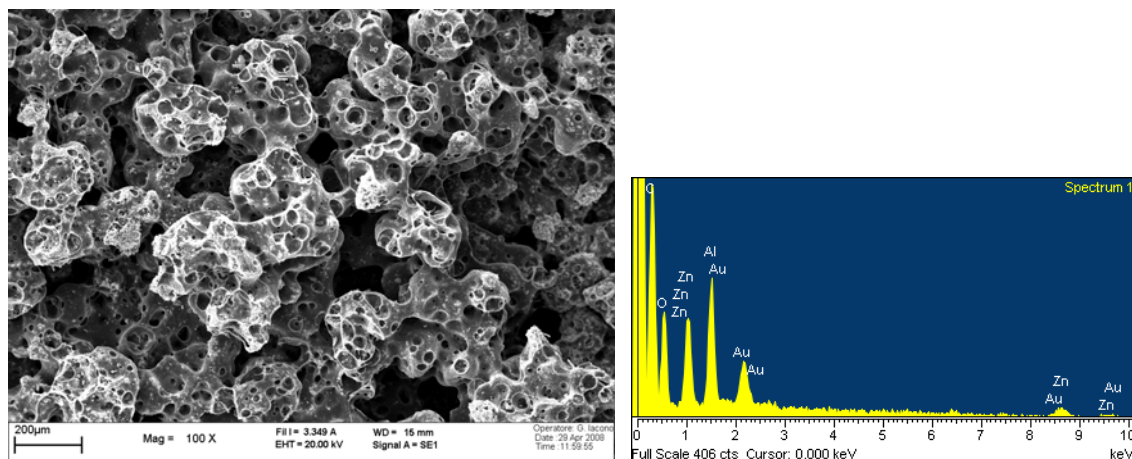


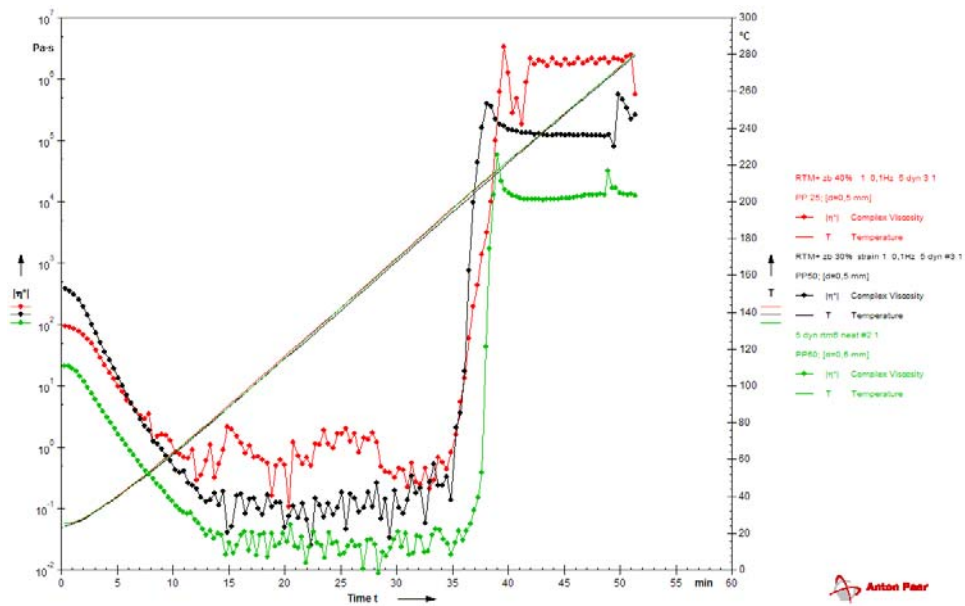
**Figure 4.15.** Scanning electron micrograph and EDS of residual of RTM6/ZB/ATH system

#### 4.2.4 Flame retardant of panels of RTM6 and inorganic compounds

The composites were prepared by mixing the epoxy resin RTM6 with all additives at percentage of 30 wt% and then the mixture was degassed for 30 minutes at 90°C in a vacuum oven to eliminate entrapped air and humidity. Afterwards the mixture was injected in the preform of 20x20cm by vacuum infusion process.

Flame retardants of panels of RTM6 and inorganic compounds were investigated by cone calorimeter under an incident flux of 35 kW/m<sup>2</sup> in according to the ASTM E1354-04 procedure for samples with thickness less than 3mm. Samples have dimensions of 100x100mm with thickness of about 3mm because they were manufactured with 8 plies of carbon fibres overlaid unidirectional at zero degree with thickness of 0.3mm each one.

Cone calorimeter data show how the best results for the flame retardant properties is at percentage of 40 wt% but rheology test, prepared at 5 °C/min, demonstrates high viscosity for this percentage and hence there are troubles during infusion. For this reason the panels were manufactured with percentage additives of 30 wt% (fig. 4.16).



**Figures 4.16.** Rheology test viscosity vs time of RTM6 neat (green), RTM6/ZB 30 wt% (blue) and RTM6/ZB 40 wt% (red).

In figure 4.17 are reported HRR curves of panels of RTM6 with carbon fibres and all additives at percentage of 30 wt%.

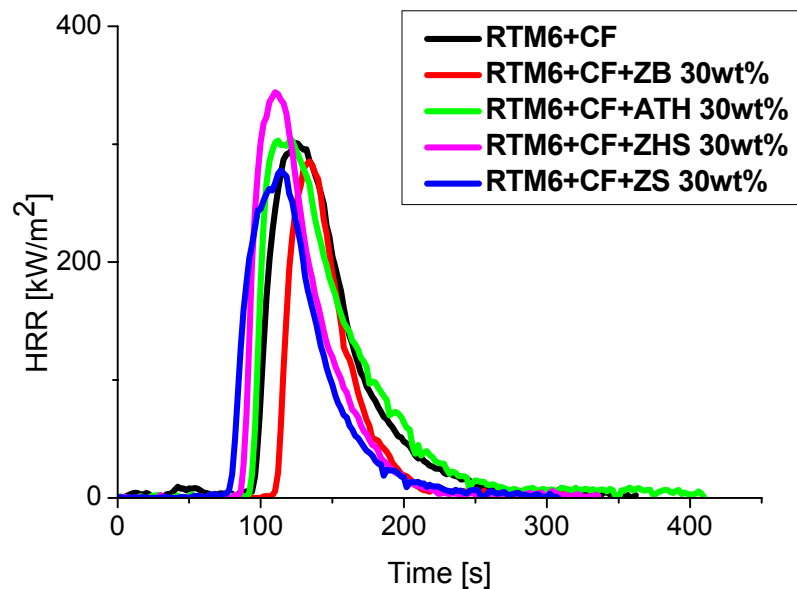


**Figure 4.17.** HRR curves of RTM6/CF/Additives system at percentage of 30 wt%.

In the figure it is shown that zinc borate retarded the time to ignition and reduced heat release rate respect to epoxy resin with carbon fibres, as is reported in table 4.11.

Samples	TTI (s)	pHRR (kW/m <sup>2</sup> )	HRR average (kW/m <sup>2</sup> )	TTP (s)	THR (MJ/m <sup>2</sup> )	TSR (m <sup>2</sup> /m <sup>2</sup> )
RTM6+CF	91	301	119	124	20	1009
RTM6+CF+ZB 30%	106	284	132	134	12	612
RTM6+CF+ATH 30%	90	303	121	122	21	969
RTM6+CF+ZHS 30%	81	344	139	110	18	876
RTM6+CF+ZS 30%	73	278	114	114	16	766

**Table 4.11.** Main cone calorimeter parameters evaluated for RTM6/Carbon Fibers/Additives system at percentage of 30 wt%.

Samples	$\Delta$ TTI (s)	$\Delta$ pHRR (kW/m <sup>2</sup> )	FIP (kW/m <sup>2</sup> *s)	FIGRA (kW/m <sup>2</sup> *s)
RTM6 neat	-	-	3.3	2.4
RTM6+CF+ZB 30%	15	17	2.7	2.1
RTM6+CF+ATH 30%	-1	-2	3.4	2.5
RTM6+CF+ZHS 30%	-10	-43	4.2	3.2
RTM6+CF+ZS 40%	-18	23	3.8	2.4

**Table 4.12.** Parameters calculated by cone calorimeter data for RTM6/Carbon Fibers/Additives system at percentage of 30 wt%.

In the table it's shown clearly that the panels with zinc borate augmented the flame retardant properties of RTM6 and carbon fibers in fact increased the TTI, reduced significantly the TSR and reduced FIP and FIGRA (table. 4.12).

The synergistic effect of zinc borate with aluminium trihydrate on panels of RTM6 and carbon fibers is shown in figure 4.18.

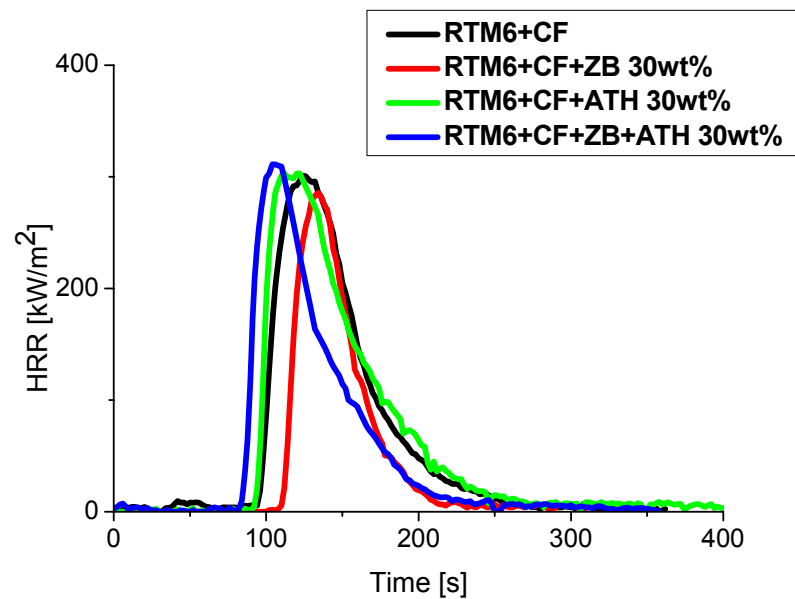


**Figure 4.18.** HRR curves of RTM6/CF/ZB/ATH system.

In this case it's shown that the synergistic effect of zinc borate didn't produce any improvement on the flame retardant properties of RTM6 and Carbon Fibers, as is reported in tables 4.13 and 4.14.

Zinc borate, from chemical, in the combustion phase is able to slow down the effect of carbon fibres because the zinc borate creates a layer of char on the surface of sample more compact than was in the presence of ZB with ATH.

Samples	TTI (s)	pHRR (kW/m <sup>2</sup> )	HRR average (kW/m <sup>2</sup> )	TTP (s)	THR (MJ/m <sup>2</sup> )	TSR (m <sup>2</sup> /m <sup>2</sup> )
RTM6+CF	91	301	119	124	20	1009
RTM6+CF+ZB 30%	106	284	132	134	12	612
RTM6+CF+ATH 30%	90	303	121	122	21	969
RTM6+CF+ZB+ATH 30%	79	311	126	104	17	788

**Table 4.13.** Main cone calorimeter parameters evaluated for RTM6/Carbon Fibers/ZB/ATH system at percentage of 30 wt%.

Samples	$\Delta$ TTI (s)	$\Delta$ pHRR (kW/m <sup>2</sup> )	FIP (kW/m <sup>2</sup> *s)	FIGRA (kW/m <sup>2</sup> *s)
RTM6 neat	–	–	3.3	2.4
RTM6+CF+ZB 30%	15	17	2.7	2.1
RTM6+CF+ATH 30%	-1	-2	3.4	2.5
RTM6+CF+ZB+ATH 30%	-12	-10	3.8	2.9

**Table 4.14.** Parameters calculated by cone calorimeter data for RTM6/Carbon Fibers/ZB/ATH system at percentage of 30 wt%.

### 4.3 Thermal mechanical analysis of RTM6 and inorganic compounds

The coefficient of thermal expansion is calculated by thermal mechanical analysis, as reported in Chapter 3.

Each result, reported in this chapter, is averaged over three replicate experiments. The thermal mechanical analysis was conducted on the samples additived at 30wt% because this percentage is resulted good by cone calorimeter test and principally to have a comparison with the panels that are produced at this percentage

In figure 4.19 is reported the CTE of RTM6 neat and it is shown clearly that there are two values of CTE in the first heating ramp and many CTE's value in the second heating ramp.

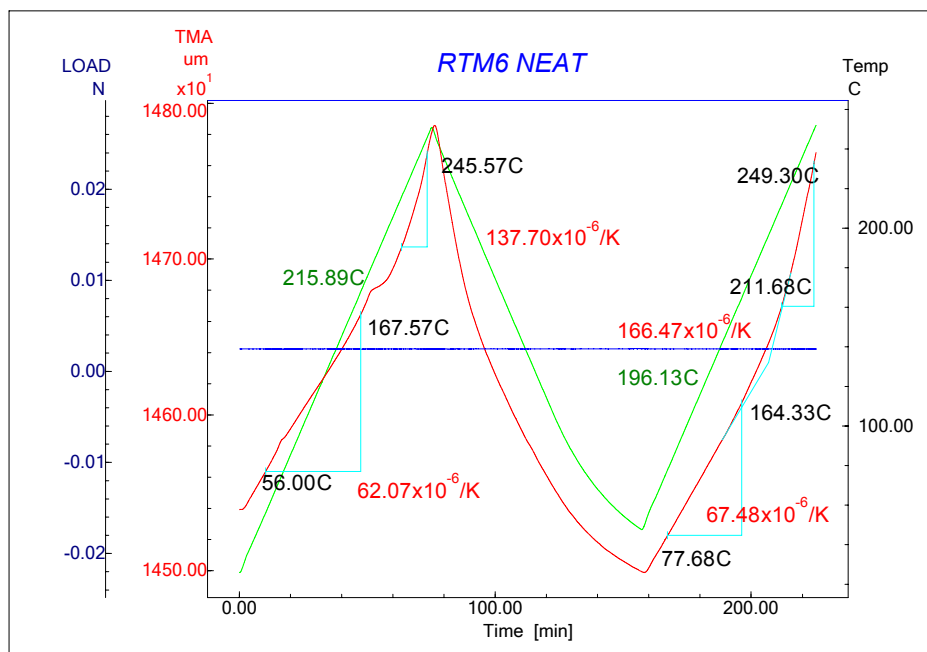


**Figure 4.19.** CTE of epoxy resin RTM6 neat

Instead in the samples of RTM6 and additives the value of CTE in the second heating ramp is only one. and it is observed that the value of CTE of RTM6/additives system is more less than the CTE of RTM6 neat

hence the influence of additives on the thermal mechanical properties of matrix is clear.

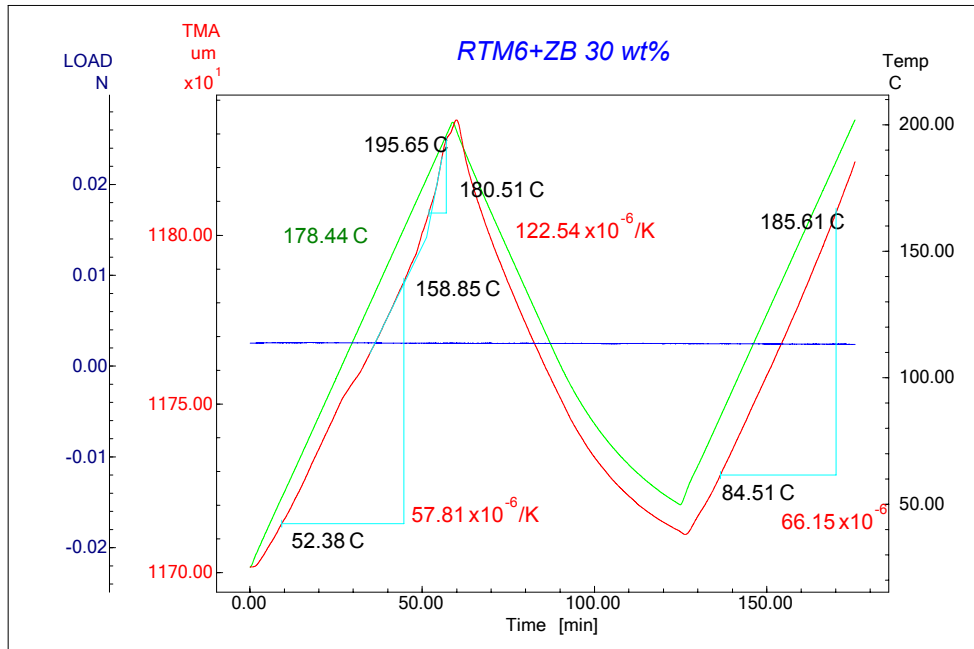


**Figure 4.20.** CTE of epoxy resin RTM6+ZB 30wt%

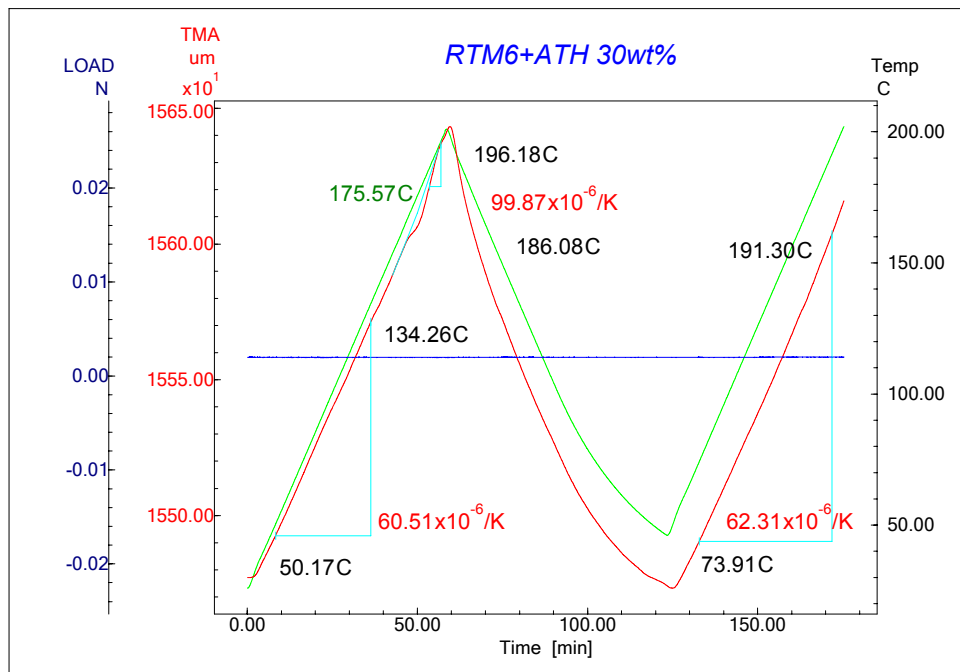


**Figure 4.21.** CTE of epoxy resin RTM6+ATH 30wt%

To observe the synergistic effect of zinc borate is calculated the CTE of RTM6/ZB/ATH 30wt% system and the results are reported in table 4.15.

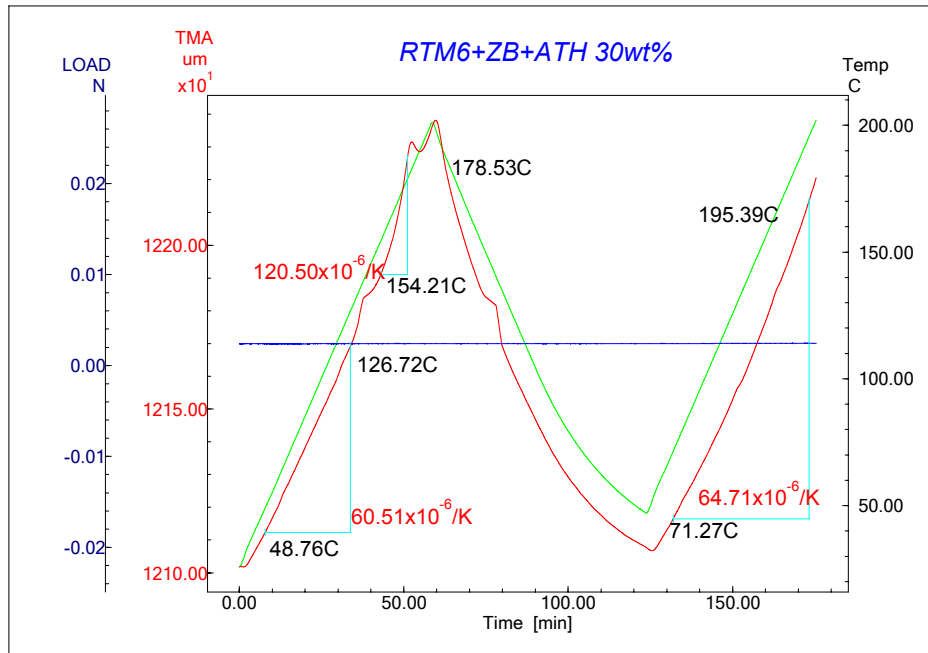


**Figure 4.22.** CTE of epoxy resin RTM6+ATH+ZB 30wt%

<b>Coefficient of Thermal Expansion (<math>10^{-6}/K</math>)</b>				
<b>Samples</b>	<b>I Heating ramp</b>		<b>II Heating ramp</b>	
RTM6 neat	60.6	132.9	67.8	165.7
RTM6+ZB 30wt%	59.5	176.7	65.6	-
RTM6+ATH 30wt%	60.5	114.9	61.2	-
RTM6+ATH+ZB 30wt%	61.2	115.7	67.1	-

**Table 4.15.** CTE of synergistic effect of zinc borate

Instead in the graph of TMA of ZS and ZHS there are two values in the second heating ramp and rather than as a ZB and ATH. This confirms, as previously seen from the cone, that the protective structure that is created is different because chemically boron and aluminium will

oxidize more easily creating alumina and boron oxide (ceramic) hence tighten the structure

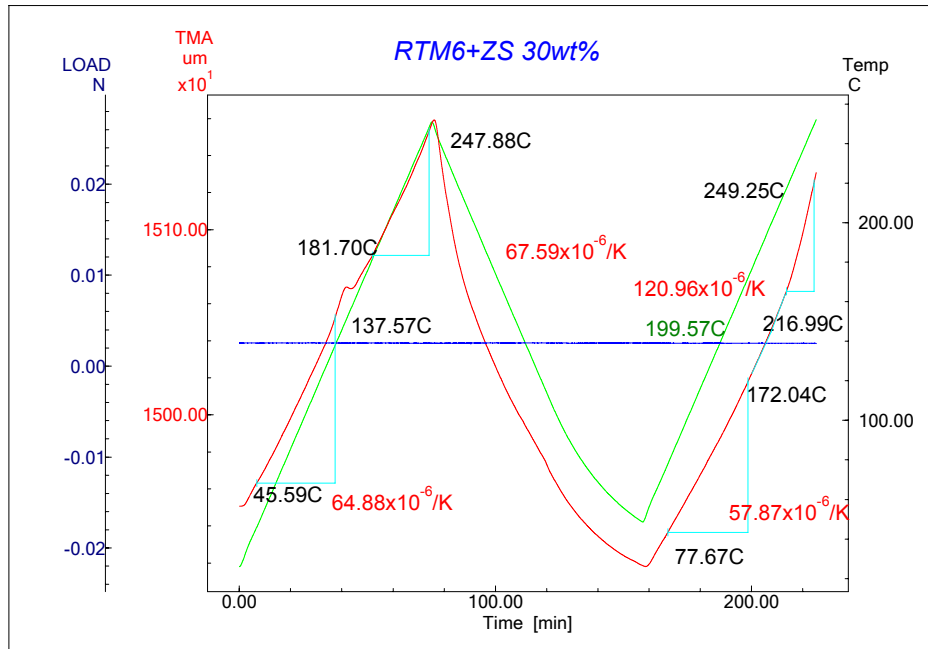


**Figure 4.23.** CTE of epoxy resin RTM6+ZS 30wt%

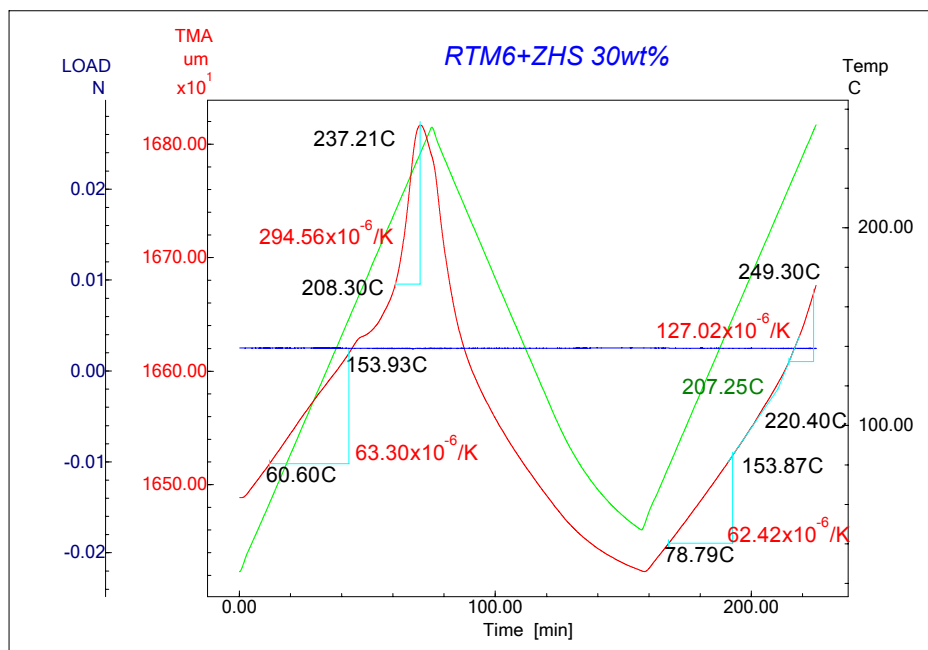


**Figure 4.24.** CTE of epoxy resin RTM6+ZHS 30wt%

In conclusion the values of coefficient of thermal expansion for both heating ramp are reported in table 4.16.

<b>Coefficient of Thermal Expansion (<math>10^{-6}/K</math>)</b>				
<b>Samples</b>	<b>I Heating ramp</b>		<b>II Heating ramp</b>	
	RTM6 neat	60.6	132.9	67.8
RTM6+ZB 30wt%	59.5	203.8	65.6	-
RTM6+ATH 30wt%	60.5	114.9	61.2	-
RTM6+ATH+ZB 30wt%	61.2	115.7	67.1	-
RTM6+ZS 30wt%	63.6	70.40	57.4	127.6
RTM6+ZHS 30wt%	62.1	289.8	61.7	126.8

**Table 4.16.** CTE of all samples of RTM6 and additives

In table 4.16 the values of CTE for all additives are reported and it is clearly observed that the influence of additives on the matrix is able to lower the CTE of epoxy resin neat.

Furthermore, it is shown the thermal mechanical analysis of panels of epoxy resin with additives produced by VIP with carbon fibres. The samples were cut to 90 degrees in the transverse direction fibres to observe the effect of carbon fibres and additives on the properties of thermal mechanical of matrix.

In the figures below the values of CTE of epoxy resin RTM6 with carbon fibres and all additives are illustrated and it is shown that the values of CTE are always lower than the CTE of single resin with fibres. This results are reported in the table 4.17.

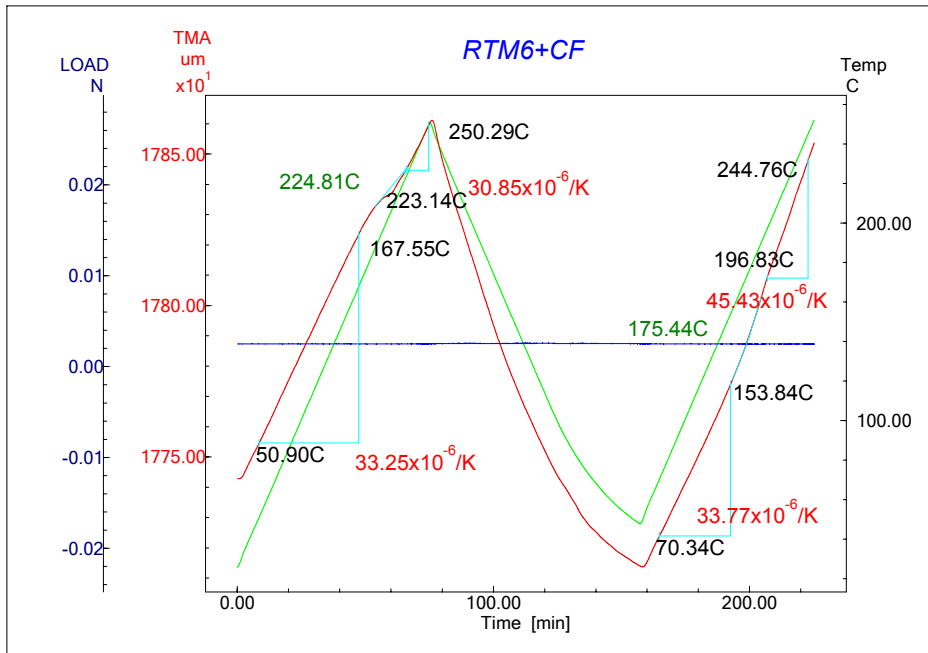


**Figure 4.25.** CTE of epoxy resin RTM6+CF

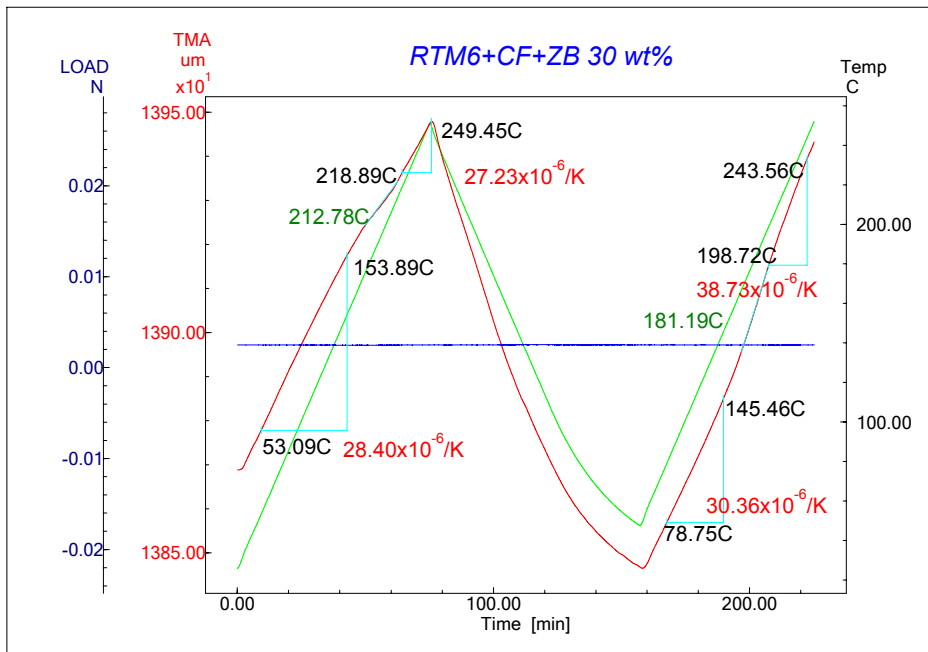


**Figure 4.26.** CTE of epoxy resin RTM6+CF+ZB 30wt%

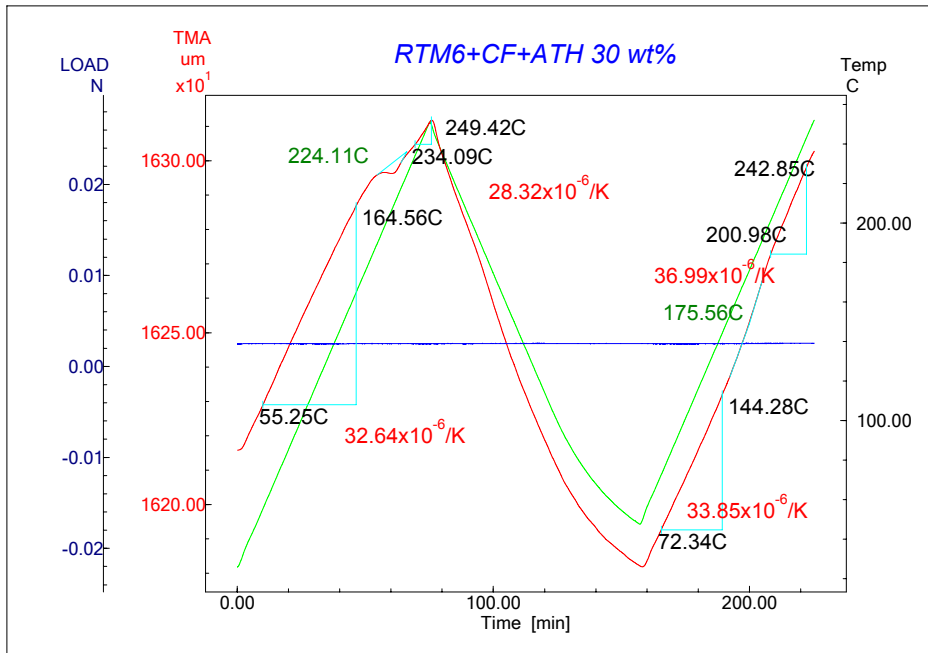


**Figure 4.27.** CTE of epoxy resin RTM6+CF+ATH 30wt%

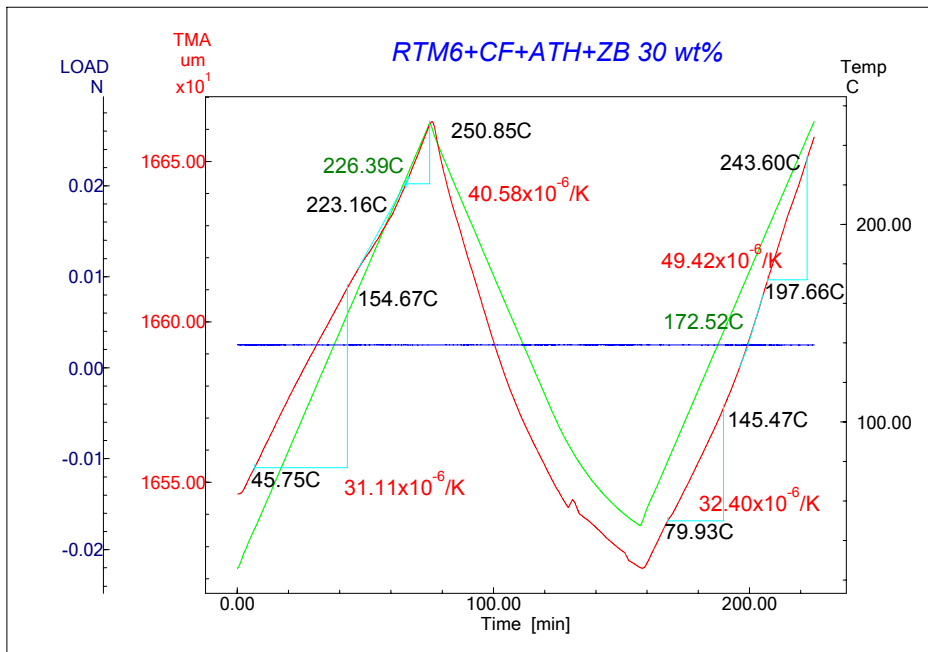


**Figure 4.28.** CTE of epoxy resin RTM6+CF+ATH+ZB 30wt%

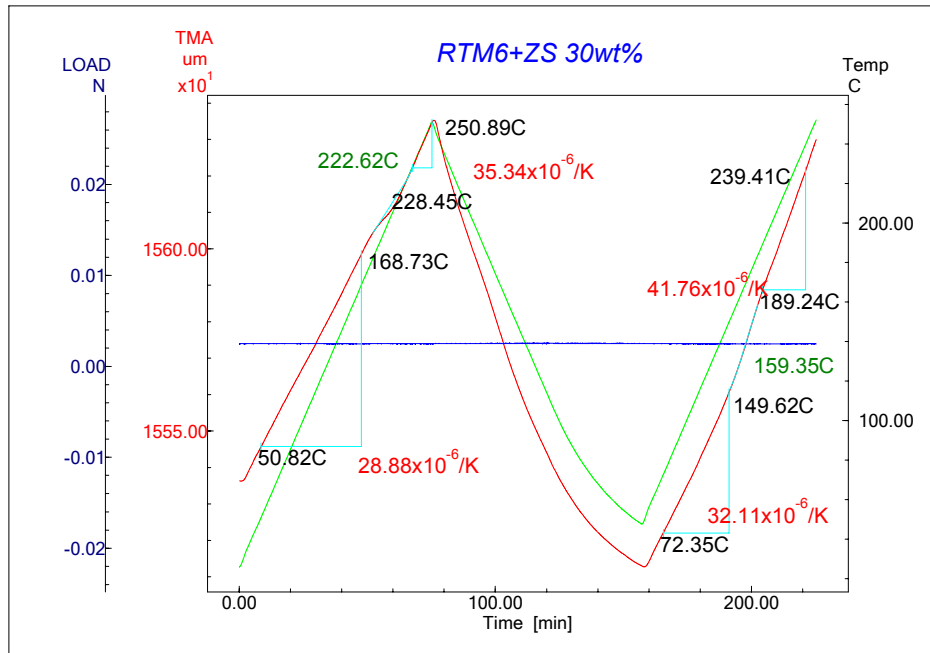


**Figure 4.29.** CTE of epoxy resin RTM6+CF+ZS 30wt%

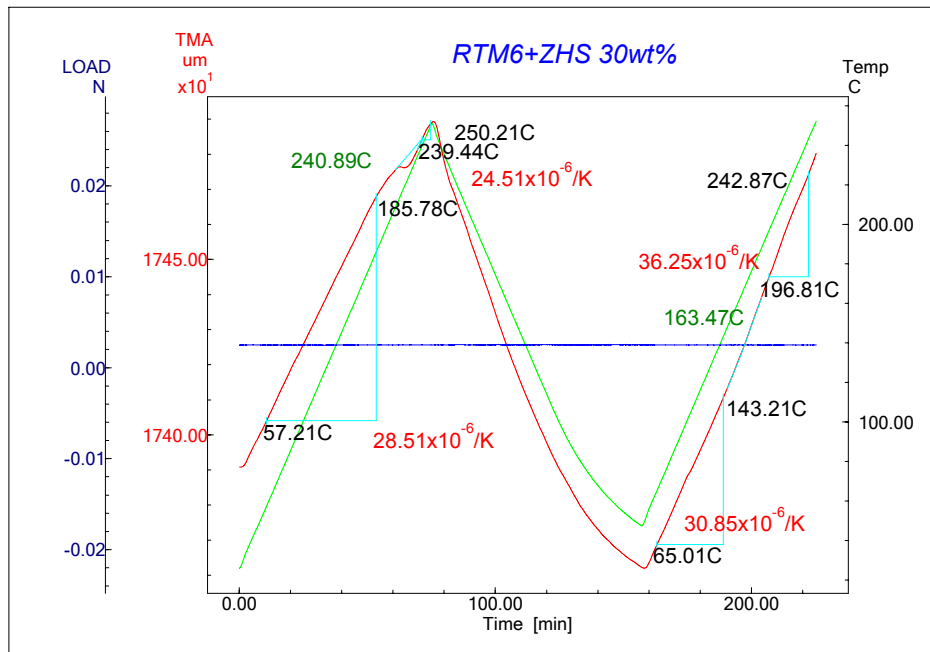


**Figure 4.30.** CTE of epoxy resin RTM6+CF+ZHS 30wt%

<b>Coefficient of Thermal Expansion (<math>10^{-6}/\text{K}</math>)</b>				
<b>Samples</b>	<b>I Heating ramp</b>		<b>II Heating ramp</b>	
	RTM6+CF	33.2	31.9	34.6
RTM6+CF+ZB 30wt%	26.5	31.7	31.1	38.6
RTM6+CF+ATH 30wt%	32.6	30.6	33.9	38.9
RTM6+CF+ATH+ZB 30wt%	29.2	29.9	30.6	39.8
RTM6+CF+ZS 30wt%	29.6	31.8	31.8	37.8
RTM6+CF+ZHS 30wt%	27.6	36.4	31.8	40.6

**Table 4.17.** CTE of all samples of RTM6+CF and all additives

In the table the thermal mechanical data of panels are reported and it is shown that the carbon fibers and the additives reduced the CTE hence increase the thermal mechanical properties of epoxy resin RTM6.

**References**

- [1] Bourbigot S., Le Bras M., Leeuwendal R., Shen K.K., Schubert D. *Polym. Degrad. Stab.* 1999, (64):419-425.
- [2] Carpentier F, Bourbigot S, Le Bras M, Delobel R, Foulon M. *Polym Degrad Stab* 2000, 69; 1: 83-92.
- [3] Wu Z., Shu W., Hu Y. *Journal of Applied Polymer Science* 2007, 103:3667-3674.
- [4] Petsom A., Roengsumran S., Ariyaphattanakul A., Sangvanich P. *Polym. Degrad. Stab.* 2003,(80):17-22.
- [5] Cusack PA., Heer MS., Monk AW. *Polymer Degradation and Stability* 1997, (58):229-237.
- [6] Ning Y, Guo S. *J. of App. Pol. Sc.* 2000; 77: 3119-3127.
- [7] Wu S, Cong P, Yu J, Luo X, Mo L. *Fuel* 2006; 85: 1298-1304.
- [8] Bourbigot S, Le Bras M, Duquesne S, Rochery M. *Macromol Mater Eng* 2004; 289: 499-511.
- [9] Le Bras M, Bourbigot S, Duquesne S, Jama C, Wilkie CA. *Royal Society of Chemistry Press: Cambridge*, 2005.
- [10] Genovese A, Shanks RA. *Polym Degrad Stab* 2007; 92: 2-13.
- [11] Samyn F, Bourbigot S, Duquesne S, Delobel R. *Thermochimica* 2007; 456: 134-144.
- [12] ScharTEL B, Hull TR. *Fire and Materials.* 2007; 31: 327-354.

# **CHAPTER 5**

## ***FLAME RETARDANT OF EPOXY RESIN WITH CARBON NANOTUBES***

### **5.1 The state of the art on flame retardant of carbon nanotubes**

Fire retardancy is one of the fields where the nanomaterials could be used successfully. Nanoparticles embedded in various polymer matrices are reported to reduce considerably the heat released from these materials [1]. The investigation of size, shape, interfaces and concentration of nanoscale silica, nano-flakes, nanotubes and other nanoparticles on the flame retardant performance increased the role of fire protected polymers within the science of materials. There is a high level of interest in using filler particles having at least one nano-dimensional scale for making polymeric nanocomposite materials with exceptional properties. One of the promising applications involves the improvement in flammability properties of polymers with nanofillers because one weak aspect of polymers is that they are combustible under certain conditions. These filled systems are attractive as possible alternatives to conventional flame retardants and furthermore they could simultaneously improve both physical and flammability properties of polymers [2].

Carbon nanotubes are candidates as flame retardant additives because of their highly elongated shape (high aspect ratio).

In literature [2-6] different authors analyzed the fire behaviours of carbon nanotubes in several matrices.

Kashiwagi et al. [2-4] found that nanocomposites based on carbon nanotubes are likewise capable of forming a continuous structured network as a protective layer without the formation of cracks that compromise the flame-retardant effectiveness. This resulted in a

significant reduction in the heat release rate (a flammability measure related to the fire intensity) with a carbon nanotube mass concentration as low as 0.5%. This protective layer consisted mainly of carbon nanotubes and it seemed to act as a heat shield for the virgin polymer below the layer. Poorly dispersed carbon nanotubes resulted in the formation of a discontinuous layer consisting of fragmented islands rather than the continuous protective network layer. Very low concentrations of the tubes yielded the same fragmented island structures as found in the clay nanocomposite measurements. The flame retardant performance of the nanocomposites containing the island structure was much poorer than that of the nanocomposites forming a continuous protective network layer. Thus, the formation of the network structured protective layer during burning, without any openings or cracks, seems to be crucial for the large reduction in heat release rate. Furthermore Kashiwagi et al. [5] suggested that this network is formed in the original sample under appropriate fabrication conditions and that this structure provides the main source of the protective layer that is formed during the burning process. This hypothesis was systematically tested with various sizes and concentrations of carbon-based nanoparticles in a PMMA matrix.

Cipiriano et al. [6] studied the effects of the aspect ratio of multi-walled carbon nanotubes (MWNTs) on the rheology and flammability of polystyrene/MWNT nanocomposites using two MWNTs having average aspect ratios (length to outer diameter) of 49 and 150. In flammability experiments they demonstrated that the larger aspect ratio particles lead to a greater reduction in mass loss rate hence they are more effective in reducing flammability.

## 5.2 Cone calorimeter test

Cone calorimeter tests were performed using a Fire Testing Technology Ltd. cone calorimeter according to the ASTM E1354-04 procedure. Samples, with nominal dimensions of 100x100x3 mm, were tested horizontally under an incident flux of 35 kW/m<sup>2</sup>. This level was chosen as it corresponds to the evolved heat during a fire for samples with thickness less than 3mm.

### 5.2.1 Flame retardant of RTM6 and MWNT Nanocyl 7000

The nanocomposites of epoxy resin and multi walled carbon nanotubes were prepared by sonication process as is reported in the Chapter 3.

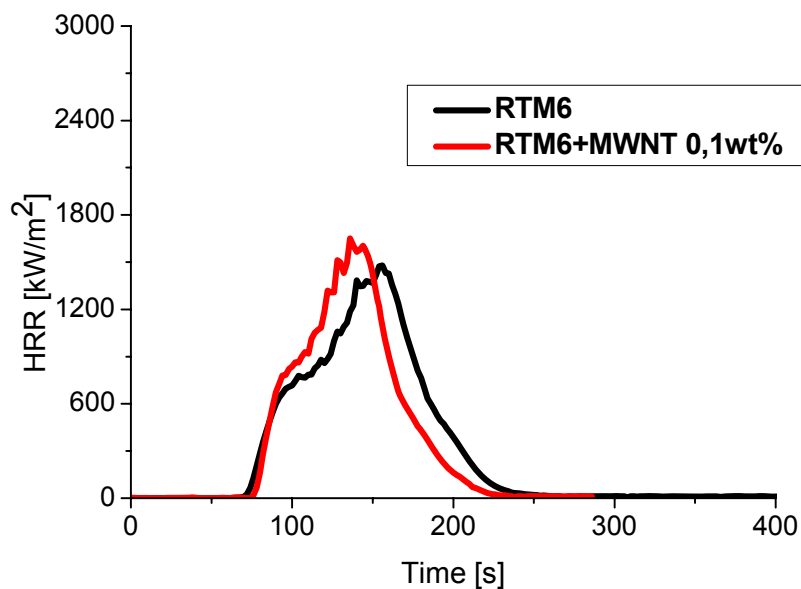


**Figure 5.1.** HRR curves of RTM6/MWNT at percentage of 0.1wt%

Samples	TTI (s)	pHRR (kW/m <sup>2</sup> )	HRR average (kW/m <sup>2</sup> )	TTP (s)	THR (MJ/m <sup>2</sup> )	TSR (m <sup>2</sup> /m <sup>2</sup> )
RTM6 neat	35	1479	614	156	117	4688
RTM6+MWNT 0.1wt%	72	1651	643	136	108	3863

**Table 5.1.** Parameters calculated by cone calorimeter data for RTM6/MWNT 0.1wt%.

In figure 5.1 it is shown that the carbon nanotubes don't influence the properties of flame retardants of matrices because the percentage used in this work is low. A small effect is shown only for the value of TTI as reported in table 5.1.

### 5.2.3 Flame retardant of panels of RTM6 and carbon nanotubes

The nanocomposites were prepared by sonication process (Chap.3) the epoxy resin RTM6 with multi walled carbon nanotubes at percentage of 0.1 wt% and then the mixture was degassed for 30 minutes at 90°C in a vacuum oven to eliminate entrapped air and humidity. Afterwards the mixture was injected in the preform of 20x20cm by vacuum infusion process. Samples were manufactured with 8 plies of overlaid unidirectional carbon fibres at zero degrees with thickness of 0.3mm each one.

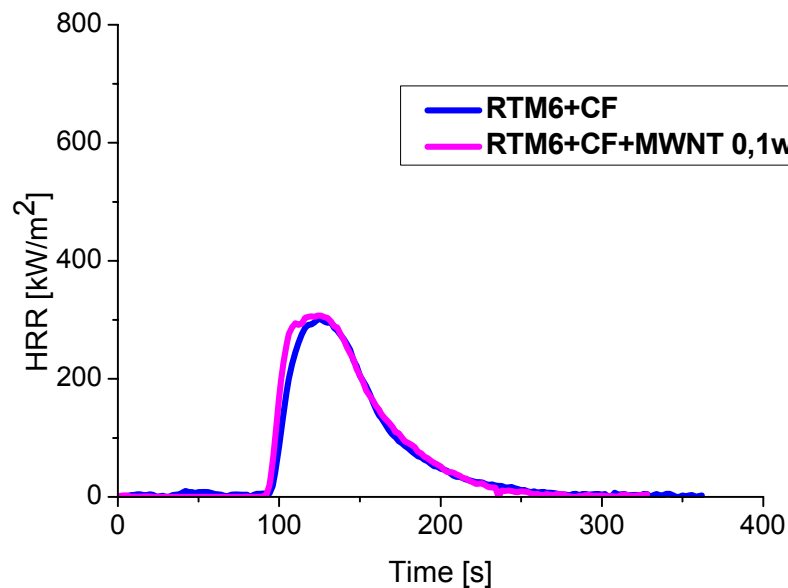


**Figure 5.2.** HRR curves of RTM6/CF/MWNT 0.1wt%

Samples	TTI (s)	pHRR (kW/m <sup>2</sup> )	HRR average (kW/m <sup>2</sup> )	TTP (s)	THR (MJ/m <sup>2</sup> )	TSR (m <sup>2</sup> /m <sup>2</sup> )
RTM6+CF	91	301	118	124	20	1009
RTM6+CF+MWNT 0.1wt%	88	306	129	124	21	1077

**Table 5.2.** Parameters calculated by cone calorimeter data for RTM6/CF/MWNT system at percentage of 0.1wt%.

As seen above, the percentage of nanotubes is not effective and the presence of unidirectional fibres does not induce changes sensitive to the distribution of flame.

### 5.3 Thermal mechanical analysis of RTM6 and carbon nanotubes

The thermal mechanical analysis was conducted on both samples of RTM6 and additives on panels with carbon fibres.

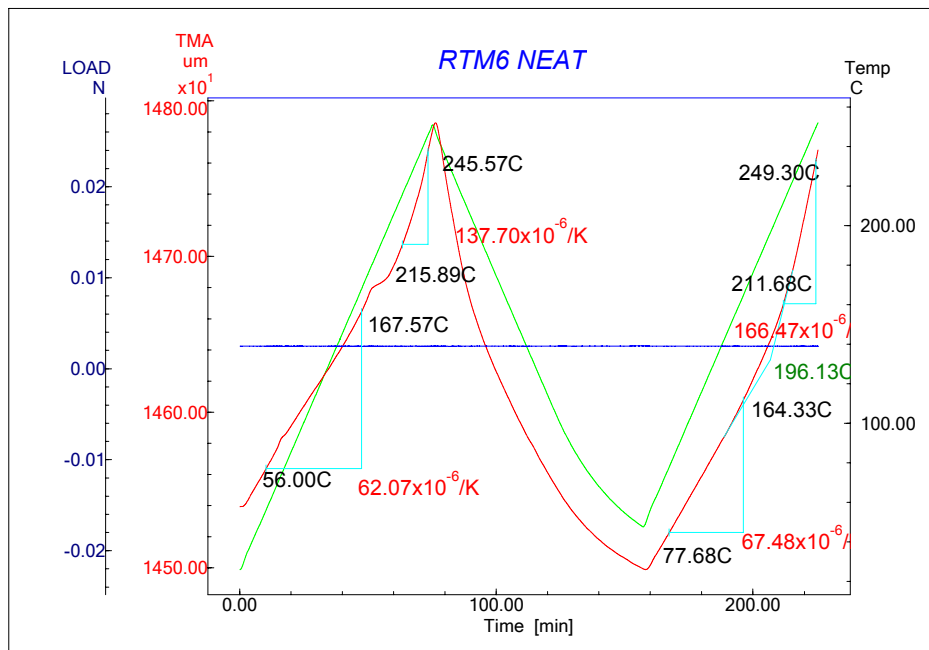


**Figure 5.3.** CTE of epoxy resin RTM6 neat

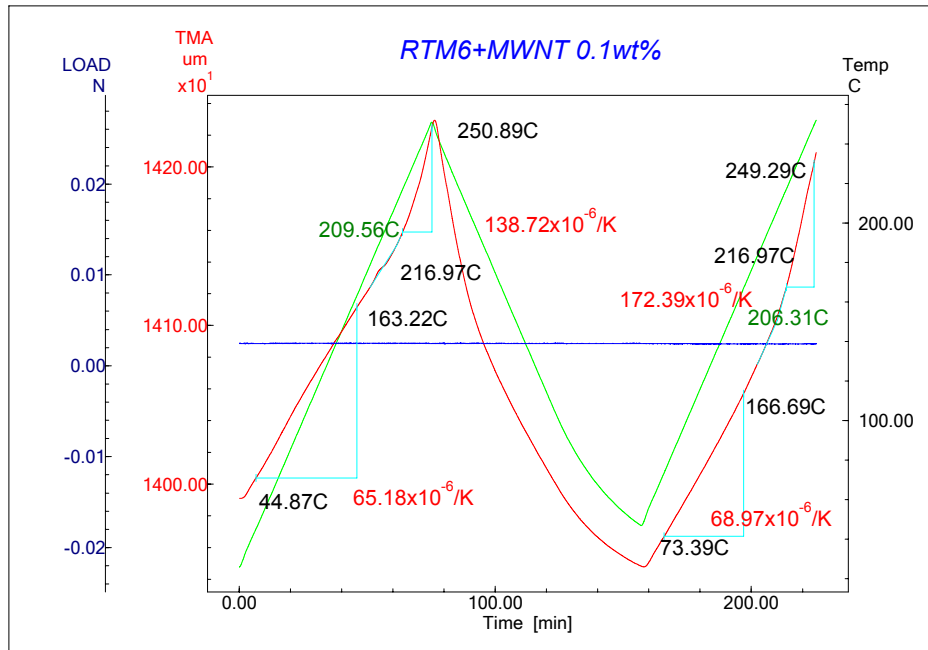


**Figure 5.4.** CTE of epoxy resin RTM6+MWNT 0.1wt%

Coefficient of Thermal Expansion ( $10^{-6}/K$ )				
Samples	I Heating ramp		II Heating ramp	
	RTM6 neat	60.6	132.9	67.8
RTM6+MWNT 0.1wt%	62.2	137.4	68.8	170.2

**Table 5.3.** CTE of RTM6 and MWNT 0.1wt%

In the figures 5.3 and 5.4 and in the table 5.3 the CTE for panels of epoxy resin added with carbon nanotubes are shown where the percentage of multi walled carbon nanotubes is too low to make an improvement on the value of CTE of RTM6 and carbon fibres.

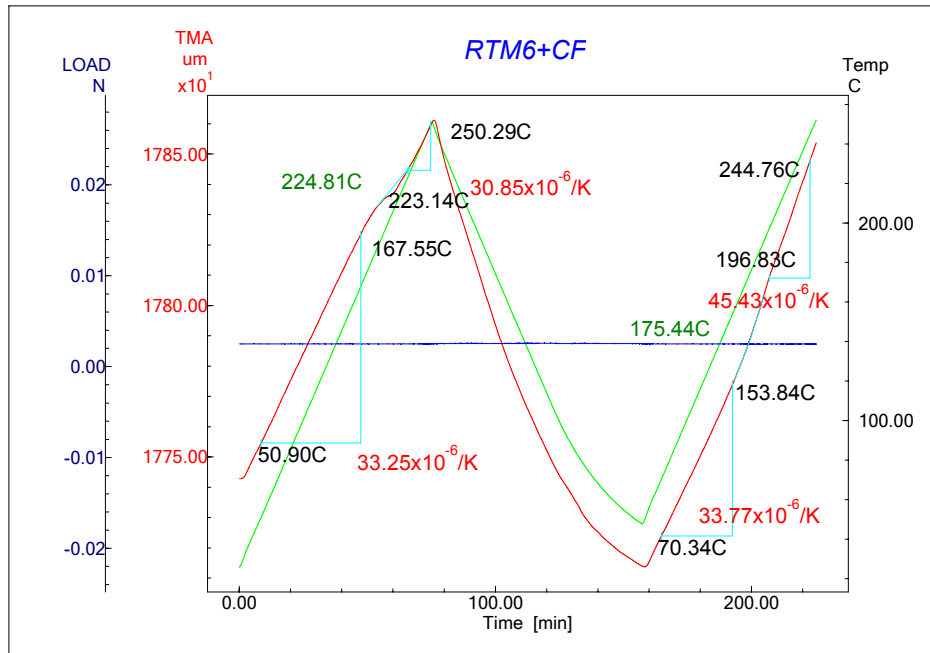


**Figure 5.5.** CTE of epoxy resin RTM6+CF

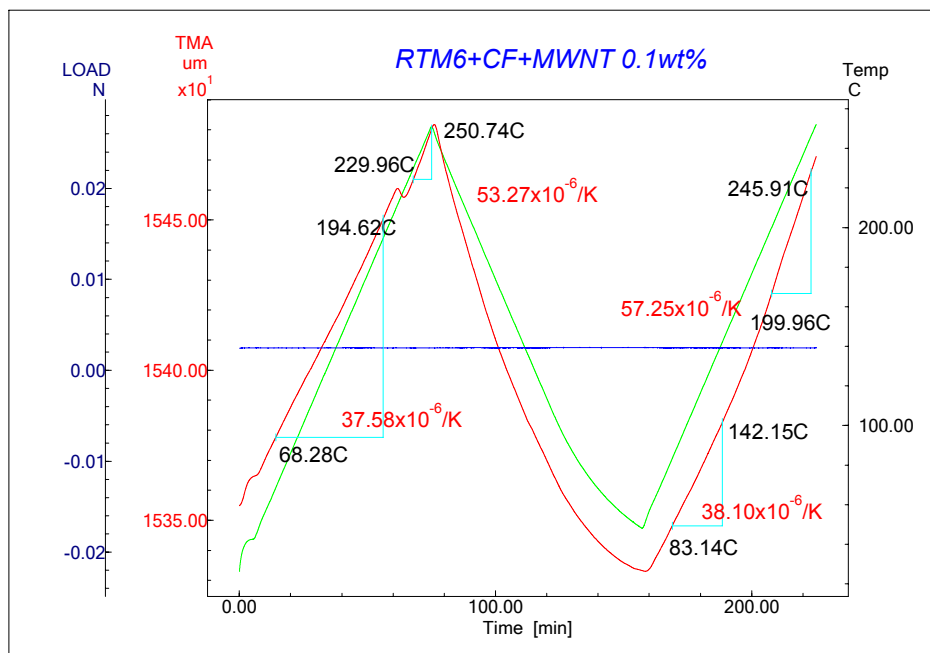


**Figure 5.6.** CTE of epoxy resin RTM6+CF+MWNT 0.1wt%

<b>Coefficient of Thermal Expansion (<math>10^{-6}/K</math>)</b>				
<b>Samples</b>	<b>I Heating ramp</b>		<b>II Heating ramp</b>	
RTM6+CF	33.2	31.9	34.6	45.2
RTM6+CF+MWNT 0.1wt%	36.7	57.7	38.3	55.3

**Table 5.4.** CTE of RTM6+CF+MWNT 0.1wt% system

Similar values are obtained for the sample with carbon fibres and carbon nanotubes in fact in table 5.4 it is shown clearly that both nanotubes and fibers don't influence CTE of RTM6/CF system.

## References

- [1] Marosfoi B., Matko Sz., Marosi PAnnaGy. *Current Applied Physics* 2006, (6):259-261.
- [2] Kashiwagi T., Du F., Winey KI., Groth KM., Shields JR., Bellayer SP., Kim H., Douglas JF. *Polymer* 2005, (46):471-481.
- [3] Kashiwagi T., Grulke E., Hilding J., Groth K., Harris R., Butler K., Shields J., Kharchenko S., Douglas J. *Polymer* 2004, (45): 4227-4239.
- [4] Kashiwagi et al. *Macromol. Rapid Commun.* 2002, (23): 761-765.
- [5] Kashiwagi T., Du F., Douglas JF., Winey KI., Harris RHJr., Shields JR. *Nature materials* 2005, (4): 5-10.
- [6] Cipiriano B.H., Kashiwagi T., Raghavan S.R., Yang Y., Grulke E.A., Yamamoto K., Shields J.R., Douglas J.F., *Polymer* 2007, 48:6086-6096.
- [7] Qian D, Dickey EC, Andrews R, Rantell T. *Appl. Phys. Lett.* 2000;76 (20):2868-2870.
- [8] Park C et al. *Chemical Physical Letters* 2002;364:303-308.
- [9] Ham HT, Choi YS, Chung JI. *Journal of Colloid and Interface Science* 2005;286 (1):216-223.
- [10] Salvetat JP, Briggs AD, Bonard JM, Bacsa RR, Kulik AJ, Stockli T, Burnham NA, Forro´ L. *Phys. Rev. Lett.* 1999;82 (5):944-947.
- [11] Choi ES, Brooks JS, Eaton DL, Haik MS, Hussaini MY, Garmestani H, Li D, Dahmen KJ. *Appl. Phys.* 2003;94:6034-
- [12] Sandler J, Shaffer MSP, Prasse T, Bauhofer W, Schulte K, Windle AH. *Polymer* 1999;40(21):5967-5971.
- [13] Xiao-Lin X, Yiu-Wing M, Xing-Ping Z. *Materials Science and Engineering R* 2005;49:89-112.
- [14] Jin L, Bower C, Zhou O. *Appl. Phys. Lett.* 1998;73 (9):1197-1199.
- [15] Choi ES, Brooks JS, Eaton DL, Al-Haik MS, Hussaini MY, Garmestani H, Li D, Dahmen KJ. *Appl. Phys.* 2003;94:5451-5473.

## **CHAPTER 6**

### ***KINETIC DEGRADATIONS: KISSINGER AND OZAWA METHODS***

#### **6.1 The state of the art on Kissinger and Ozawa methods for epoxy resin**

To study the accelerated ageing of polymers and to obtain the kinetic parameters of decomposition such as the apparent activation energy we must to extrapolate according to the environment where the materials are used. It is important to consider the degradation mechanisms both in the environments where they are used both when they are under accelerated ageing conditions.

Thermogravimetric analysis is often used to determine decomposition reactions and to evaluate the thermal stability. The mass loss is controlled by time in isothermal conditions or by temperature during the heating rate. Changes in mass can be associated with solvent or water desorption/absorption, oxidation or reduction and decomposition. Dynamic TG tests tend to be shorter and the mechanism of degradation may be studied over a large temperature range with typical heating rate. Regnier et al. [1] in a previously work on polyimide polymer system compared several methods to calculate thermal kinetic parameters. They showed that Van Krevelen, Horowitz-Metzger, Coats Redfern and Mac-Callum-Tanner methods gave a similar apparent activation energy. All kinetic parameters calculated by using these methods showed equally good agreement with the experimental data. Afterwards Regnier et al. [2] investigated the thermal degradation of epoxy/carbon composites in dynamic conditions. The activation energy have been evaluated employing Kissinger's method assuming first order reaction or the Osawa's method which gives an estimated activation energy for the overall degradation.

Kiefer et al. [3] mentioned that the sample preparation had an effect on the kinetic results. It does seem that the kinetic parameters are divided into two groups, however, depending whether or not the sample contained fibres. He observed that the resin is affecting the fibre.

Wang et al. [4] studied the degradation behaviours of epoxy resins containing various flame retardant components by Kissinger, Flynn-Wall-Ozawa and Horowitz-Metzger methods. They demonstrated that the activation energy at lower degree of the degradation decreased by incorporation of flame retardant components, while increased at higher degree of the degradation.

Chiang et al. [5] prepared epoxy nanocomposites containing silicon and phosphorus and compared with pure epoxy by Kissinger's method. They found that the activation energies of thermo-oxidative degradation for epoxy nanocomposites are less than those of thermo-oxidative degradation for pure epoxy in first stage of thermo-oxidative degradation. However, the activation energies of thermo-oxidative degradation for epoxy nanocomposites are more than those of thermo-oxidative degradation for pure epoxy in second stage of thermo-oxidative degradation.

In the dynamic and isothermal TGA measurements the mass loss is detected in function of temperature and kinetic of degradation is based on  $n^{\text{th}}$  order reaction mechanism and, in the many cases, the rate of degradation is a linear function of temperature by a constant, dependent of temperature, by Arrhenius equation:

$$\frac{d\alpha}{dt} = Kf(\alpha) \quad (1)$$

with

$$k = Af(\alpha) \exp\left(\frac{-E}{RT}\right) \quad (2)$$

The combination of (1) e (2) gives:

$$\frac{d\alpha}{dt} = Af(\alpha)\exp\left(\frac{-E}{RT}\right) \quad (3)$$

If heating rate  $\beta=dT/dt$  is constant, the variation in degree of conversion can be analysed as a function of temperature and this temperature being dependent on the time of heating:

$$\frac{d\alpha}{dT} = \frac{A}{\beta}f(\alpha)\exp\left(\frac{-E}{RT}\right) \quad (4)$$

The integrated form of this equation generally is expressed as:

$$g(\alpha) = \int_0^{\alpha} \frac{d\alpha}{f(\alpha)} = \frac{A}{\beta} \int_0^T \exp\left(-\frac{E}{RT}\right) dT \quad (5)$$

where  $g(\alpha)$  is the integrated form of the conversion dependence function. Different kinetics methods (differential and integral) were applied in this study.

**Kissinger method** [6] makes it possible to determine the values of activation energy without a precise knowledge of the reaction mechanism and analyzes the changes in the thermo-gravimetric data through the change of scan rate of heating,  $\beta$ , depending on the temperature of the maximum peak in DTG curve. That way you get that:

$$\ln\left(\frac{\beta}{T_{\max}^2}\right) = \left\{ \ln \frac{AR}{E} + \ln \left[ n(1 - \alpha_{\max})^{n-1} \right] \right\} - \frac{E}{RT_{\max}} \quad (6)$$

where  $T_{\max}$  is the temperature corresponding to the inflection point of thermo degradation curves which corresponds to the maximum reaction rate,  $\alpha_{\max}$  is the conversion at  $T_{\max}$ , and  $n$  is the reaction order.

Assuming that  $f'(\alpha_{\max}) = n(1 - \alpha_{\max})^{n-1} \cong \text{const.}$  the activation energy  $E$  can be determined from a plot of  $\ln(\beta/T_{\max}^2)$  against  $1/T_{\max}$ .

With ***Flynn-Wall-Ozawa method*** [7-9] it is possible to get values of activation energy applying Doyle's approximation to the integration of Eq.(5). You get that :

$$\log \beta = \log \left[ \frac{AE}{g(\alpha)R} \right] - 2.315 - 0.4567 \frac{E}{RT} \quad (7)$$

Using Eq.7, it is possible to plot  $\log \beta$  against  $1/T$  and to consider the slope of straight line which result with a various value of conversion. The graph that result report  $E$  in function of conversion degree.

## 6.2 Kinetic degradations of RTM6 and inorganic compounds

For obtaining the kinetic information, such as the activation energy, the TGA study has been conducted with the variation of the heating rates. The dynamic experiments were carried out at different heating rates 5, 7.5, 10 and 20 °C/min from ambient to 800°C with TA 2950 thermobalance in nitrogen and air atmosphere. For each experiment were used approximately 10 mg of materials and the kinetics parameters of interest, as activation energy relating to initial degradation of mixtures, were obtained by Kissinger and Flynn-Ozawa-Wall methods.

In figure 6.1 thermogravimetric analysis of the epoxy resin RTM6 in the nitrogen atmosphere are reported. The epoxy resin shows only one step of degradation and the onset temperature is around 350°C while the maximum temperature on the DTG curves shows a little difference in the heating rate.

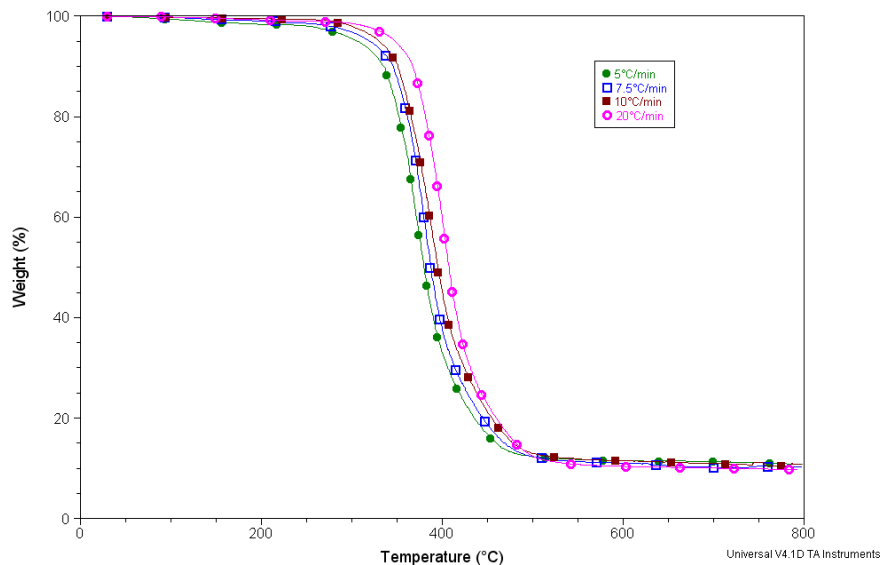


**Figure 6.1.** TGA thermograms of RTM6 neat in nitrogen atmosphere

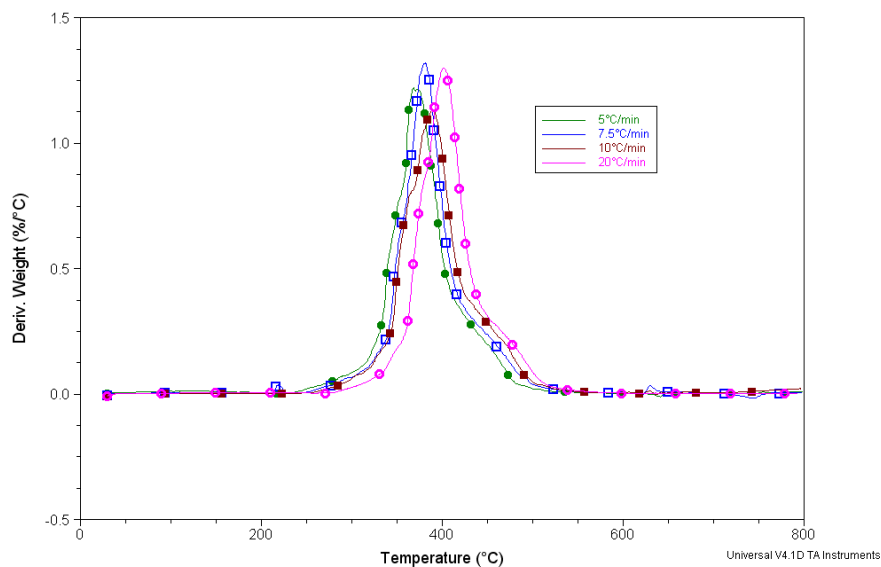


**Figure 6.2.** DTG thermograms of RTM6 neat in nitrogen atmosphere

In table 6.1, the onset temperature and maximum temperature for epoxy system neat are reported along with the corresponding heating ramp.

Heating rate (°C/min)	T <sub>onset</sub> (°C)	T <sub>max</sub> (°C)
5°C/min	305	372
7.5°C/min	320	381
10°C/min	330	388
20°C/min	348	403

**Table 6.1.** T<sub>onset</sub> and T<sub>max</sub> of epoxy resin RTM6 in nitrogen atmosphere

In air atmosphere, two different degradation steps spanning the whole investigated temperature range are noticeable, the first step occurring at 350°C and a second much broader step within around 500-550°C (fig. 6.3 and 6.4). The second step was attributed to a decomposition of the non-volatile residues formed in the first step

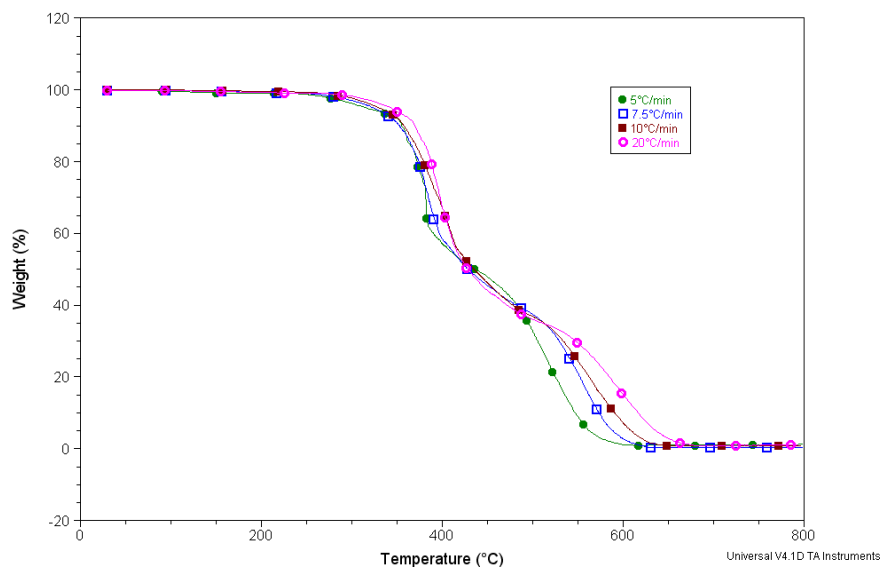


**Figure 6.3.** TGA thermograms of RTM6 neat in air atmosphere

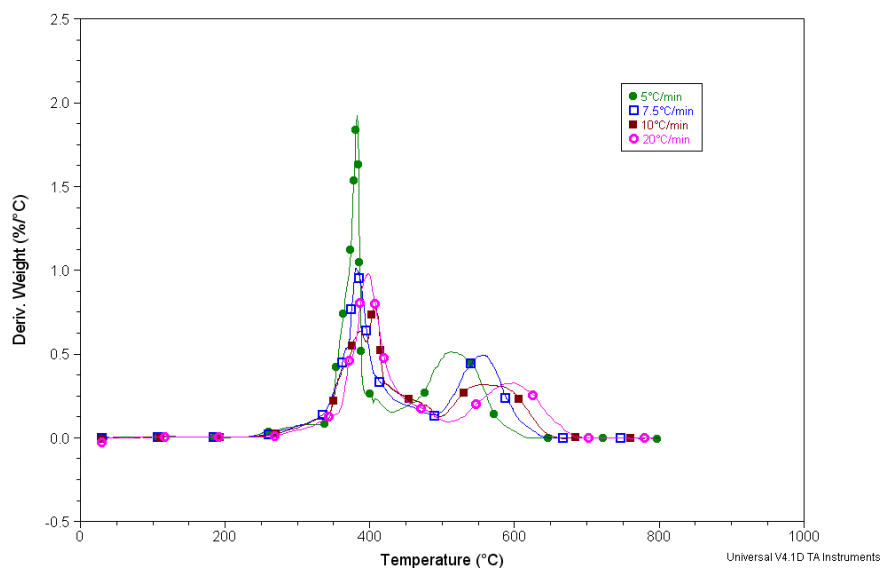


**Figure 6.4.** DTG thermograms of RTM6 neat in air atmosphere

In table 6.2 are reported  $T_{\text{onset}}$  and  $T_{\text{max}}$  of epoxy resin in air atmosphere for each step.

<b>I STEP</b>		
Heating rate (°C/min)	$T_{\text{onset}}$ (°C)	$T_{\text{max}}$ (°C)
5°C/min	354	378
7.5°C/min	351	383
10°C/min	354	406
20°C/min	357	398
<b>II STEP</b>		
Heating rate (°C/min)	$T_{\text{onset}}$ (°C)	$T_{\text{max}}$ (°C)
5°C/min	475	517
7.5°C/min	524	556
10°C/min	523	568
20°C/min	544	597

**Table 6.2.**  $T_{\text{onset}}$  and  $T_{\text{max}}$  of epoxy resin RTM6 in air atmosphere

The Kissinger method was employed to obtain the apparent activation energy ( $E_a$ ) in air or nitrogen from several scan with different heating rate ( $q$ ). Figures 6.5 and 6.6 represent the Kissinger plots of the epoxy resin degraded in nitrogen and air atmosphere.

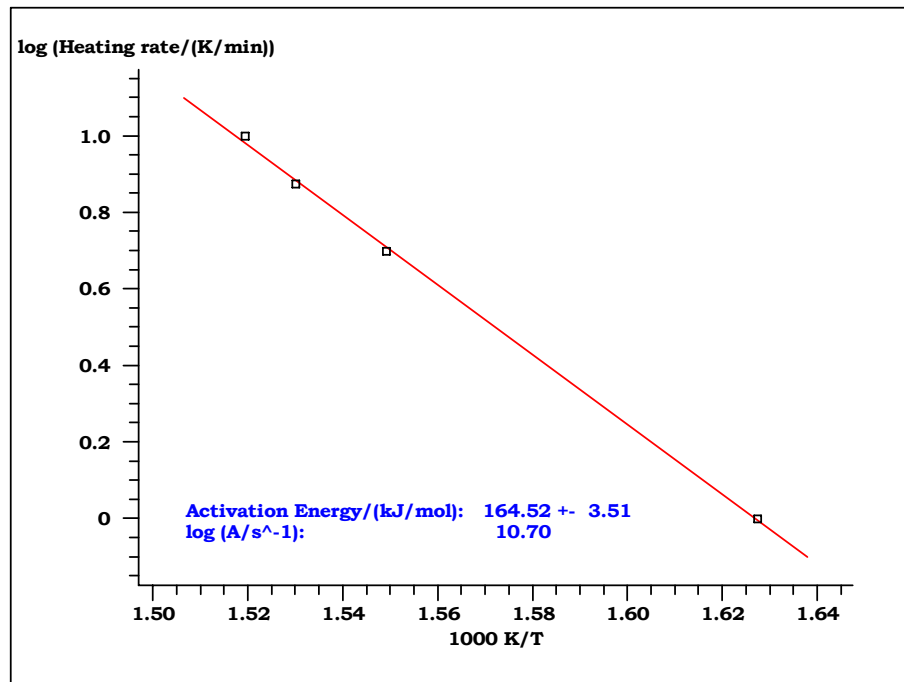


**Figure 6.5.** Kissinger graphs for RTM6 data in nitrogen atmosphere

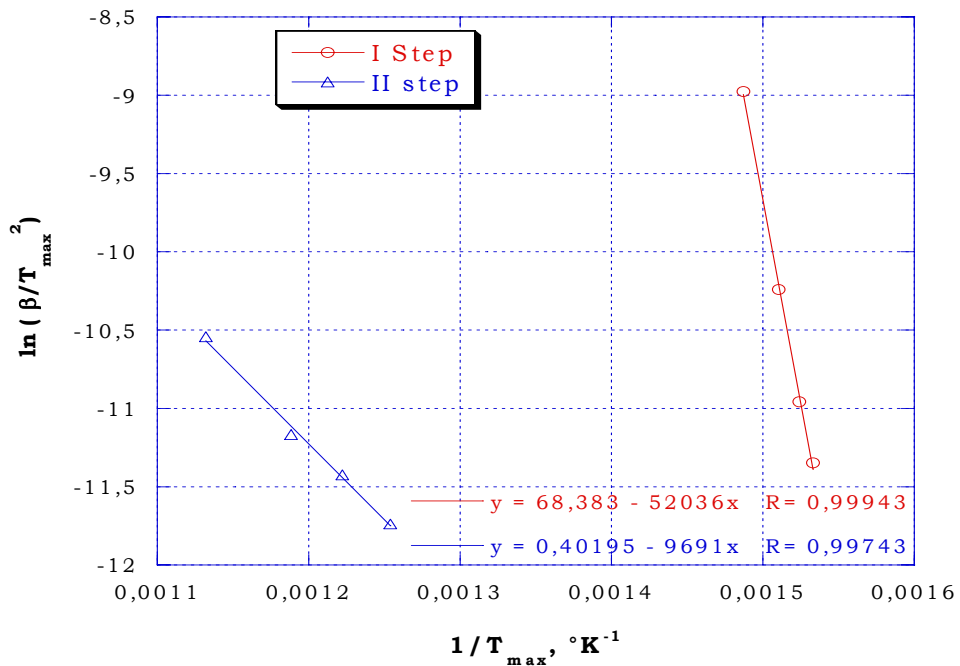


**Figure 6.6.** Kissinger graphs for RTM6 data in air atmosphere

<b>RTM6 NEAT</b>	<b>KISSINGER in nitrogen atmosphere</b>	
	$E_a$ (kJ/mol)	164.52
	<b>KISSINGER in air atmosphere</b>	
	<b>I STEP</b>	<b>II STEP</b>
	$E_a$ (kJ/mol)	
	81.6	115.7

**Table 6.3.** Kissinger data for epoxy resin RTM6 in nitrogen and air atmosphere

The kinetic parameters calculated in nitrogen flow present activation energy values higher than  $E_a$  obtained in air flow. In fact activation energy value in nitrogen flow is 164.52 kJ/mol instead in air flow is 81.6 kJ/mol for first step and 115.7 KJ/mol for second step.

The Flynn-Ozawa-Wall method was also carried out for calculating the activation energy only in nitrogen atmosphere. In figures 6.7 and 6.8 it is reported respectively the Ozawa analysis and activation energy, calculated with Ozawa methods, for epoxy resin RTM6. It is possible to notice that in the nitrogen atmosphere the  $E_a$  increase from conversion zero to 20%, after  $E_a$  is a constant from  $\alpha=0.2$  to  $\alpha=0.7$  and than increase until to  $\alpha=0.85$ .

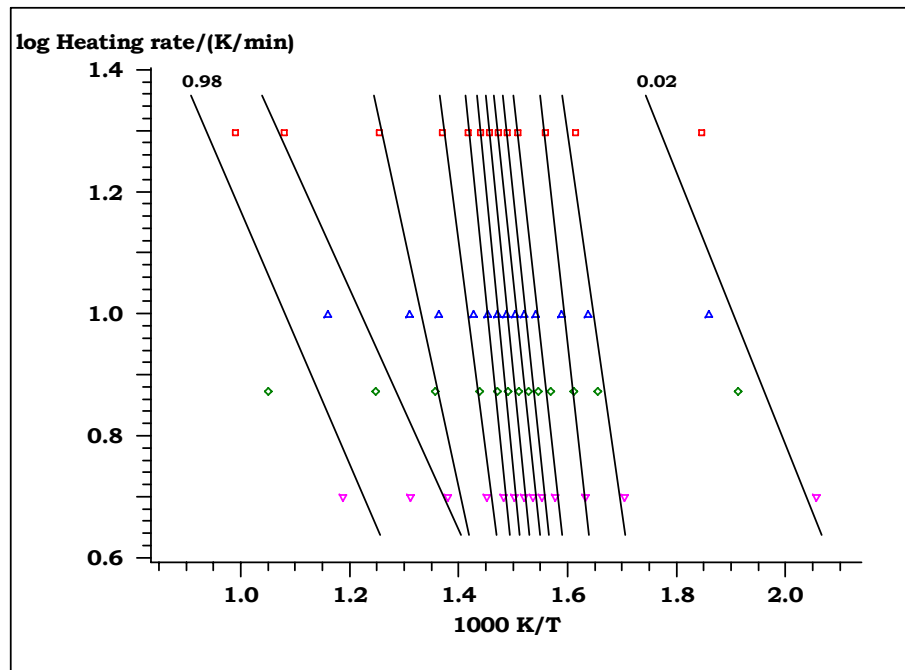


**Figure 6.7.** Ozawa analysis for RTM6 in nitrogen atmosphere

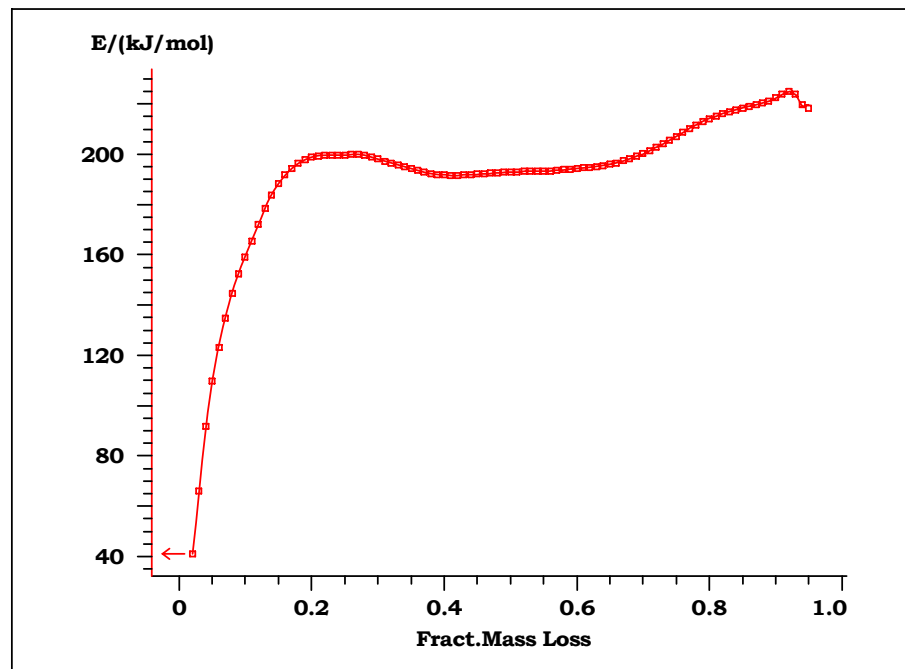


**Figure 6.8.** Energy of activation calculated with Ozawa method for RTM6 in nitrogen atmosphere

The thermogravimetric derivate signal for RTM6/ZB 30 wt% system is showed in figure 6.9 for nitrogen atmosphere and in figure 6.10 for air atmosphere.

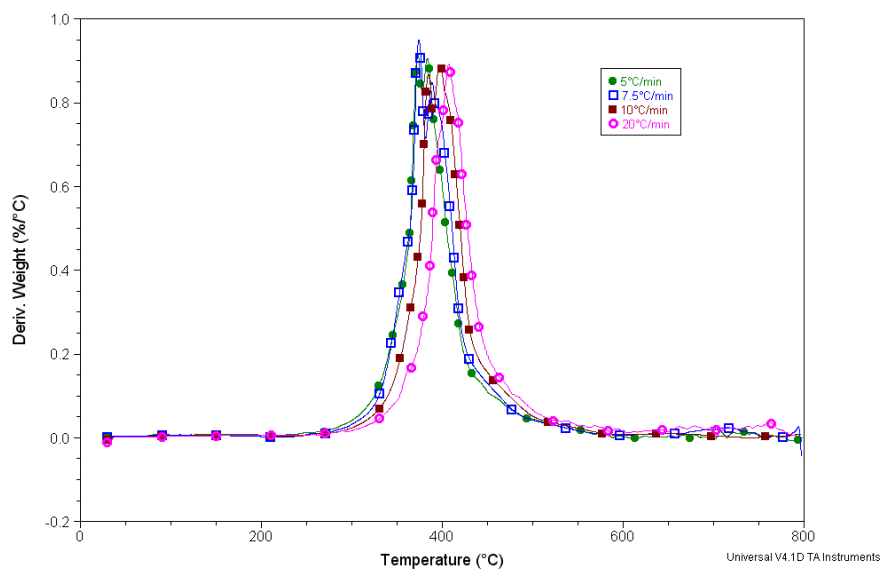


**Figure 6.9.** DTG thermograms of RTM6+ZB 30wt% in nitrogen atmosphere

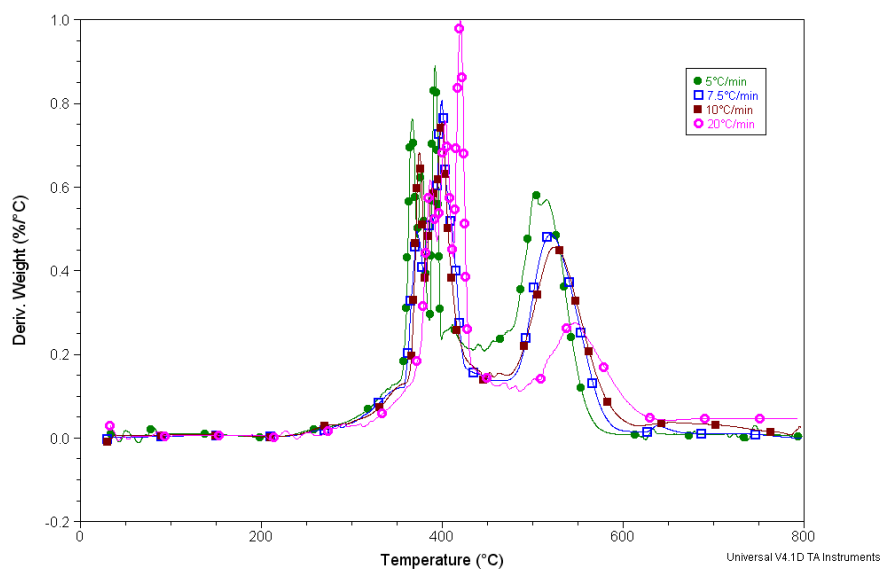


**Figure 6.10.** DTG thermograms of RTM6+ZB 30wt% in air atmosphere

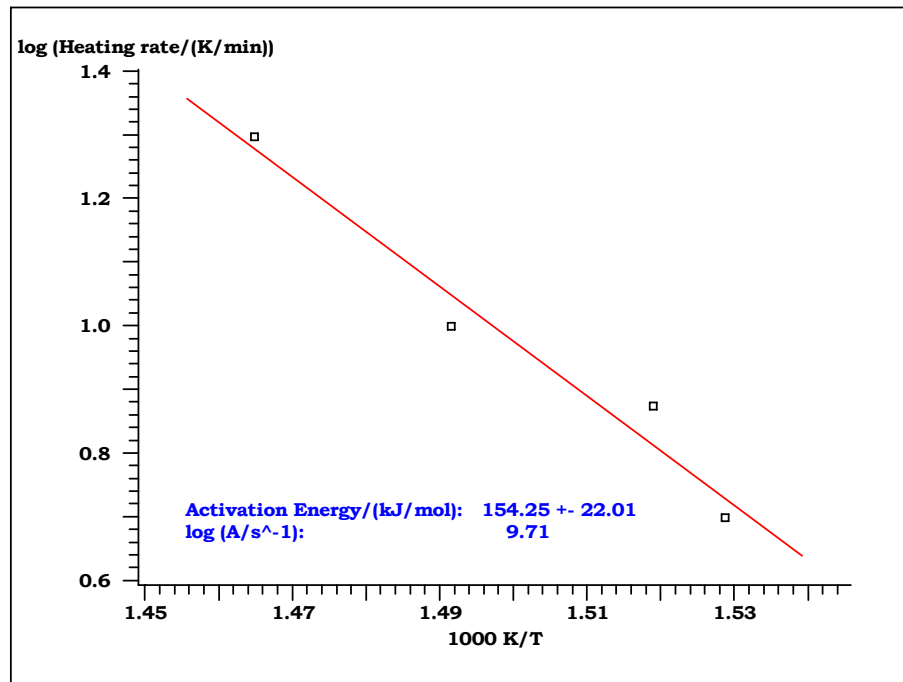


**Figure 6.11.** Kissinger graphs for RTM6+ZB 30wt% data in nitrogen atmosphere

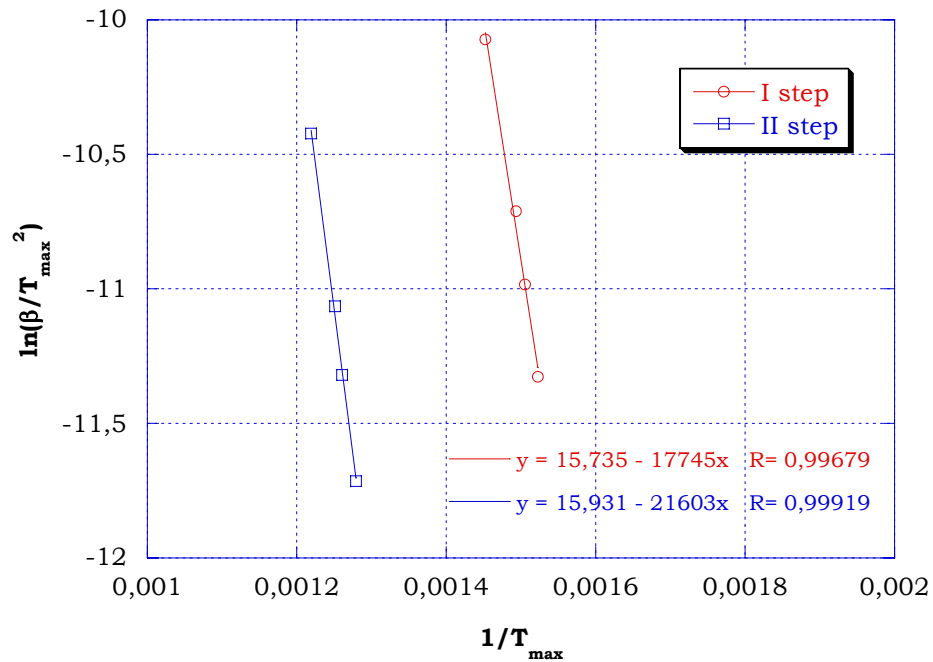


**Figure 6.12.** Kissinger graphs for RTM6+ZB 30wt% data in air atmosphere

The Kissinger analysis in nitrogen atmosphere has demonstrated that the activation energy  $E_a$  is less than the value of epoxy resin hence it doesn't achieve the energy for the degradation of RTM6 neat. Instead in the Kissinger analysis, in air atmosphere, it is shown that the value of

$E_a$  in the second step is higher than the value of RTM6 in fact at the temperature lower 500°C a char on the surface that protects the matrix is produce.

<b>RTM6+ZB 30wt%</b>	<b>KISSINGER in nitrogen atmosphere</b>	
	$E_a$ (kJ/mol)	154.25
	<b>KISSINGER in air atmosphere</b>	
	<b>I STEP</b>	<b>II STEP</b>
	$E_a$ (kJ/mol)	
	147.54	179.62

**Table 6.4.** Kissinger data for RTM6+ZB 30wt% in nitrogen and air atmosphere

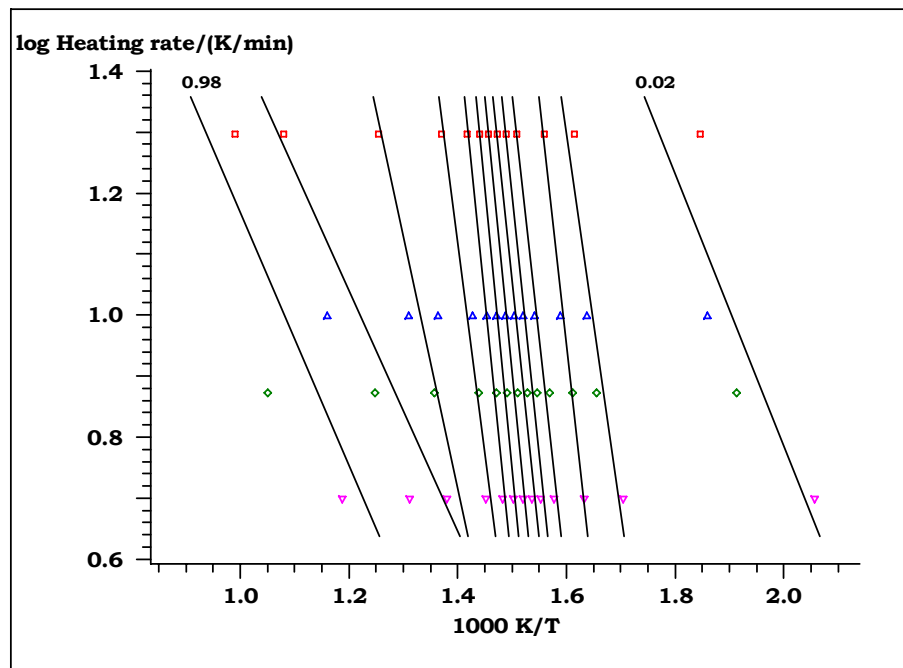


**Figure 6.13.** Ozawa analysis for RTM6+ZB 30wt% in nitrogen atmosphere

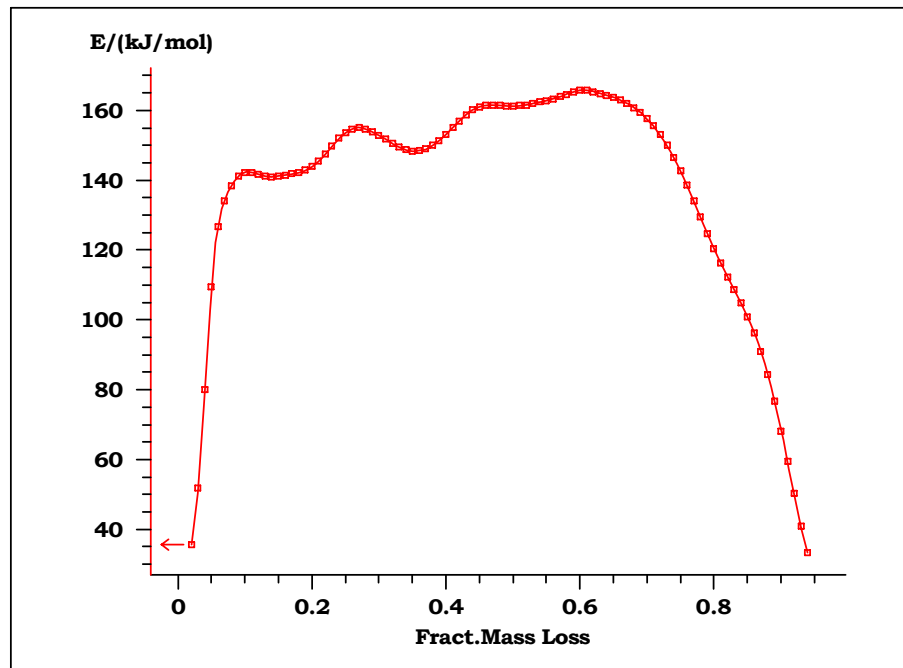


**Figure 6.14.** Energy of activation calculated with Ozawa method for RTM6+ZB 30wt% in nitrogen atmosphere

In the nitrogen atmosphere, the Ozawa analysis confirms the positive effect of zinc borate on the epoxy resin RTM6 because with low conversion values the activation energy  $E_a$  is less than 50kJ/mol while for conversion degrees between 0.1 and 0.8 a multi-step degradation process is shown. The presence of this step means that several layers of char on the surface of the RTM6 have been created.

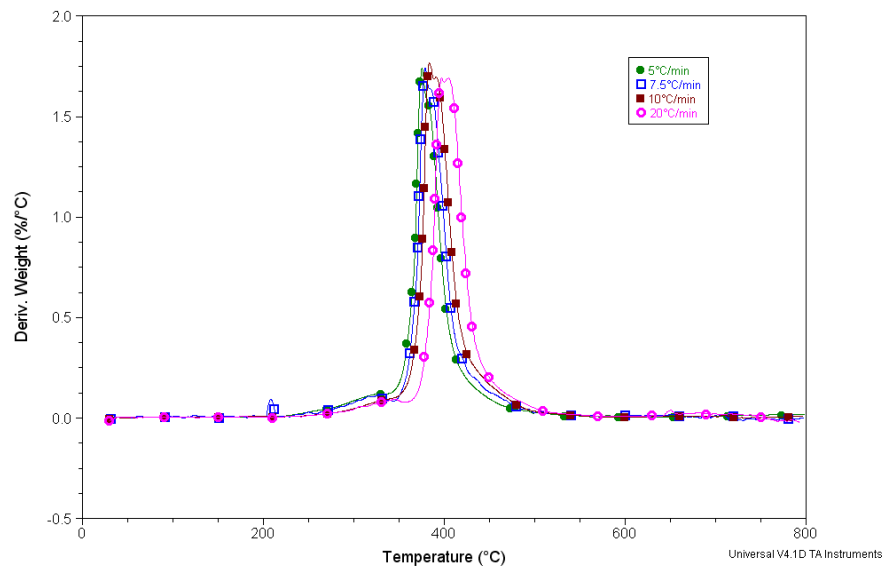


**Figure 6.15.** DTG of RTM6+ATH 30 wt% in nitrogen atmosphere

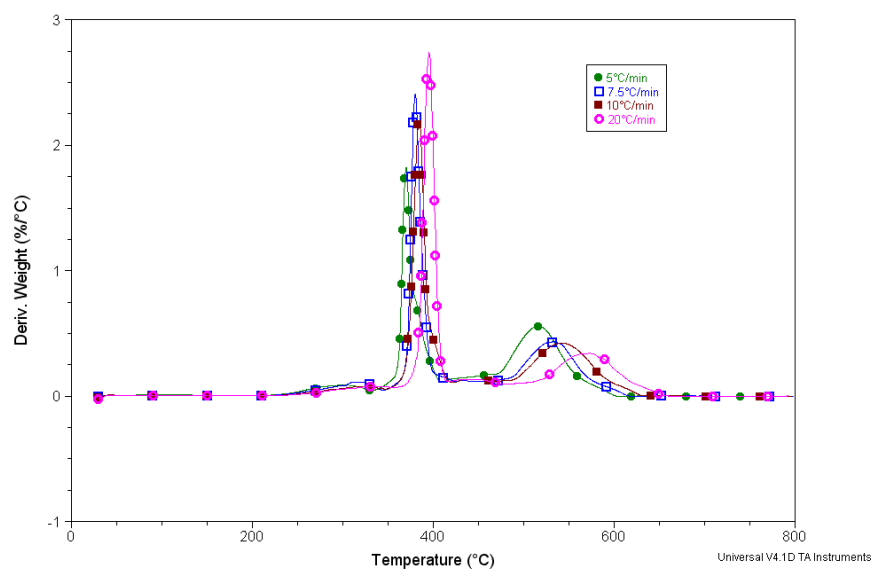


**Figure 6.16.** DTG of RTM6+ATH 30 wt% in air atmosphere

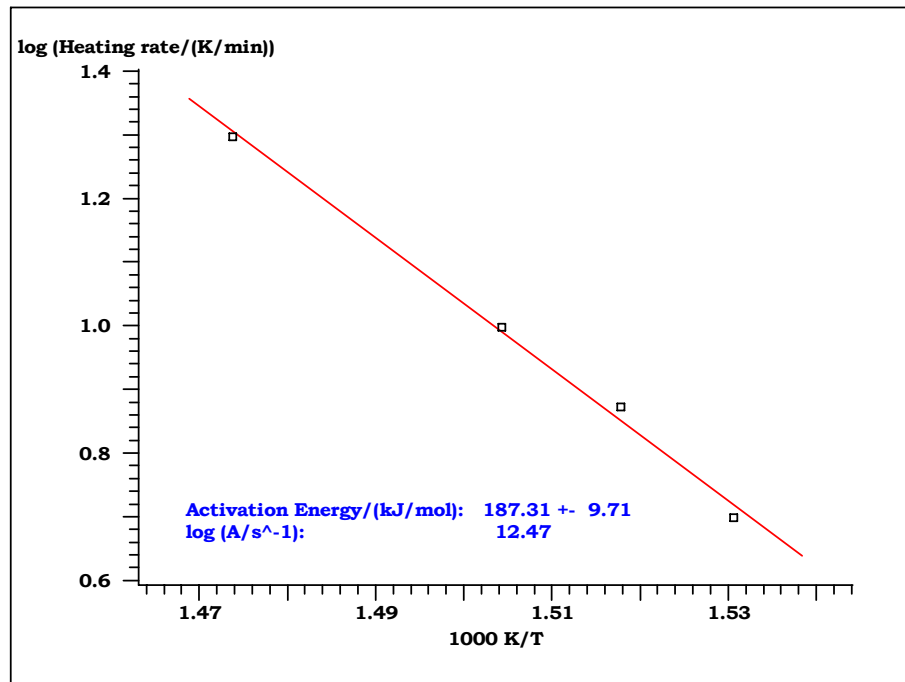


**Figure 6.17.** Kissinger graphs for RTM6+ATH 30 wt% data in nitrogen atmosphere

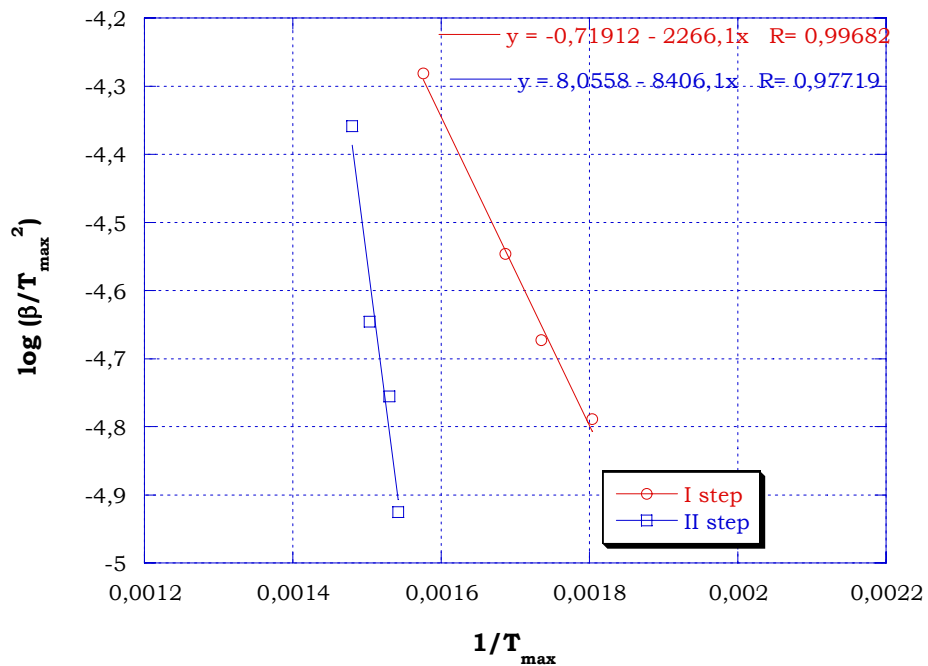


**Figure 6.18.** Kissinger graphs for RTM6+ATH 30 wt% data in nitrogen atmosphere

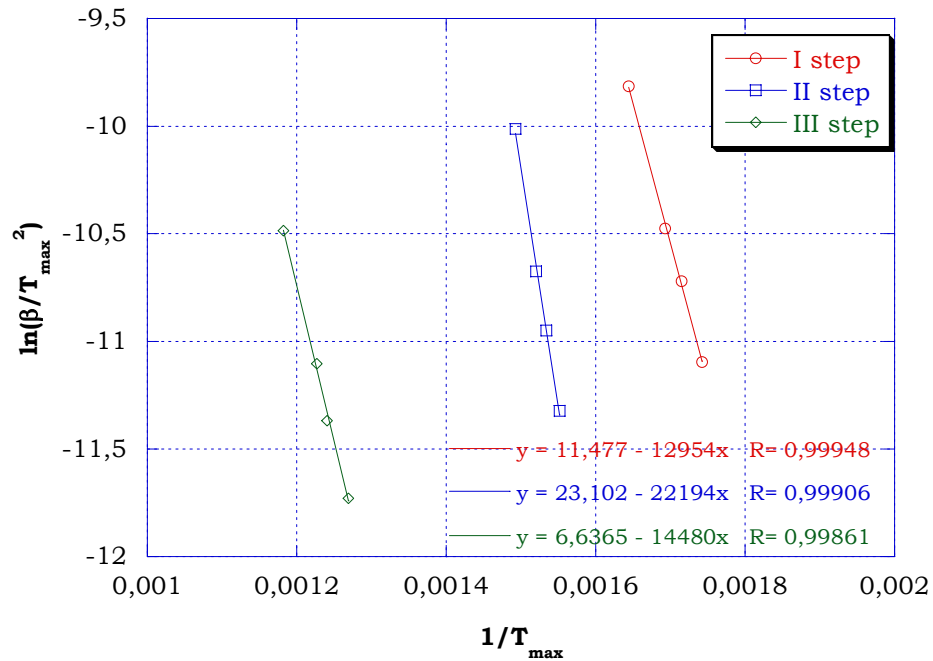


**Figure 6.19.** Kissinger graphs for RTM6+ATH 30 wt% data in air atmosphere

RTM6+ATH 30wt%	KISSINGER in nitrogen atmosphere		
	I STEP		II STEP
	E <sub>a</sub> (kJ/mol)		
	18.841	69.89	
	KISSINGER in air atmosphere		
	I STEP	II STEP	III STEP
	E <sub>a</sub> (kJ/mol)		
107.7	184.5	120.4	

**Table 6.5.** Kissinger data for RTM6+ATH 30wt% in nitrogen and air atmosphere

In this case there are three degradation steps in the Kissinger analysis in air atmosphere of aluminium trihydrate. By varying the temperature the following process occurred sequentially:

- dehydration of hydroxyl groups,
- formation of aluminized layer protection,
- pyrolysis of char.

For every step it is possible to associate the activation energy, which is greater than  $E_a$  of RTM6 hence it represents a slower degradation

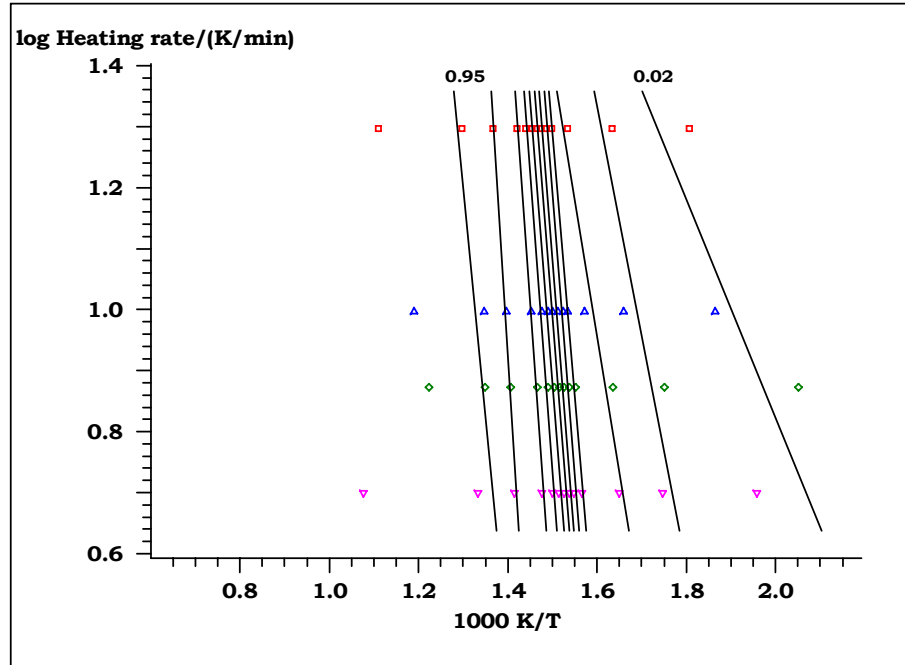


**Figure 6.20.** Ozawa analysis for RTM6+ATH 30wt% in nitrogen atmosphere

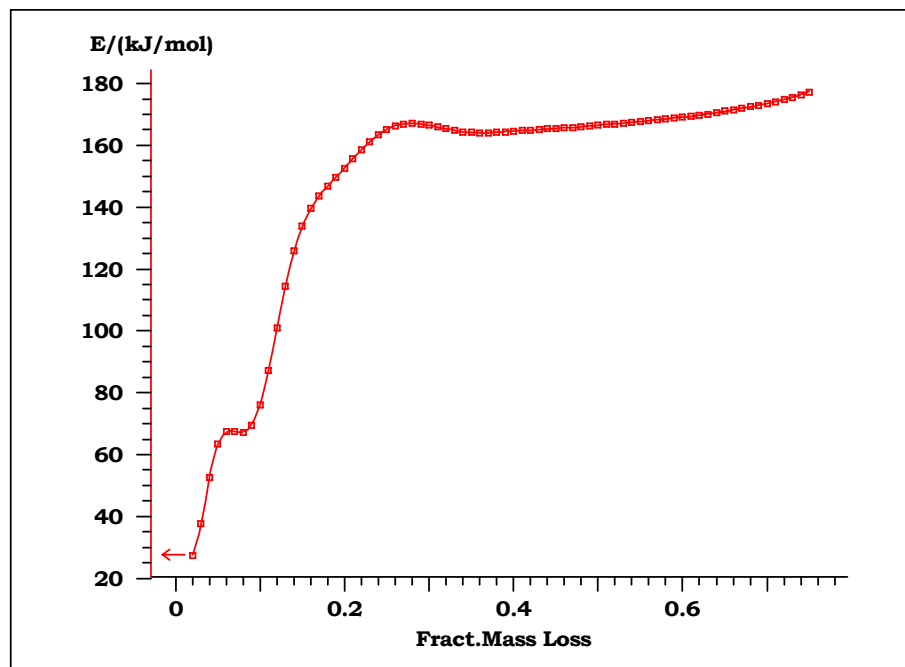


**Figure 6.21.** Energy of activation calculated with Ozawa methods for RTM6+ATH 30wt% in nitrogen atmosphere

In the Ozawa analysis it is demonstrated that the  $E_a$  starts to lower values than both RTM6 and ZB in fact  $E_a$  starts to 25 kJ/mol and two different steps are observed. In the first step  $E_a$  is 70 kJ/mol for  $\alpha=0.1$  while in the second step  $E_a$  is 160 kJ/mol with conversion degree  $\alpha$  between 0.2 and 0.7.

The TGA thermograms of the epoxy resin containing zinc borate and aluminium trihydrate is reported in figures 6.22 and 6.23 to study the kinetic parameters for synergistic effects of zinc borate.

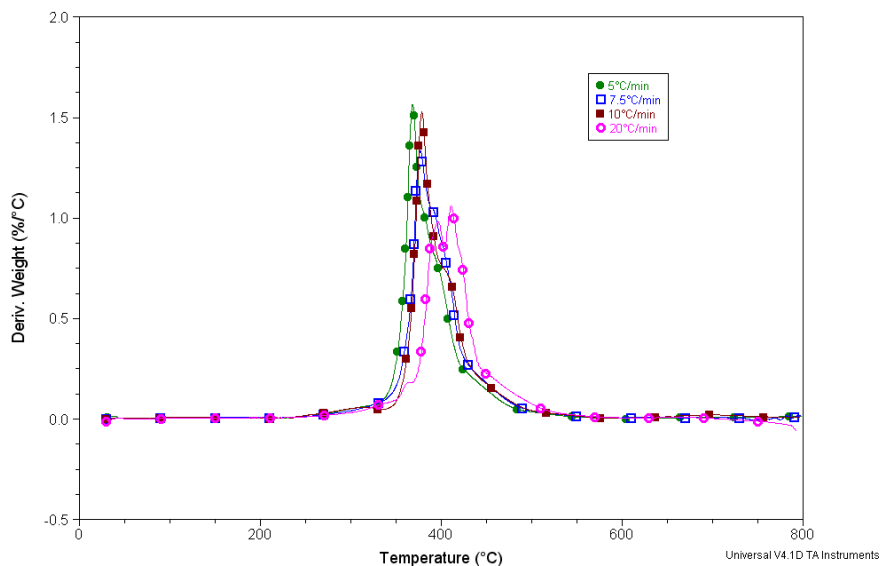


**Figure 6.22.** DTG of RTM6+ATH+ZB 30 wt% in air atmosphere

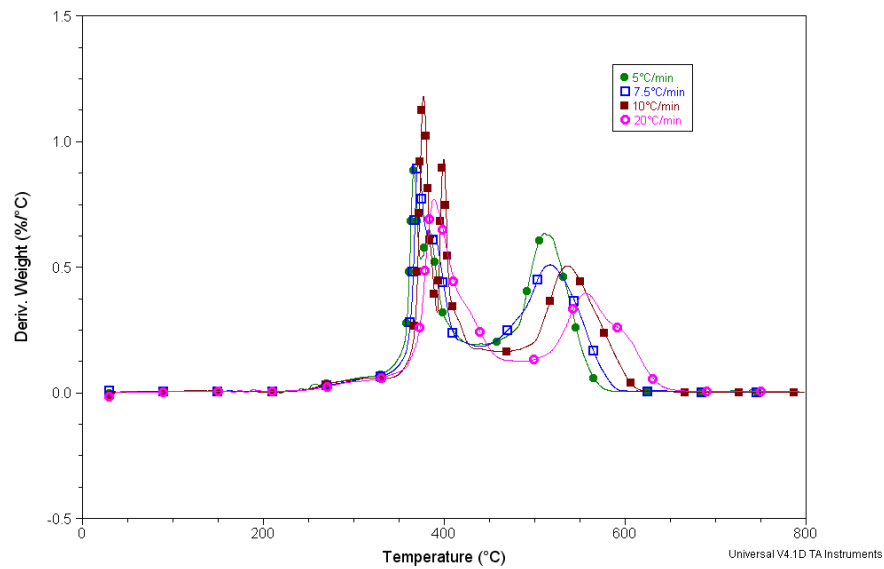


**Figure 6.23.** DTG of RTM6+ATH+ZB 30 wt% in air atmosphere

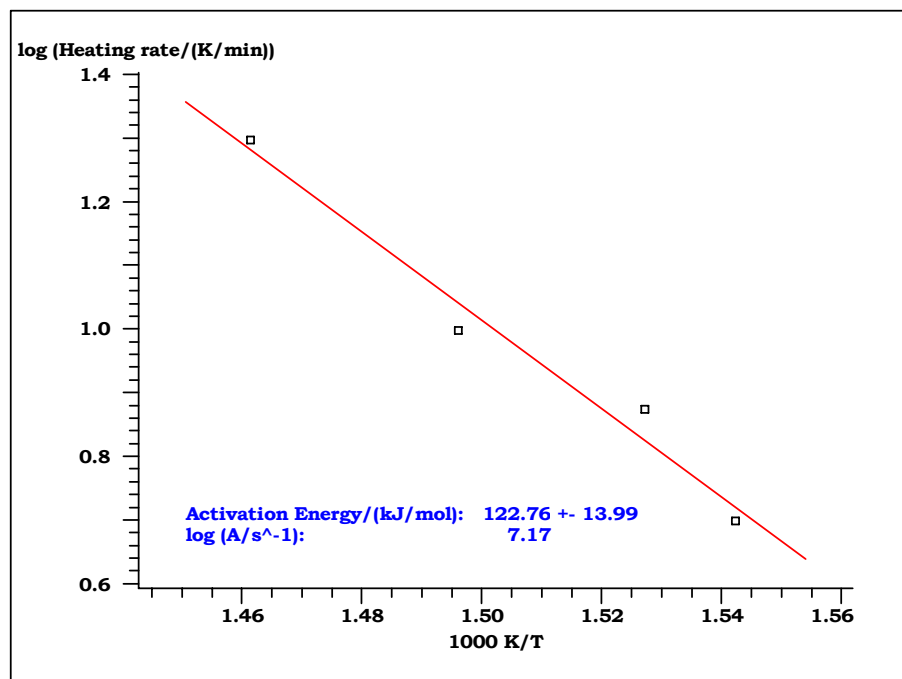


**Figure 6.24.** Kissinger graphs for RTM6+ATH+ZB 30 wt% system data in nitrogen atmosphere

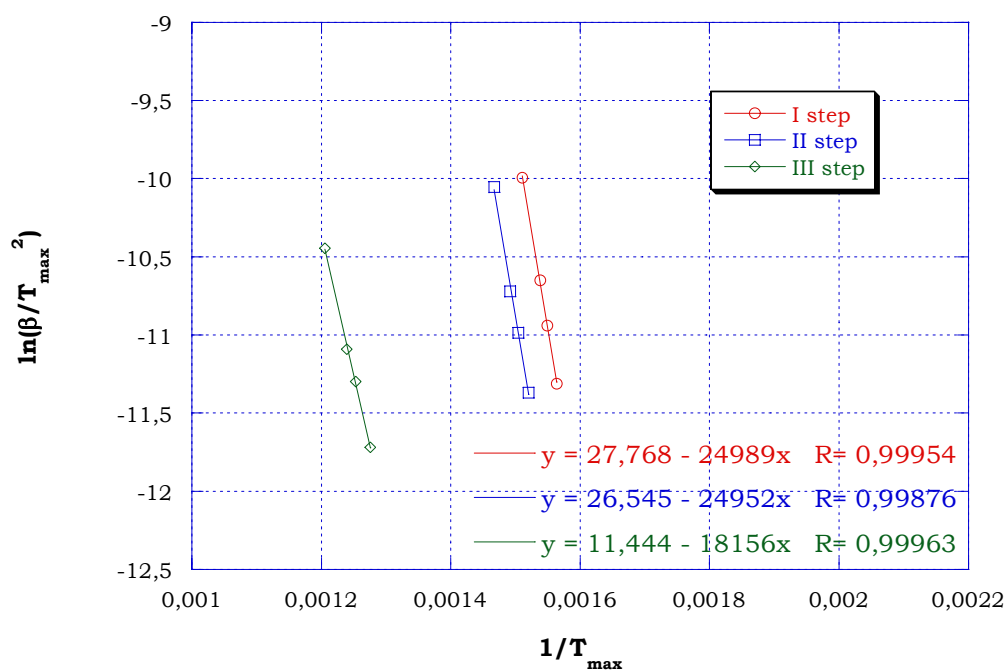


**Figure 6.25.** Kissinger graphs for RTM6+ATH+ZB 30wt% system data in air atmosphere

<b>RTM6+ATH+ZB 30wt%</b>	<b>KISSINGER in nitrogen atmosphere</b>		
	$E_a$ (kJ/mol)	122.76	
	<b>KISSINGER in air atmosphere</b>		
	<b>I STEP</b>	<b>II STEP</b>	<b>III STEP</b>
	$E_a$ (kJ/mol)		
	207.7	207.5	150.9

**Table 6.6.** Kissinger data for RTM6+ATH+ZB 30wt% in nitrogen and air atmosphere

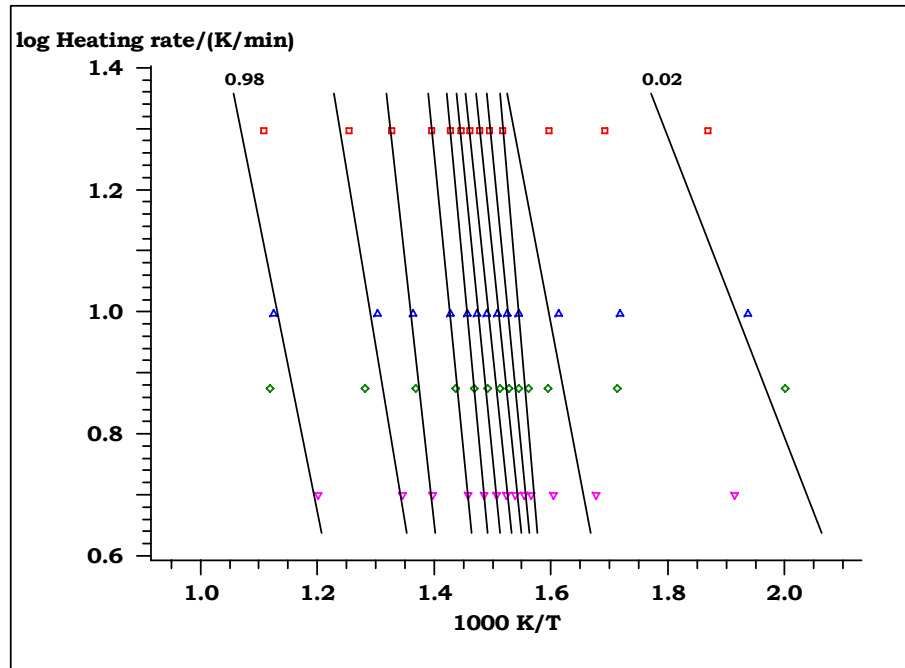


**Figure 6.26.** Ozawa analysis for RTM6+ATH+ZB 30wt% system in nitrogen atmosphere

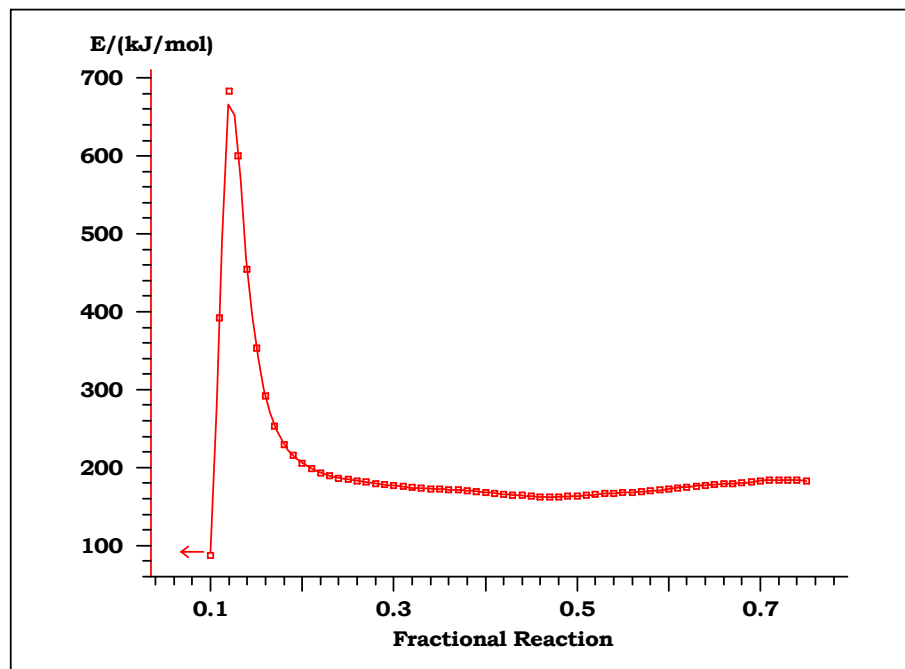


**Figure 6.27.** Energy of activation calculated with Ozawa methods for RTM6+ATH+ZB 30wt% system in nitrogen atmosphere

The presence of both additives is clear in the Kissinger analysis and the synergistic effect is shown in the Ozawa analysis because at low levels of alpha  $E_a$  is higher. In fact  $E_a$  increases for values of alpha around 0.1 and remains constant value of 200 kJ/mol throughout the range of conversion. Consequently it is necessary a higher energy than in respect to the same additives taken individually and RTM6 neat to complete the degradation process.

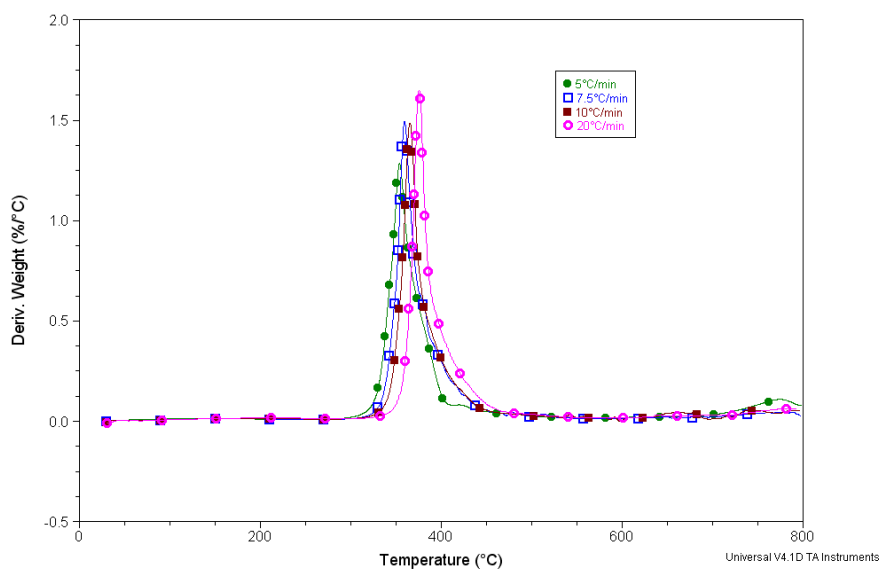


**Figure 6.28.** DTG of RTM6+ZS 30 wt% in nitrogen atmosphere

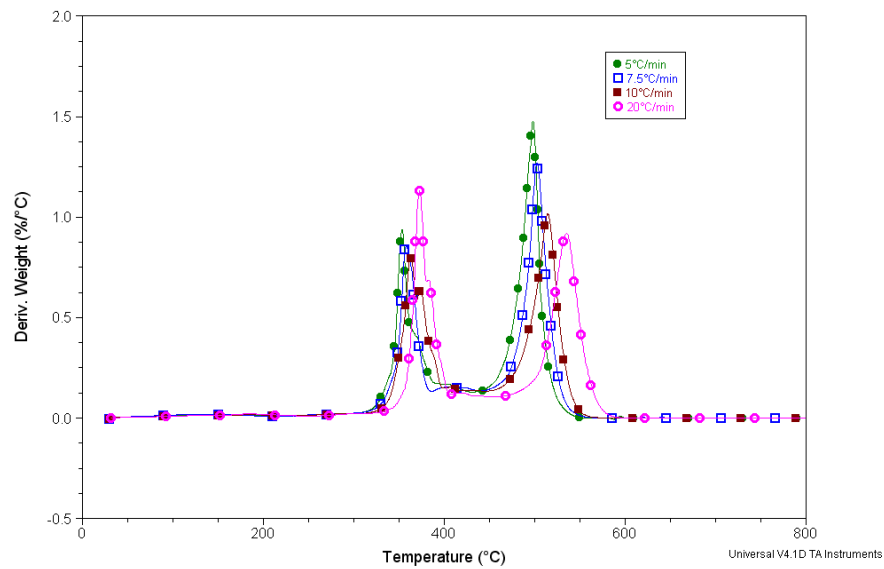


**Figure 6.29.** DTG of RTM6+ZS 30 wt% in air atmosphere

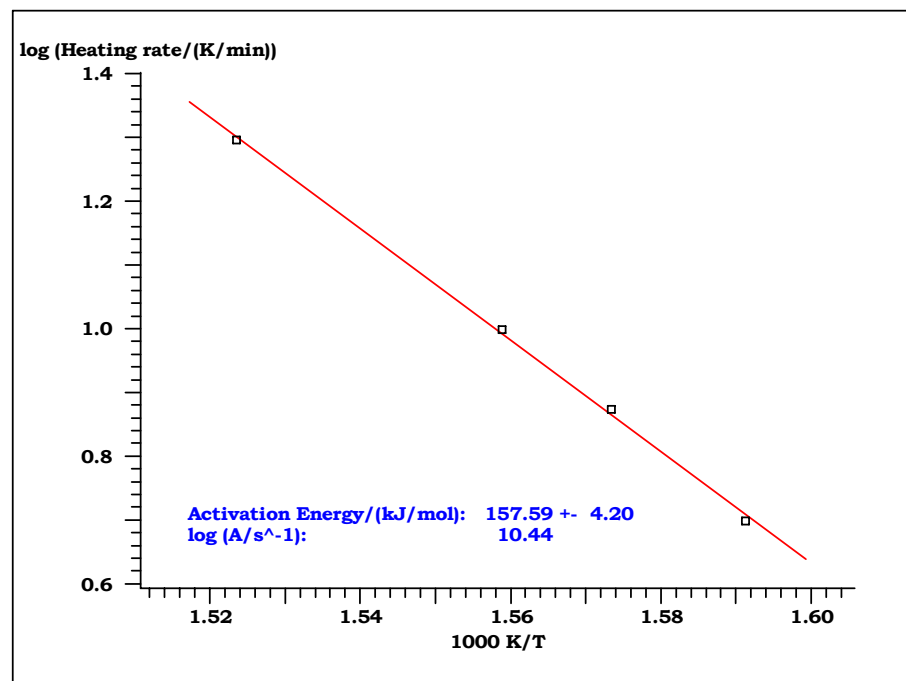


**Figure 6.30.** Kissinger graphs for RTM6+ZS 30 wt% data in nitrogen atmosphere

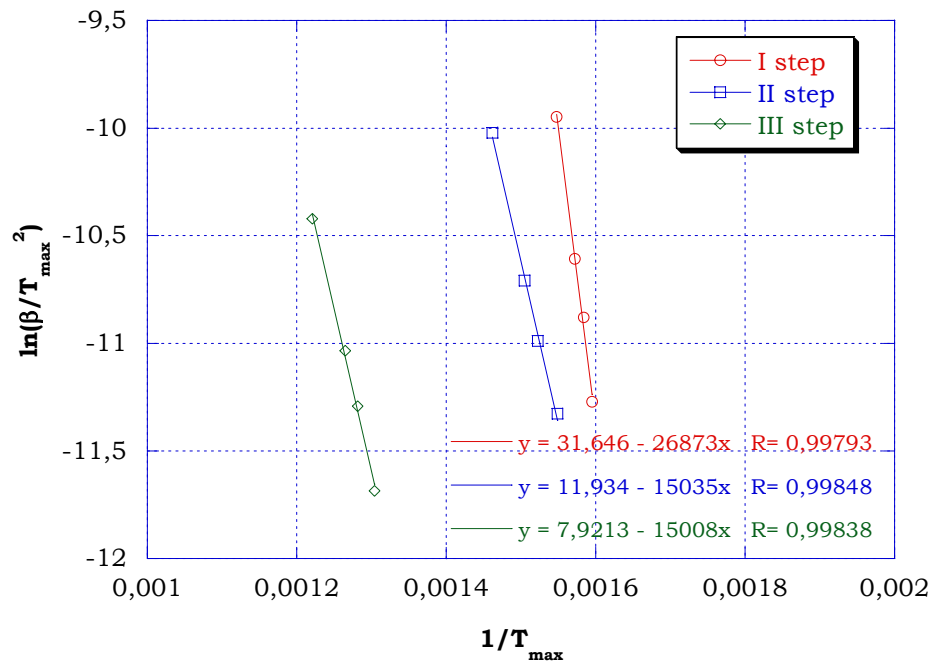


**Figure 6.31.** Kissinger graphs for RTM6+ZS 30 wt% data in air atmosphere

RTM6+ZS 30wt%	<b>KISSINGER in nitrogen atmosphere</b>		
	E <sub>a</sub> (kJ/mol)	157.6	
	<b>KISSINGER in air atmosphere</b>		
	<b>I STEP</b>	<b>II STEP</b>	<b>III STEP</b>
	E <sub>a</sub> (kJ/mol)		
	223.4	125	124.8

**Table 6.6.** Kissinger data for RTM6+ZS 30wt% in nitrogen and air atmosphere

Zinc stannate is similar to ATH for Kissinger analysis because also in this case there are three degradation steps. The discussion on the structure of char isn't like ATH because there isn't the aluminium and because the second and third degradation step need a lower energy to be completed hence it is explained that the protection action is partly missing.

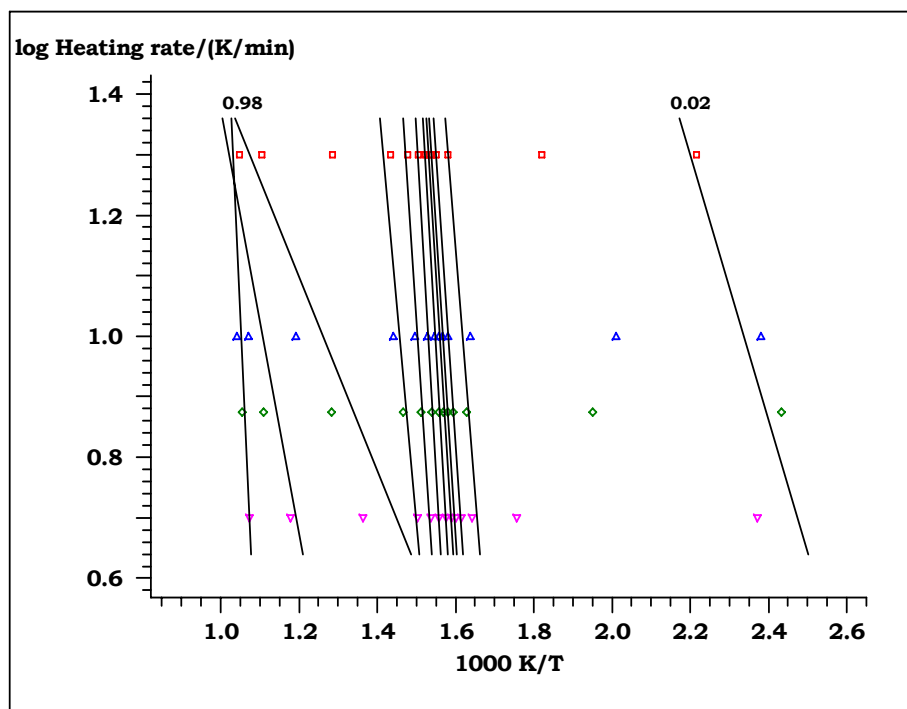


**Figure 6.32.** Ozawa analysis for RTM6+ZS 30wt% in nitrogen atmosphere

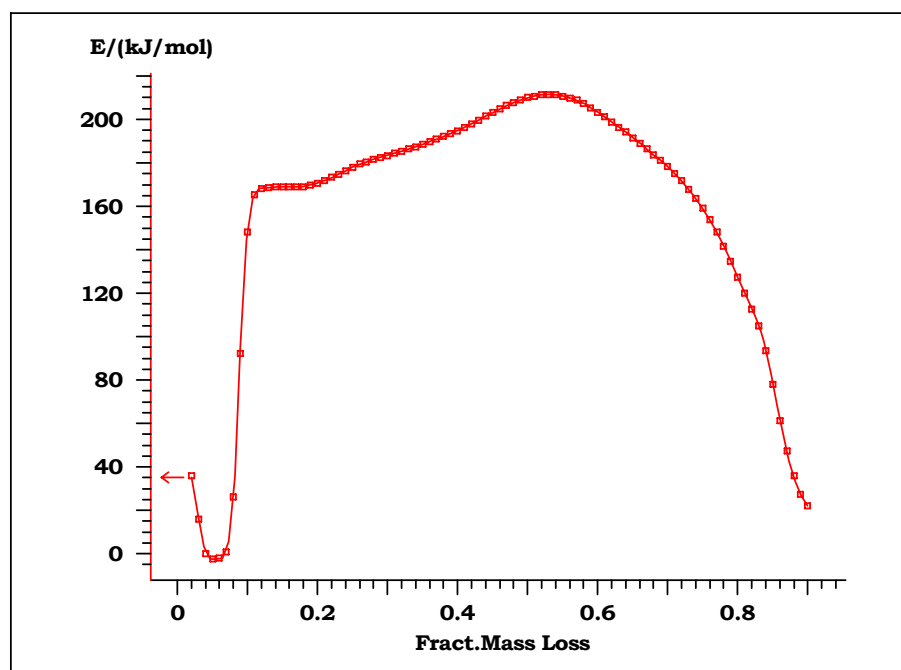


**Figure 6.33.** Energy of activation calculated with Ozawa methods for RTM6+ZS in nitrogen atmosphere

In the Ozawa analysis in nitrogen atmosphere the activation energy has a maximum peak of 200 kJ/mol around to  $\alpha=0.6$  and neither a constant evolution nor several degradation steps are shown.

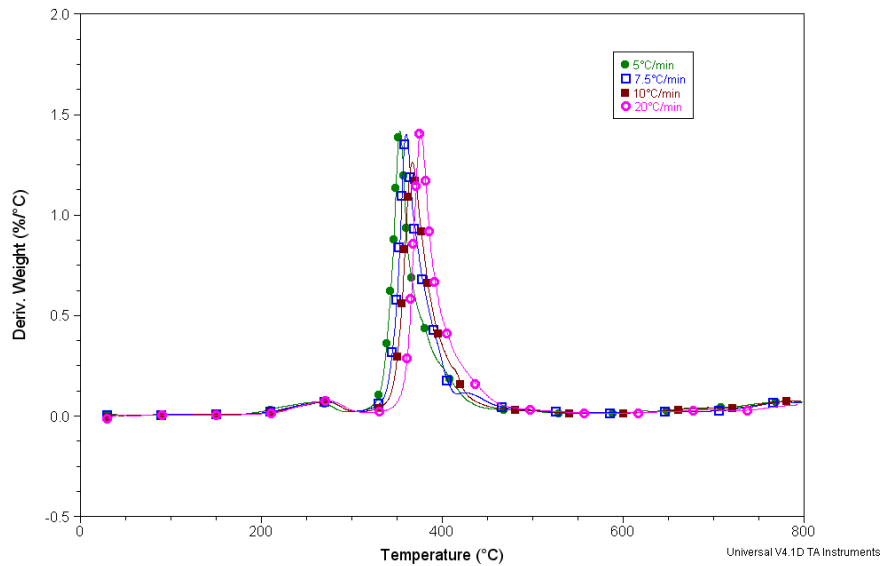


**Figure 6.34.** DTG of RTM6+ZHS 30 wt% in nitrogen atmosphere

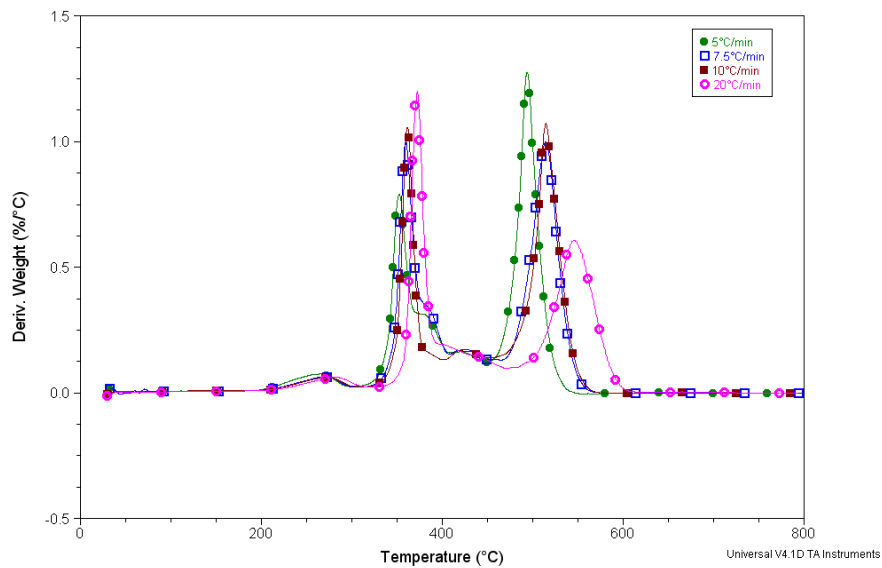


**Figure 6.35.** DTG of RTM6+ZHS 30 wt% in air atmosphere

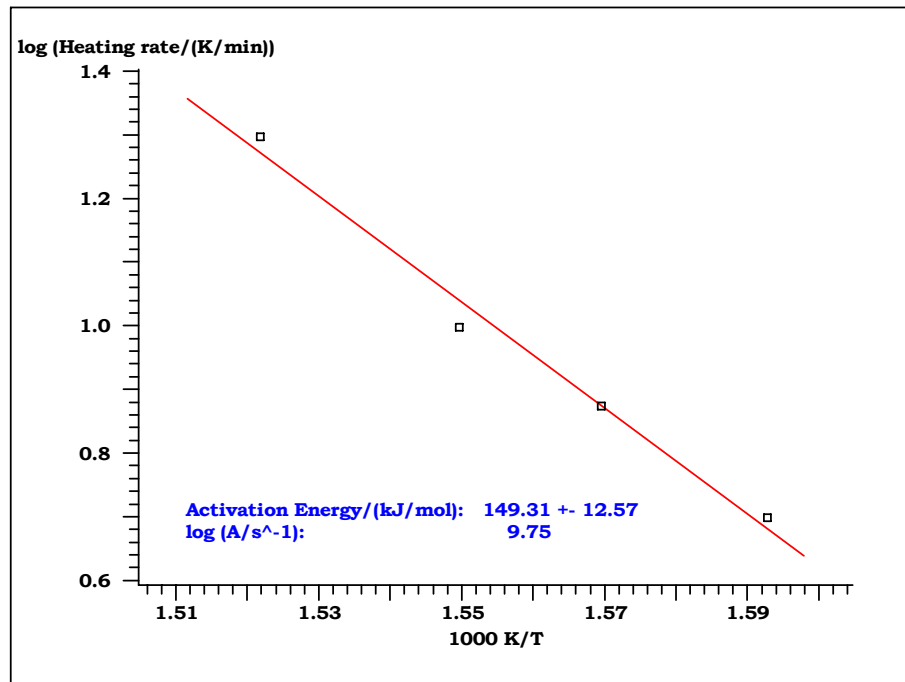


Figure 6.36. Kissinger graphs for RTM6+ZHS 30 wt% data in nitrogen atmosphere

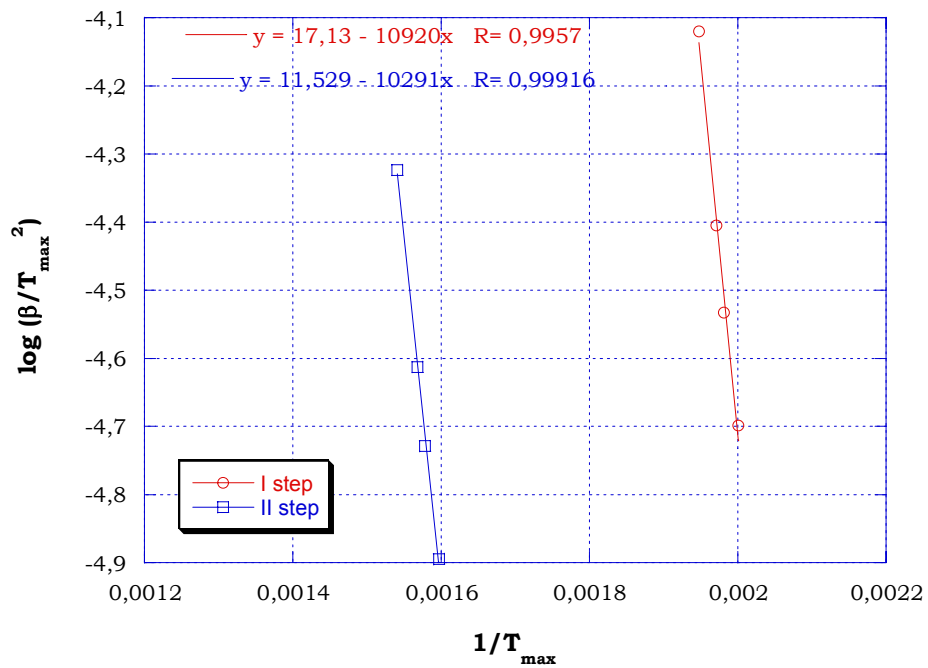
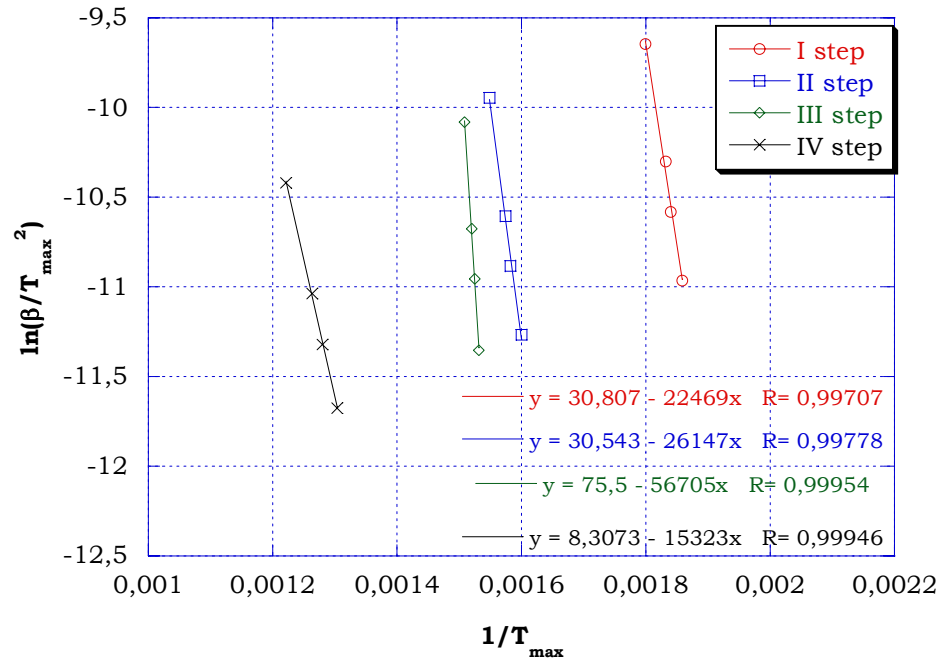


Figure 6.37. Kissinger graphs for RTM6+ZHS 30 wt% data in nitrogen atmosphere



**Figure 6.38.** Kissinger graphs for RTM6+ZHS 30 wt% data in air atmosphere

RTM6+ZHS 30wt%	KISSINGER in nitrogen atmosphere			
	I STEP		II STEP	
	E <sub>a</sub> (kJ/mol)			
	90.8		85.564	
	KISSINGER in air atmosphere			
	I STEP	II STEP	III STEP	IV STEP
	E <sub>a</sub> (kJ/mol)			
186.8	217.4	471.5	127.4	

**Table 6.7.** Kissinger data for RTM6+ZHS 30wt% in nitrogen and air atmosphere

Zinc hydroxystannate shows four degradation steps therefore the degradation mechanism is particularly complex and to create the protective layer a high energy contribution (471 kJ/mol) is necessary.

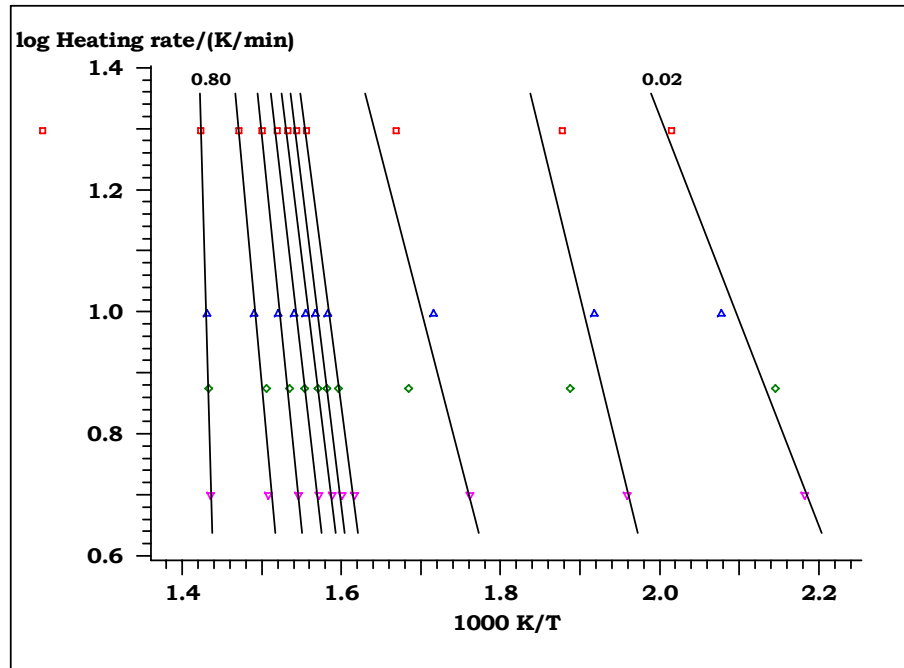


**Figure 6.39.** Ozawa analysis for RTM6+ZHS 30wt% in nitrogen atmosphere

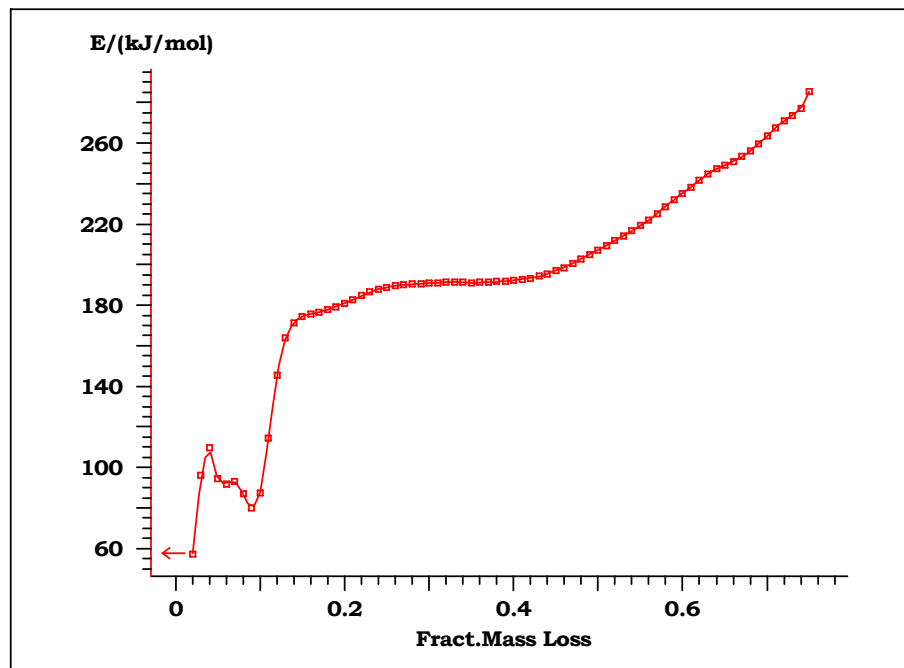


**Figure 6.40.** Energy of activation calculated with Ozawa methods for RTM6+ZHS in nitrogen atmosphere

In the Ozawa analysis there are several steps and  $E_a$  is constant at the value of 180 kJ/mol between alpha 0.1 to 0.5 and  $E_a$  increases until

270 kJ/mol where is obtained to complete the degradation process of degradation

### 6.3 Kinetic degradations of RTM6 and carbon nanotubes

The thermal properties of CNTs/polymer composites also attracted many attentions from polymer scientists because CNTs have very high thermal stability [10-14]. Yang et al. [11] reported the effect of single-walled carbon nanotubes (SWNTs) on the thermal stability of acrylonitrilebutadiene styrene (ABS)/SWNTs composites. They found that the addition of SWNTs destabilized ABS and caused the composites to degrade at lower temperatures. Probst et al. [12] revealed that MWNTs promote the degradation of polyvinyl alcohol. In contrast, Kashiwagi et al. [13] observed an increased thermal stability of MWNTs/polypropylene (PP) composites. The same effect of MWNTs on PP was found by Yang et al. [14]. From the above publications, both promoting and hindering effects of CNTs on the thermal stability of polymer are found. The structure of the polymer matrix and the interaction between CNTs and the matrix may be the key factors for the thermal degradation behaviour of CNTs filled polymer composites.

DTG curves of RTM6 with 0.1wt% MWNTs under nitrogen and air environments are showed in figures 6.39 and 6.40 respectively. One step decomposition is found under nitrogen atmosphere, while two step decomposition (second step from 450°C to 700°C) are found under air atmosphere.

Heating rate (°C/min)	T <sub>onset</sub> (°C)	T <sub>max</sub> (°C)
5°C/min	317	376
7.5°C/min	334	387
10°C/min	334	391
20°C/min	348	404

**Table 6.8.** T<sub>onset</sub> and T<sub>max</sub> of RTM6+MWNT 0.1wt% in nitrogen atmosphere

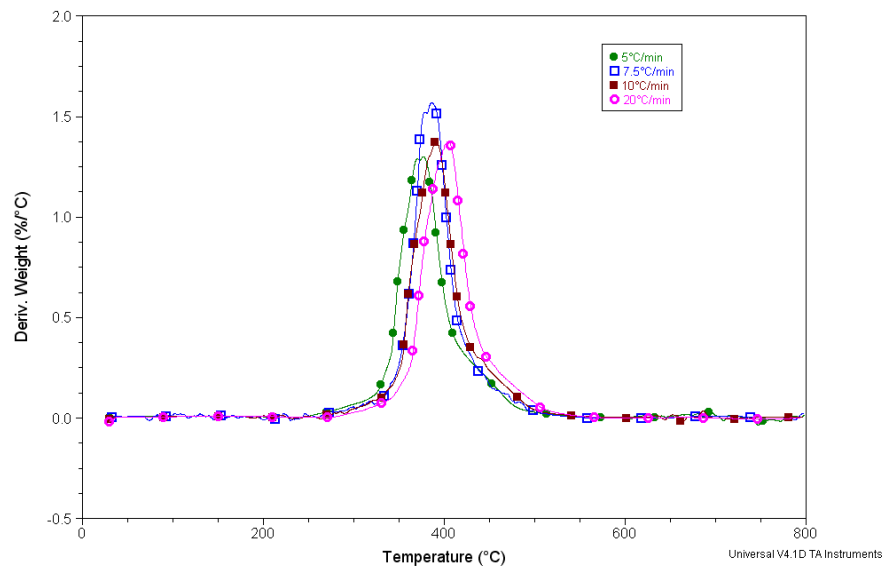


**Figure 6.41.** DTG of RTM6+MWNT 0.1wt% in nitrogen atmosphere

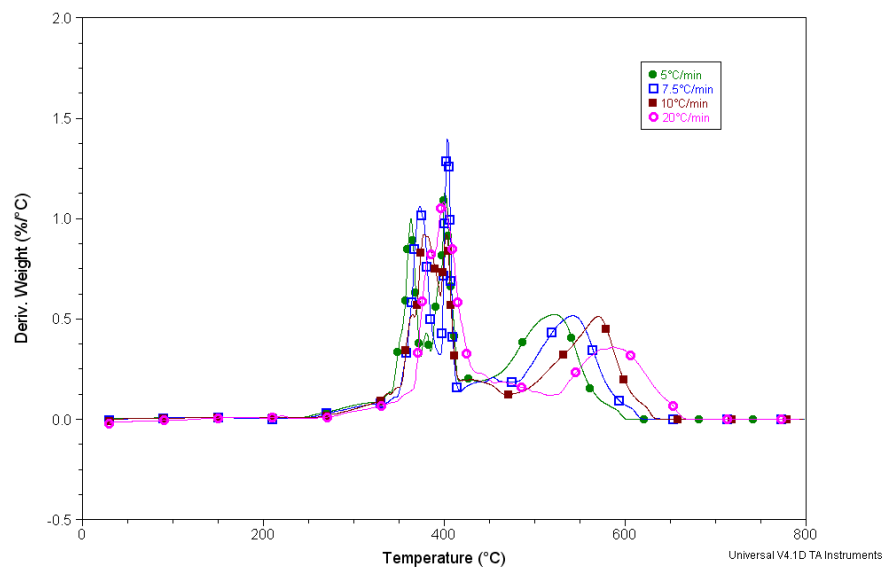


**Figure 6.42.** DTG of RTM6+MWNT 0.1wt% in air atmosphere

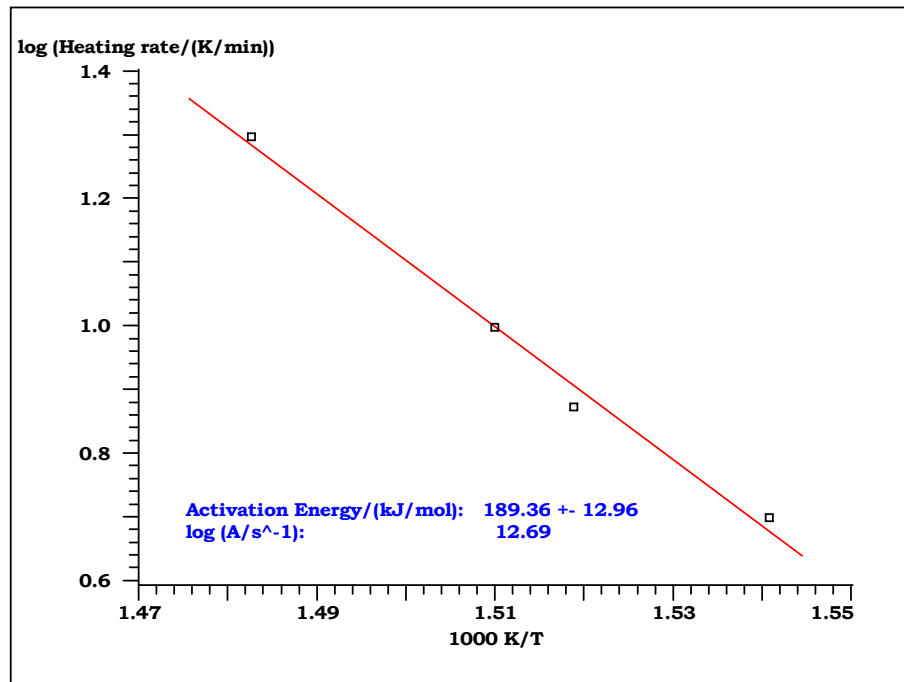


**Figure 6.43.** Kissinger graphs for RTM6+MWNT 0.1wt% data in nitrogen atmosphere

The  $E_a$  of neat RTM6 is found to be 164 KJ/mol while MWNTs/RTM6 composites is found to be 189 KJ/mol, suggesting that the MWNTs increase the thermal stability of RTM6 under nitrogen atmosphere.

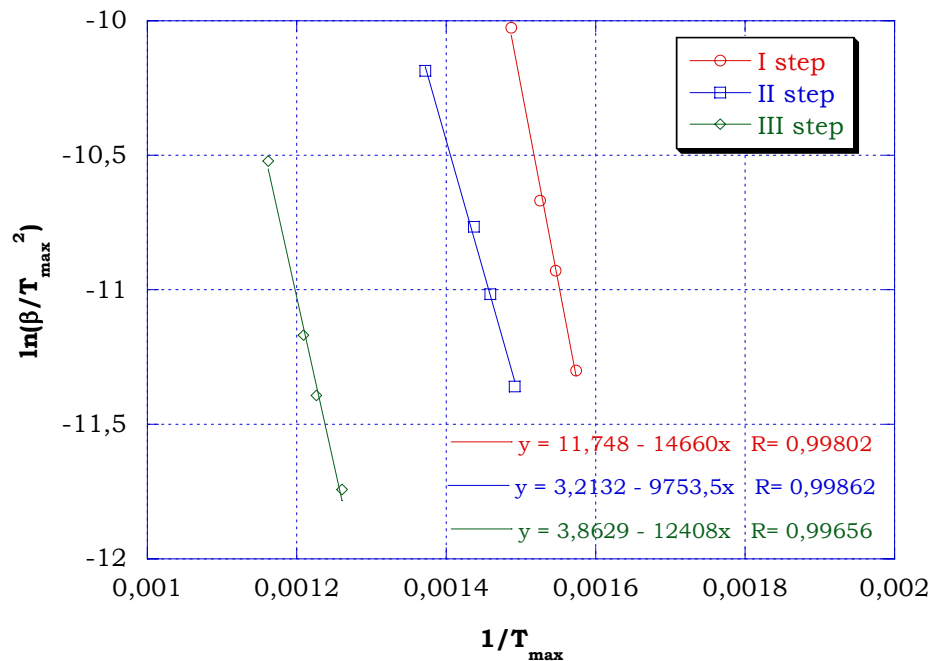


**Figure 6.44.** Kissinger graphs for RTM6+MWNT 0.1wt% data in air atmosphere

There are three steps although the small amount of carbon nanotubes demonstrates that the degradation process has been altered. The first step is given by the of epoxy resin with carbon nanotubes. The second step is divided in two steps where in the first is lower than of the resin and the second step is the pyrolysis of the char that happens with an additional energy contribution.

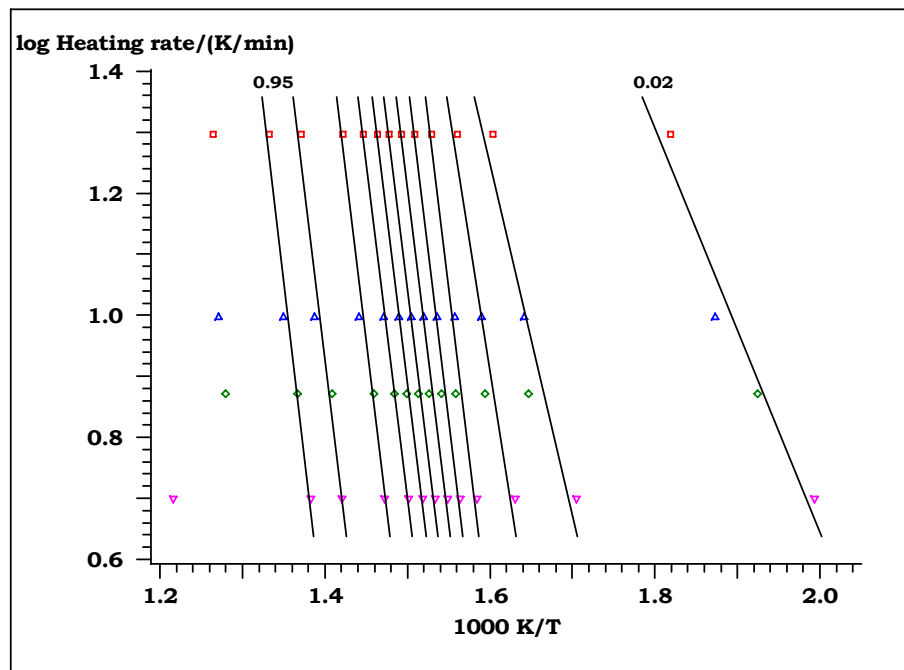


**Figure 6.45.** Ozawa analysis for RTM6+MWNT 0.1 wt% in nitrogen atmosphere

In the Ozawa data a higher thermal stability than RTM6 is shown because  $E_a$  starts by higher values but it is stable at about 200 kJ/mol for  $\alpha$  between 0.1 and 0.9.

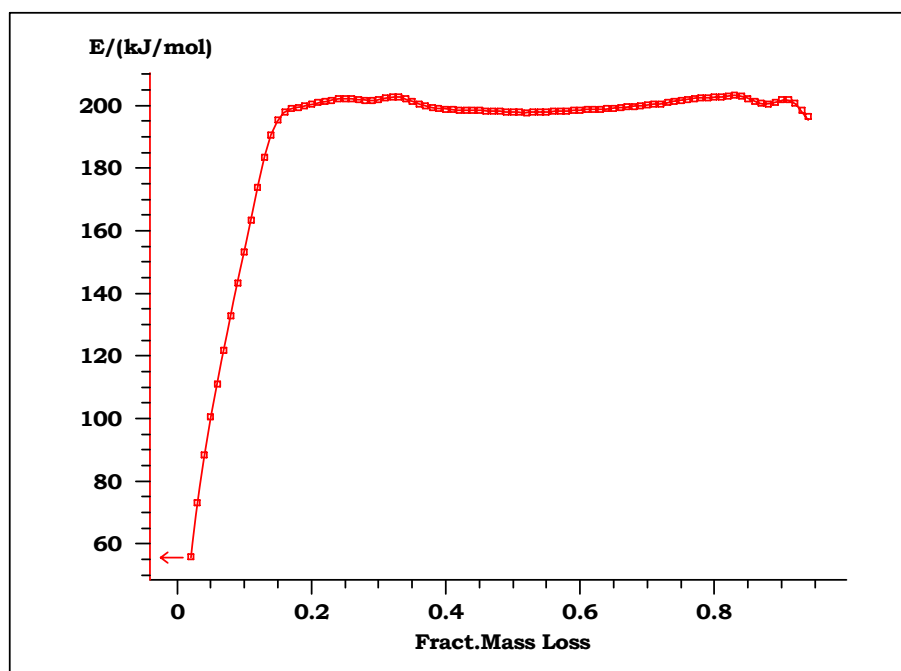


**Figure 6.46.** Energy of activation calculated with Ozawa methods for RTM6+MWNT 0.1 wt% in nitrogen atmosphere

## 6.4 Analysis of residue

In the figure 6.47 a graph comparing dynamic measurements carried out with scan rate of 10°C/min in air flow on all the samples tested in this study is reported. It is possible to notice that addition of zinc compounds in the epoxy matrix does not induce big differences in the first two stages of degradation except for the initial temperature of degradation that increase for samples containing ZS and ZB. For the samples containing ZHS and ATH there is a difference in the first step of degradation which occurs at around 220°C and these temperature is characteristic of dehydration of crystallisation water. For the samples with ZS and ZB the loss of crystallisation water occur at higher temperatures and this process is concomitant with the first step of epoxy matrix degradation which happens in airflow at a temperature of about 350°C and concern the dehydration of hydroxyl functions.

The char oxidation stage occurs for the RTM6 neat in the temperature range (513-627°C) instead for the samples containing flame retardant

zinc compounds, this range of temperature decrease. It is possible to notice large differences for the residue of dynamic experiments carried on samples flame retardants in oxidant atmosphere (tab 6.9). The flame retardant zinc based promote char formation more efficiently at temperatures lower than the epoxy RTM6. Zinc borate in the epoxy matrix RTM6 induce formation of stable char at 554°C and residue is about 32% of initial weight with weight loss in the third stage of 24% RTM6 with ZS form the char stable at the same temperature of sample containing ZB but the residue in this case is lower than ZB (27%). Similarly RTM6 with ZHS show a residue equal at 14%, lower than the initial addition of flame retardant in the resin matrix (20%) and the char formation occurs at temperatures of 551°C.

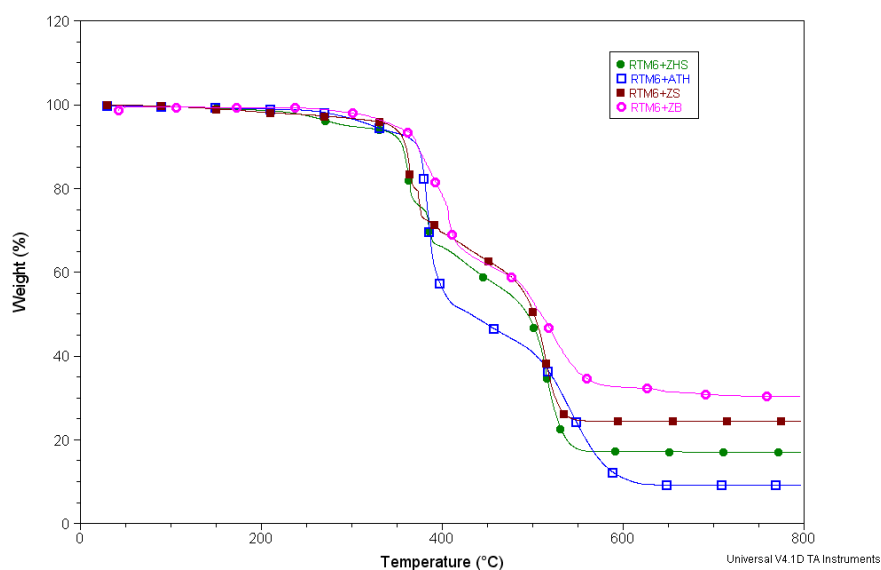


**Figure 6.47.** Comparison of additives at 10°C/min in dynamic mode and in air atmosphere

Sample	Temperature (°C)			% weight loss III stage	% of char at 800°C
	at 10% weight loss	charring stage	initial char formation		
<b>RTM6</b>	357	530-604	636	38	1
<b>RTM6+ZS</b>	359	492-527	555	35	24
<b>RTM6+ZHS</b>	356	498-530	559	40	17
<b>RTM6+ZB</b>	376	485-558	554	24	32
<b>RTM6+ATH</b>	374	509-582	628	36	9

**Table 6.9.** Analysis of last step of degradation in air flow

According to the Flynn-Ozawa-Wall analysis data it is possible to notice that in air flow for RTM6 during the first stage of degradation occur chain scission by thermolysis and there is the formation of thermally more stable molecular compounds. To destroy this compound it is needed another stage of degradation that occurs with activation energy and temperatures higher than first stage. In the presence of flame retardant compounds the second and third stage of degradation concerns the segments of chain liberated that migrates in the surface of samples. A parts of these segments are volatiles but most of these segments react with zinc compounds and form a layer of char stable that delay the oxidation of matrix. The sample containing ZB shows higher efficiency of this process in the formation of char in the epoxy matrix.

## References

- [1] Regnier N., Guibe C. *Polymer Degradation and Stability* 1997, 55:165.
- [2] Regnier N., Fontaine S. *Journal of Thermal Analysis and Calorimetry* 2001, 64:789.
- [3] Kiefer R., Yue J., Hinkley J. *Journal of Advanced Materials* 1995, 26:55.
- [4] Wang Q., Shi W. *Polymer Degradation and Stability* 2006, 91:1747-1754.
- [5] Chiang C.L., Ma C.C.M., Wang F.Y., Kuan H.C. *European Polymer Journal* 2003, 39:825-830.
- [6] Kissinger HE. *Anal Chem* 1957, 29:1702-1706.
- [7] Flynn JH, Wall LA. *J Res Nat Bur Stand A Phys Chem* 1996, 70A:487.
- [8] Ozawa T. *Bull Chem Soc Jpn* 1965, 38:1881.
- [9] Doyle CD. *Nature* 1965, 207:240.
- [10] Beyer G. *Fire Mater* 2002;26(6):291-3.
- [11] Yang SY, Castilleja JR, Barrera EV, Lozano K. *Polym Degrad Stab* 2004;83:383-8.
- [12] Probst O, Moore EM, Reasaco DE, Grady BP. *Polymer* 2004;5:4437-43.
- [13] Kashiwagi T, Grulke E, Hilding J, Harris R, Awad W, Douglas J. *Macromol Rapid Commun* 2002;23(13):761-5.
- [14] Yang J, Lin YH, Wang JF, Lai MF, Li J, Liu JJ, et al. *J Appl Polym Sci* 2005;98: 1087-91.

# **CHAPTER 7**

## **CONCLUSIONS AND FUTURE PERSPECTIVES**

### **7.1 Conclusions**

In this work the flame retardant and thermal mechanical properties of an monocomponent epoxy resin additived with micro and nano fillers are studied. The experimental study is based on cone calorimeter analysis and thermo-mechanical analysis and on the study of kinetic parameters by Kissinger and Ozawa methods.

Through the cone calorimeter test it has been demonstrated that the zinc borate resulted as the best additive as it concerns the 30% and 40% percentages. Furthermore, the flame retardant effect of zinc borate on the Epoxy resin neat is highlighted when it is synergistically used with ATH; instead, as ZS and ZHS are concerned, ZHS performs better at the above mentioned percentages. This comes up also by Kissinger analysis (performed both in nitrogen atmosphere and in air atmosphere) as ZHS shows two steps in nitrogen atmosphere (so as ATH does) and epoxy resin neat shows one step. In air atmosphere, ZHS shows four steps and epoxy resin neat shows two steps. As the Ozawa model is concerned, the union of ZB and ATH improves the activation energy.

From the residue analysis, we can notice that ZB is the best additive both regarding the char-formation temperature both regarding the morphology.

Thermo-mechanical analysis shows that all the additives provide an improvement of the composites thermal expansion coefficient, such as it decreases upon the addition of additives respect to the neat resin.

About nanotubes, the used percentage is too low to observe any meaningful effects in all of the analyses undertaken in this study.

To conclude, zinc borate is, in the light of all performed analyses, the best additive; the percentages where the effect of the additive can be sensibly observed are 30 and 40%.

## **7.2 Future Perspectives**

From our conclusions, it is possible to suggest further studies on ZHS and on its synergistic effect and an investigation on a possible synergy between the used additives and the nanotubes. As for nanotubes, they should be chosen with a higher statistical percolation threshold, so to use a higher additivation percentage.

Moreover, an interesting topic for future work is the comprehension of the degradative mechanisms related to additives in terms of their chemical properties and their interaction with the resin. This study can be carried out by means of FTIR and XRD analysis. The study of the actual mechanisms of degradation during the different heating steps could lead to a better knowledge of kinetic parameters of the composite systems.

About fibres reinforced resin composites, the study of the effects of different lay-up methods on the thermal properties of the additivated composites, could lead to the improvement of their flame retardant properties.